ALMA MATER STUDIORUM
UNIVERSITY OF BOLOGNA

SCHOOL OF SCIENCE

Laurea Magistrale in Analisi e Gestione dell'Ambiente
Curriculum in Water and Coastal Management

# EXPLORING CHLOROPHYLL-A SATELLITE DERIVED DATA TO CHARACTERISE THE COASTAL WATERS OF THE SOUTH OF PORTUGAL

Thesis in: Advanced Technologies and Decision Support Systems in Water and Coastal Management

Supervisor

***Dr. Sónia Cristina***

Presented by:

**Endalkachew Yeshewas MUCHE**

Co-supervisor

***Prof. Clara Cordeiro***

Unique session Academic year: 2020/2022

# Acknowledgments

First and foremost, I express my sincere gratitude to my supervisors Dr. Sónia Cristina and Prof. Clara Cordeiro for all their attention, dedication, valuable advice, guidance, and friendly approach throughout the work of this thesis.

The work was carried out under Erasmus Mundus Programme with funding from European Union. I am thankful to Erasmus Programme for providing a scholarship to do my masters studies.

I would like to extend to thank to the Centre for Marine and Environmental Research (CIMA)-University of Algarve (UAlg) for offering me an internship to collect the data sets used in this study.

I thank the Copernicus Marine Service for providing free and open marine data on ocean colour, SST, and nutrient, which are utilised in this study.

I would like to express my deepest gratitude to Dr. Sónia Cristina who is the host tutor for my internship, and given me the necessary training on SNAP software, which are utilised in this work.

I would like to thank Prof. Clara Cordeiro for the great help on R software, providing me the initial training for this work.

I am also thankful to Prof. Alice Newton, Prof. Elena Fabbri, and Prof. Irene Laiz who is the EMJMD WACOMA Coordinators for all their considerate guidance, kindness, and support during the tenure. I also pay my sincere thanks to all WACOMA technical staff and administrative staff for their support, tolerance, and encouragement.

Finally, I am very much grateful to all my family, friends, and my colleagues for all their support along the way.

# Abstract

The chlorophyll-a (Chl-*a*) concentration can be used as the main indicator of the productivity, trophic condition, and proxy of phytoplankton biomass in coastal, and oceanic waters. This ecological indicator will provide useful information for reliable monitoring systems and government policy (e.g., European directives); however, assessment of Chl-*a* using *in situ* measurements in coastal and oceanic waters has some economic challenges and gives a restricted view of the dynamics of the phytoplankton. To overcome this limitation this study used Chl-*a* datasets from the Copernicus Marine Environment Monitoring Service (CMEMS), that provide merged multi-sensor ocean colour products. This study aimed to characterise the inter-annual variability of the Chl-*a* concentration retrieved by multi-ocean colour sensors data and relate these variabilities to the coastal environmental changes in five stations in the south coast of Portugal. Statistical analyses were performed to help the understanding and the characterisation of Chl-*a* at the coastal water stations along the southern Portugal coast based on 17 years of data (2002-2019). In addition, a comparison between Chl-*a* and physical (sea surface temperature (SST)) and chemical (nutrients) parameters were made to understand the inter-annual variability in these coastal waters. The extracted Chl-*a* values in the study area showed a seasonal cycle where the Chl-*a* is triggered in early spring. A clear negative relationship between Chl-*a* and SST was found in all stations. In the study area, a positive correlation was found between Chl-*a* and nutrients ($NH_4^+$, $NO_3^-$, $PO_4^{-3}$, and $SiO_4^{-4}$). Results show that SST and nutrients influence the Chl-*a* concentration availability in the study area. The Chl-*a* retrieved by satellite data reveals to be an efficient alternative tool and valuable approach to study environmental conditions of the coastal water, especially in response to eutrophication, which is the common management issue in coastal waters.



**Keywords:** Remote Sensing; Chlorophyll-a; Physical-chemical variables; Inter-annual variability; Coastal waters

# Table of contents

# List of Figures

# List of Tables

# Glossary and Acronyms

| | |
|---|---|
| **ACF** | Auto Correlation Function |
| **API** | Algal Pigment Index |
| **AVHRR** | Advanced Very High-Resolution Radiometer |
| **CCCs** | Coastal Counter Currents |
| **CCI** | Climate Change Initiative |
| **CDOM** | Coloured Dissolved Organic Matter |
| **Chl-*a*** | Chlorophyll-a |
| **CI** | Colour Index |
| **CMEMS** | Copernicus Marine Environmental Monitoring Service |
| **CSM** | Cape Santa Maria |
| **CSV** | Cape São Vicente |
| **CZCS** | Coastal Zone Colour Scanner |
| **ENSO** | El Niño Southern Oscillation |
| **EOF** | Empirical Orthogonal Function |
| **ESA** | European Space Agency |
| **GES** | Good Environmental Status |
| **HAB** | Harmful Algal Bloom |
| **HPLC** | High Performance Liquid Chromatography |
| **IBI** | Iberian-Biscay-Ireland |
| **IP** | Iberian Peninsula |
| **IPC** | Iberian Poleward Current |
| **IQR** | Interquartile Range |
| **IUS** | Iberian Upwelling system |
| **L3** | Level-3 |
| **L4** | Level-4 |
| **Max** | Maximum |
| **MERIS** | MEdium Resolution Imaging Spectrometer |
| **Min** | Minimum |
| **MODIS** | MOderate resolution Imaging Spectro-radiometer |
| **MODIS_AQUA** | MODIS sensor carried on AQUA satellite |
| **MODIS_TERRA** | MODIS sensor carried on TERRA satellite |
| **MPA** | Marine Protected Area |
| **MSFD** | Marine Strategy Framework Directive |
| **NAO** | North Atlantic Oscillation |
| **NIR** | Near Infra-Red band |
| **NOAA** | National Oceanic and Atmospheric Administration |
| **NRT** | Near-Real-Time |
| **OC** | Ocean Colour |
| **OC-CCI** | Ocean Colour Climate Change Initiative |
| **OCTAC** | Ocean Colour Thematic Assembly Centre |
| **OLCI** | Ocean and Land Colour Instrument |
| **OLCI-3A** | Ocean and Land Colour Instrument from the Sentinel-3A |

| | |
|---|---|
| **PC** | Portuguese Current |
| **PDO** | Pacific decadal oscillation |
| **PDO** | Pacific decadal oscillation |
| **PFTs** | Phytoplankton Functional Types |
| **PU** | Production Unit |
| **Q1** | 1st quartile or 25th percentile |
| **Q3** | 3rd quartile or 75th percentile |
| **$R_{rs}$** | Remote Sensing Reflectance |
| **$r_s$** | Spearman's correlation coefficient |
| **SeaWiFS** | Sea viewing Wide Field of view Sensor |
| **SNAP** | Sentinel Application Platform |
| **SNPP** | Suomi National Polar-orbiting Partnership |
| **SPC** | South Portugal Coast |
| **SPM** | Suspended Particulate Matter |
| **SST** | Sea Surface Temperature |
| **SWPC** | Southwest coast of Portugal |
| **UI** | Upwelling index |
| **VIIRS** | Visible Infrared Imaging Radiometer Suite |
| **WFD** | Water Framework Directive |

# Chapter 1: Introduction

Interest in marine phytoplankton has increased in recent years due to its significance in regulating climate by producing and consuming greenhouse gases (Tiffany *et al.* 2012). Marine phytoplankton represents less than 1% of global photosynthesis and is responsible for more than 45% of the world's annual net primary production (Falkowski *et al.* 2004, Simon *et al.* 2009). Their role is significant in contributing to 50% of atmospheric oxygen and regulating the carbon dioxide concentration by sequestering annually 20-35% of the worldwide carbon dioxide emissions (Tweddle *et al.* 2018). Marine phytoplankton is not only control carbon dioxide and release oxygen but also they are a vital elements of the marine food chain in the oceanic environment (Falkowski 1997, Falkowski *et al.* 2004). Therefore, changes in the composition of phytoplankton influence the marine ecosystem through trophic interaction between food chains and nutrients (Agirbas & Karadeniz 2020). Additionally, the quick response mechanism of phytoplankton against changes in environmental drivers is a good indicator of the tropic state and is associated with symptoms of eutrophication (Baban 1996, Sheela *et al.* 2011). The consequences of eutrophication can be minimised by identifying the physio-chemical parameters that limit the algal growth and primary productivity (Loureiro et al., 2005). Thus, accounting the phytoplankton primary production is vital to improve our understanding of oceanic biogeochemical cycles (Uitz *et al.* 2010).

Pigments are a powerful means of recognizing nano- and pico-phytoplankton in the ocean, and can be used for mapping phytoplankton populations and monitoring their abundance and composition (Trees *et al.* 2000, Roy *et al.* 2006, Wright & Jeffrey 2006). Photosynthetic phytoplankton contains one or more types of chlorophyll as part of pigments in light-harvesting (Trees *et al.* 2000, Wright & Jeffrey 2006). The role of chlorophyll-a (Chl-*a*) is to absorb light for photosynthesis (Hendry 1996). Photosynthetic pigments can provide information about environmental conditions for a given coastal areas, and reveal the phytoplankton community composition (Roy *et al.* 2006). Chl-*a* has been used as a proxy for monitoring phytoplankton biomass (Gibb 2000). It has been used as the main indicator of the productivity, trophic condition and as a proxy for phytoplankton biomass in estuaries, coastal and oceanic systems for a long period of time (Gibb 2000, Boyer *et al.* 2009, Sheela *et al.* 2011, Goela *et al.* 2014). In addition, Chl-*a* can also be used to support the management of Blue Economy economic sectors (such as fisheries, offshore aquaculture, and marine and coastal tourism) and to provide

useful information for reliable monitoring systems and government policy (e.g., European directives).

The basic assessment of Chl-*a* concentration can be performed using *in situ* measurements (Boss & Behrenfeld 2010); however, this approach provides data with a sparse temporal and spatial coverage and gives only a restricted view of the dynamics of the phytoplankton in relation to human activities. Due to its global and repeated coverage, satellite-based remote sensing offers a unique observational approach suitable for regular measurement of physical and biological properties over large regions of the ocean (McGillicuddy *et al.* 2001). The use of satellite-based ocean colour remote sensing can be more advantageous than *in situ* measurement for the detection, monitoring, and generation of massive series of data, especially in terms of spatial and temporal observation that can be used to study changes in the coastal and oceanic waters (Cristina *et al*. 2016). Ocean colour sensors onboard satellites measures the water-leaving reflectance from the sea surface to quantify the significant optical constituent such as Chl-*a* ( Morel & Prieur 1977). Several scientific studies have been using time series of Chl-*a* retrieved by ocean colour sensors to provide information on the water quality (Novoa *et al.* 2012, Harvey *et al.* 2015, Gohin *et al.* 2019), seasonal and inter-annual dynamics of the Chl-*a* concentration (Mélin *et al.* 2011, Goela *et al.* 2014, Cristina *et al.* 2016, Yu *et al.* 2019, Moradi 2021a), harmful algal blooms detection (Shen *et al.* 2012), primary production (Carretero *et al.* 2019), fishery management (Wilson 2011) and coastal management (Klemas 2011, Kratzer *et al.* 2014). There is a need for additional works to improve its ability for spatial and temporal observation of the major seasonal and inter-annual patterns in biological and oceanographic data (Mélin *et al.* 2011, Goela *et al.* 2016). There is also a need to understand and analyse this massive dataset to characterise the inter-annual variability of the global or regional changes in the coastal waters for the future development of new strategies intended for sustainable management. This study will address the efficiency of the use of Chl-*a* retrieved by ocean colour sensors on the characterization of the inter-annual variability of the Chl-*a* concentration changes in southern Portugal.

## 1.1 Scope of the Study

### 1.1.1 Hypotheses

The physio-chemical parameters influence the variability of Chl-*a* in the southern Portugal coastal zone.

### 1.1.2 Aim and Objectives

This study aimed to characterise the inter-annual variability of the Chl-*a* concentration retrieved by ocean colour sensors data and to relate these variabilities to the coastal environmental changes in southern Portugal. This was mainly achieved by statistical analyses of data spanning 17 years (2002-2019), including Chl-*a,* SST, and nutrients ($NH_4^+$, $NO_3^-$, $PO_4^{-3}$, and $SiO_4^{-4}$) acquired in the Copernicus Marine Service for the coastal waters of five study stations (Station 1 (off Aljezur), Station 2 (off Sagres), Station 3 (off Portimão), Station 4 (off Ria Formosa) and Station 5 (off Guadiana Estuary)) by assessing their temporal changes on yearly, monthly, seasonal, and inter-annual time series.

The specific objectives of this thesis are:

1. To study the inter-annual variability of Chl-*a* in the south coast of Portugal;
2. To explore the impact of SST and nutrients variables on Chl-*a* satellite product using statistical methodologies;
3. To compare the temporal variability of the above variables among the study stations.

### 1.1.3 Research Questions (RQ)

This study intends to address the following g research questions:

1. What is the seasonal behaviour of the Chl-*a* concentration along the southern Portugal coast?
2. What is the impact of the physical and chemical variables on Chl-*a* at the coastal waters?
3. Which stations in southern Portugal are more susceptible to the impacts of environmental variables on the variation of the Chl-*a*?
4. How helpful is the measurement of Chl-*a* for coastal managers and the characterisation of coastal waters using open-source satellite data?

# Chapter 2: Background and Literature Review

## 2.1 Phytoplankton for marine management

The marine phytoplankton species are dominated by microscopic unicellular organisms with a size ranging between 0.4-200 μm that obtain energy through photosynthesis, and therefore drifts in the surface of the ocean, down to 200 m in the clearest waters (Barlow *et al.* 2007, Simon *et al.* 2009). In coastal waters, phytoplankton is efficient filters for nutrient inputs and will respond rapidly to biotic and abiotic changes (Loureiro *et al.* 2006). Phytoplankton distribution in the oceans is governed by the adaptation of various communities to changing environmental conditions of temperature, nutrient and water column stability (Barlow *et al.* 2007, Blondeau *et al.* 2014). Wherever the nutrient concentrations are high, the large phytoplankton cell tends to dominate in turbulent water, while smaller cells are prominent in stratified waters wherever regenerated forms of nitrogen are found (Barlow *et al.* 2007). The enrichment of nutrients in the water column can cause an increase in the phytoplankton biomass, resulting in a range of undesirable disturbances to the organism present in the water and the quality of coastal water (Gohin *et al.* 2019). This excessive growth of phytoplankton biomass in the water column is one of the indicators for eutrophication (J. G. Ferreira *et al.* 2011). Eutrophication impacts on marine goods and services, human health, and economic activities, is still threatening and damaging many coastal ecosystems worldwide (Greenhalgh & Selman 2008, Brito *et al.* 2020). In Europe, approximately 65% of coastlines displays a sign of eutrophication (Cabrita *et al.* 2015). In response to eutrophication on the coastal zones, phytoplankton management must be accounted in marine management processes, to maintain clean, healthy, safe, productive and biologically diverse seas (Tweddle *et al.* 2018).

Marine phytoplankton is considered for assessment of "good ecological status" within the European Union (EU) Water Framework Directive (WFD, 2000/60/EC) (European Commission 2000) and the "good environmental status" within EU Marine Strategy Framework Directive (MSFD, 2008/56/EC ) (European Commission 2008). Within the WFD, the Chl-*a* has been widely used as indicator for the assessment of ecological status using the phytoplankton biological quality element (J. G. Ferreira *et al.* 2011, Tweddle *et al.* 2018). Under the MSFD the Descriptor 5- Eutrophication, use Chl-*a* as an indicator of direct effects of nutrient enrichment which is the primary symptoms of eutrophication (Cabrita *et al.* 2015, Brito *et al.* 2020).

The knowledge and understanding about coastal phytoplankton can be used to assist in ecosystem-based sustainable management of our oceans. Marine phytoplankton management should be considered and incorporated by legislators, policy makers, marine managers, and stakeholders because of the important role marine phytoplankton play in a healthy ecosystem (Farmer *et al.* 2012, Tweddle *et al.* 2018). Consideration of phytoplankton indicators should also be incorporated within management processes for potential marine protected area (MPA) creation, towards mobile species utilizing marine space where there are increased phytoplankton concentrations, and for sustainable resource use such as commercial fisheries (Tweddle *et al.* 2018).

## 2.2 Chl-*a* the proxy of phytoplankton biomass

Pigment analysis offers the best technique for identifying and monitoring phytoplankton in the ocean; however, special condition must be employed to use them as a marker, as they are sensitive to light and heat, as well as their content per cell varies with environmental factors such as nutrients (Wright & Jeffrey 2006, Agirbas & Karadeniz 2020).

Phytoplankton contains three types of pigments involved in light harvesting and photoprotection, namely, chlorophylls, carotenoids and biliprotiens (Wright & Jeffrey 2006). Photosynthetic phytoplankton contains one or more types of chlorophyll as part of the light-harvesting complexes in their chloroplasts(Wright & Jeffrey 2006). Chl-*a* has long been recognised as a unique molecular marker of oceanic phytoplankton biomass (Gibb 2000). The role of Chl-*a* is to absorb light for photosynthesis (Agirbas & Karadeniz 2020). Chl-*a* reflects the overall growth and loss process in oceanic waters, and it is easy to measure compared to algal biomass. Photosynthetic pigments can provide information about environmental conditions and trophic status for a given area.

## 2.3 Important factors impacting the distribution and variability of Chl-*a*

The environmental drivers that influence nutrient and light availability is crucial for supporting the phytoplankton growth in coastal oceans. Understanding the chemical drives (nutrient) and physical drivers such as sea surface temperature (SST), climatic oscillations (e.g., El Niño and the Pacific decadal oscillation (PDO) among other), river discharge, coastal upwelling, eddies in the coastal oceans, and frontal zones (the boundary between different water masses) helps to explain the Chl-*a* distribution and variability in the coastal region.

Yu *et a*l. (2019) have shown the inter-annual variability of Chl-*a* levels increases during El Niño strong southwest monsoon along the southeast of Vietnam. Likewise, Nababan *et al*. (2011) found higher Chl-*a* levels in the northeaster Gulf of Mexico during a strong El Niño event observed during 1997 to 1998 period; and found that higher Chl-*a* levels near the coast were induced by river discharge and wind-driven upwelling. Nababan *et al*. (2011) found that the river discharge and wind-driven upwelling as the major factors influencing the surface Chl-*a* variability for the north-eastern Gulf of Mexico between 1997 and 2000. In their study, during the spring of 1998 a strong upwelling event was observed along the coast due to the El Niño Sothern Oscillation event and caused the Chl-*a* concentration four times higher than during the same period in 1999-2000 (Nababan *et al.* 2011).

Signorini *et al.* (2015) have found that at a global scale the Chl-*a* distribution is largely controlled by ocean circulations. The El Niño southern oscillation impacts the global growth of phytoplankton via changes in SST, wind, and sea surface level (Wilson & Adamec 2001, Racault *et al.* 2017). Racault *et al*. (2017) found that during Eastern Pacific and Central Pacific types of El Niño casued an impact on oceanic phytoplankton. Conversely, Wilson and Adamec (2001) found that the dominant response increased Chl-*a* during the La Niña event in the eastern pacific in 1999.

Kahru *et al*. (2007) demonstrated that the eddies in the coastal oceans played an important role in determining the Chl-*a* variability in the northeaster tropical Pacific. The boundary between different water masses, which is called frontal zones are usually associated with high Chl-*a* and biomass levels (Signorini & McClain 2007).

Martinez *et al*. (2009) have proved that the PDO can impact the regional Chl-*a* level distribution in the basin of the Pacific Ocean. Also found that, global phytoplankton abundances are related to basin-scale oscillations of the physical ocean (PDO and the Atlantic Multidecadal Oscillation). In their studies a basin response of phytoplankton related to large-scale climate oscillators has been shown. Phytoplankton is often nutrient-limited, they grow when nutrients are made available through the upwelling of cold nutrient-rich water from below. Any change in the stratification of the ocean surface has a potential effect on phytoplankton growth, which may happen at different spatial and temporal scales (Martinez *et al.* 2009).

Signorini *et al*. (2015) have revealed the seasonal variability of Chl-*a* concentrations increases in the North Pacific, Indian Ocean, North Atlantic and South Atlantic gyres for a 16-

year (1998–2013) analysis using Chl-*a* retrievals from ocean colour satellite data. Their study revealed that, the surface warming trend over the 16 year period has shown biomass reduction and low Chl-*a* level (Signorini *et al.* 2015).

Kahru *et al*. (2010) have demonstrated that, the global time series of satellite-derived wind and surface Chl-*a* concentration showed a negative correlation in areas with deep mixed layers of the subpolar gyres, the eastern tropical Pacific, and the eastern tropical Atlantic; and positive correlation in areas with shallow mixed layers of the tropics and subtropical gyres. These patterns interpreted the main limiting factor that control phytoplankton growth, i.e., nutrient control phytoplankton biomass in areas with a positive correlation between Chl-*a* and wind speed control phytoplankton biomass in areas with a negative correlation with Chl-*a* and wind speed (Kahru *et al.* 2010).

The studies of Cravo *et al.* (2010) and Cardeira *et al*. (2013) developed in the south Portuguese coast also revealed significant relationships between Chl-*a* and specific environmental processes, such as coastal upwelling. Both studies reveals that the coastal waters show higher Chl-*a* concentrations after the occurrence of upwelling events. Cravo *et al*. (2010) showed that, the amount of Chl-*a* and nutrients transported through the upwelling filaments was significant. Consequently, the filaments in the SW Iberia played a key role in the seaward export of matter (nutrients, gases, and phytoplankton) with an important impact on the regional oceanography of the region.

## 2.4 Measuring Chl-*a* concentration

The basic assessment of measuring Chl-*a* concentration is generally performed using *in situ* measurements and satellite remote sensing methods. *In situ* measurements relies on manually collecting water samples on the field and taken back to the laboratory for chemical analysis of Chl-*a* concentration. This approach, however, is challenged by the cost of operation at sea, the complexity of instrument measurement, and the regional and seasonal variability of seawater (Zibordi *et al.* 2012). Furthermore, this method is a time-consuming, labour intensive, needs skilled human resources to do the laboratory analysis and provides insufficient spatial and temporal coverage of coastal and oceanic waters.

With limited resources and logistical constraints on *in situ* monitoring method, satellite remote sensing offers a cost-effective solution for large scale coastal water quality monitoring (IOCCG 2018). Satellite remote sensing monitoring is a promising tool to acquire information

without physical contact. This approach brings many advantages, for example, it can efficiently acquire water quality information for a large area of coastal water; it can provide observations for remote locations often logistically difficult and expensive to reach using *in situ* monitoring approaches; frequent revisit times provide observations adequate for time-series analysis and event monitoring (IOCCG 2018). This approach also has its own limitations, ocean colour sensors onboard on satellites only provide Chl-*a* concentration in days with clear cloud conditions and of the upper layer of the ocean, i.e. the first attenuation depth, while its vertical distribution throughout the entire euphotic zone is not taken into account (Blondeau-Patissier *et al.* 2004, Rivas *et al.* 2006).

## 2.5 Ocean colour remote sensing

Ocean colour remote sensing makes use of ocean colour sensors, with a narrow field of view that measures the water leaving reflectance from the sea surface at several wavelengths in the visible and near-infrared domains of the electromagnetic spectrum to quantify the optical significant constituent such as Chl-*a*, suspended particulate matter (SPM) and coloured dissolved organic matter (CDOM) (IOCCG 2000).

Since the seventies with the launch of the Coastal Zone Colour Scanner (CZCS; 1978-1986) several other ocean colour sensors such as MEdium Resolution Imaging Spectrometer (MERIS, 2002-2012); Sea-viewing Wide Field-of-view Sensor (SeaWiFS, 1997-2010), MOderate Resolution Imaging Spectroradiometer (MODIS, Terra/2000-present and Aqua/2002-present), Visible Infrared Imaging Radiometer Suite (VIIRS, 2012-present) and Ocean and Land Colour Instrument (OLCI, 2016-present) have been providing Chl-*a* datasets at a global and regional scale for monitoring marine environment (Gohin *et al*. 2019, Moradi 2021) the use of this datasets have been revealed that Chl-*a* can efficiently reflect the phytoplankton dynamics (Yu *et al.* 2019).

To increase the spatial and temporal coverage of Chl-*a* datasets provided by single satellite sensors, the Climate Change Initiative (CCI) program of the European Space Agency (ESA) (http://www.esa-oceancolour-cci.org), and the GlobColour (http://www.globcolour.info) project of the Copernicus Marine Environment Monitoring Service (CMEMS) have generated merged multi-sensor ocean colour products. The CMEMS provides time-series of multi-sensor Chl-*a* datasets over Case-I and Case-II waters in global oceans and for European regional seas (Moradi 2021).

Three algoritihms have been used to retrive Chl-*a* in the CMEMS GlobColour and CCI ocean color product since 2018 (Garnesson *et al.* 2019). These are, the Color Index (CI) approach (Hu *et al.* 2012) restricted to relatively clear water, the common approach OCx (where x represents the number of bands used in the algorithm, OC3,OC4 or OC4Me) for mesotrophic water and OC5 algorithm for complex waters along the coastal zone (Gohin *et al.* 2002). The wavelengths used for the Chl-*a* estimation algorithm in different sensors including, OC3M (443, 488, 547 nm) for MODIS, OC3V(443, 486, 550 nm) for VIIRS , OC3S (443, 490, 555 nm) for SeaWiFS, and OC4Me (443, 490, 510, 560 nm) is the semi-analytical algorithm developed for MERIS for estimating the Algal Pigment Index 1 (API 1) (Morel & Antoine 2007, Harshada *et al.* 2021).

The Ocean Colour Thematic Assembly Centre (OCTAC) builds and operates the European ocean colour operational service within CMEMS providing global, European, and regional (Arctic Ocean, Atlantic Ocean, Baltic Sea, Black Sea, and Mediterranean Sea) high quality core ocean colour products based on Earth Observation from ocean colour missions (Von Schuckmann *et al.* 2016, Volpe *et al.* 2019). The data product files from the CMEMS OCTAC are disseminated by two product levels: Level-3 (L3) and Level-4 (L4) (Colella *et al.* 2021). L3 products are the daily composite products as obtained by merging ocean colour sensors data. L4 products are a daily interpolated and weekly/monthly mean composites product obtained by merging variables derived from multiple measurements. L4 are those products for which a temporal averaging method or an interpolation technique is applied to fill in missing data values(Colella *et al.* 2021).

## 2.6 Application of Chl-*a* in several studies

*In situ* and ocean remote sensing has been applied to monitor Chl-*a* distribution in coastal regions. Recently more and more researchers employed this emerging satellite remote sensing tool to study the distribution and variability of Chl-*a*. Most studies on environmental monitoring using remote sensing method have proved its advantages and potentials to environmental monitoring. For example, for water quality monitoring, Arabi *et al.* (2020) integrate the *in situ* and multi-sensor satellite observations for effective water quality monitoring in coastal areas. Their study of integration the spatial-temporal water constituent concentrations data obtained from *in situ* measurements and satellite images finds applications for the detection of anomaly events and serves as a warning for management actions in the complex coastal waters of the Wadden Sea. Similarly, Novoa *et al.* (2012) assessed the

ecological status of Basque coastal water bodies in the north of Spain using satellite imagery from MODIS sensor. In their study, OC5 algorithm corresponded most accurately with *in situ* measurements performed in the area. They developed classification of water bodies, based upon satellite-derived Chl-*a*, which could improve considerably the assessment of water quality.

Studies as the one of Gurlin *et al.* (2011) used the MERIS and MODIS to test the performance of near infra-red models for the remote estimation of Chl-*a* concentrations in turbid productive coastal and estuarine waters. Their study concluded MERIS two-band model estimated Chl-*a* concentrations slightly more accurately than the MODIS model in coastal water. The comparable results from several near infra-red models, calibrated for inland and coastal waters around the world, indicate a high potential for the development of a simple universally applicable near infra-red algorithm.

Xi *et al.* (2020) studied for global retrieving of Chl-*a* concentrations of phytoplankton functional types (PFTs) from multi-sensor merged ocean colour products or Sentinel-3A OLCI data from the GlobColour archive in the frame of the CMEMS. They applied an empirical orthogonal function (EOF) method to retrieve Chl-*a* concentrations of multiple PFTs using extensive global data sets of *in situ* pigment measurements and matchups with satellite ocean colour products. The study results show that the approach predicts well Chl-*a* concentrations of most of the mentioned PFTs.

Wang *et al.* (2021) assessed the first-ever near-real-time (NRT) global daily Chl-*a* anomaly products that can be used to detect and identify algae blooms from satellite ocean colour measurements such as those from the VIIRS onboard the Suomi National Polar-orbiting Partnership (SNPP) and NOAA-20. They introduced two new VIIRS global Level-3 Chl-*a* anomaly products, Chl-*a* anomaly in difference ΔChl-*a* and Chl-*a* anomaly ratio (or its relative difference) ΔrChl-*a*. The study found out that with both data, global abnormal algae biomass events can be more reliably identified and detected.

Studies from Waite & Mueter (2013), Yu *et al.* (2019) and Corredor-Acosta *et al.* (2020) have shown how the use of satellite observation data can contributed to the understanding of the spatial distribution and temporal variability of Chl-*a*. They explored the relationship between the Chl-*a* and environmental drivers (Sea surface height, SST, freshwater discharge, and coastal upwelling). Their results suggested that the Chl-*a* concentration in each of temporal and spatial variability are associated with environmental drivers.

### 2.6.1 Previous Studies in the South Coast of Portugal

Also, in the Portuguese coast the Chl-*a* have been explore in different studies firstly access buy in situ samplings and in the last years using in situ and remote-sensing sampling strategies.

The in situ sampling carried out by Loureiro *et al.* (2005) to study the dynamic of local microplankton community, production, and respiration at Sagres (SW Portugal) relative to coastal upwelling have revealed that this oceanographic phenomena is the primary factor to affect the distribution of the microplankton at the study area.

Goela *et al*. (2014) also made here study in the SW coast of Portugal on off Sagres stations and established a CHEMTAX methodology to assess the relative contribution of the total Chl-*a* concentration from the main phytoplankton classes. They carried out sampling campaigns for four years off the SW coast of Portugal and taken samples were used for the determination of Chl-*a* and other phytoplankton pigments by High Performance Liquid Chromatography (HPLC). It is noted that in their pigment result, the diatoms dominated from early spring to summer coinciding with coastal upwelling event in the region. The contribution of cyanobacteria to total Chl-*a* was generally low, however there were occasional sampling campaigns where it was exceptional high.

Mendes *et al.* (2011) studied the distribution and composition of phytoplankton assemblages in the Nazaré submarine canyon (Portugal) during an upwelling event using conventional pigment analysis. They recorded a high Chl-*a* concentrations in the canyon head, near the coast.

The studies of southern Portugal coastal waters using ocean colour remote sensing were also conducted. Cardeira *et al.* (2013) assessed the Chl-*a* and chemical signatures, affected by meteorological, topographic, and oceanographic processes mainly occurring in the South Portuguese coast. Their study is based on the upwelling event that took place in the year 2006. Five sections named: Guadiana, Cape Santa Maria, Quarteira, Portimão and Cape São Vicente (CSV) covering the entire region, including the main areas of influence from the main rivers outflow and lagoon, were selected for characterization of Chl-*a* and nutrients (nitrate, phosphate, and silicate). They estimated Chl-*a* concentration using eight-day composite satellite images of MODIS, with a spatial resolution of 4 km. They also took a water sample for the determination of nutrients and Chl-*a*. The study claimed, in the coastal stations high Chl-*a* (maximum 3.1 µg/L) and low nutrient concentrations were observed, particularly in the retention area close to the western limit of the Guadiana River.

In Portugal, the implementation of marine European Directives that work with problems related to eutrophication has been explored by Cristina et al. (2015) with respect to the MSFD and by Brito et al., (2020) with respect to the WFD. The first study test how Chl-a retrieved from the MERIS ocean colour sensor can contribute to the monitoring of an MSFD Descriptor 5-eutrophication for "good environmental status" (GES) and the second study integrate in situ and ocean colour data to evaluate ecological quality under the WFD.

Caballero *et al.* (2020) showed the capabilities of Sentinel-2A/B satellites mission of the Copernicus programme in combination with *in situ* data for monitoring harmful algal bloom (HAB) in the SW Iberian Peninsula. Their study proved that the S2A/2B twin satellites have a suitable capability for supporting the environmental monitoring of small HAB bloom in the Guadiana Estuary. They concluded that the Copernicus product is crucial for water quality monitoring and for ecological and management purposes at regional and national scales.

Ferreira *et al.* (2021) assessed the phytoplankton bloom in the Western Iberian Coast (WIC) using a multi-sensor long-term ocean colour remote sensing dataset with daily resolution. They found out the Chl-*a* concentration ranging from <0.5 mg $m^{-3}$ (low productive oceanic regions) to >3 mg $m^{-3}$ (productive coastal areas). Based on the result they identified the most productive areas in the northern and central section of the WIC and the Gulf of Cadiz. They found out spring is the most productive season of the year, and the northern and central section of the WIC and the Gulf of Cádiz are the most productive areas. Similarly, Navarro & Ruiz (2006) evaluated the temporal and spatial distribution of Chl-*a* concentration in the Gulf of Cadiz (SW Spain) using remote sensing data. They find out that, in coastal areas the maximum Chl-*a* appears in spring followed by summer, mainly due to the presence of several processes that favour the nutrient entrance, such as upwelling events and river discharge. Ferreira *et al.* (2019) also investigated the drivers of Chl-*a* variability in the WIC by using CMEMS satellite data. They found out a positive annual trend of Chl-*a* near Northern coastal WIC, and a negative trend in Southern areas near the Gulf of Cádiz. In the Southern oceanic region, positive Chl-*a* anomalies were found to be associated with high concentrations of nitrogen.

Krug *et al.* (2017) evaluated the patterns in seasonal and inter-annual variability in phytoplankton and underlying environmental determinants within southwest area off the Iberian Peninsula to assess whether the climate variability affects the regions in different ways. They found out that, the climate-sensitive local environmental variables (SST, upwelling, and

river discharge) emerged as the most influential Chl-*a* predictors, and large-scale climate indices (e.g., North Atlantic Oscillation) showed significant but minor effects.

# Chapter 3: Data and Methods

## 3.1 Study Area

The study area lies on the northeast Atlantic coast in the orientation of the South-Western coast of the Iberian Peninsula (IP), covering from 37.5º N to 36.5º N and from 9.5º W to 6.5ºW on the south coast of Portugal (Algarve) (Fig. 3.1). To characterise the Chl-*a* in key regions, five significant study stations were selected approximately 5 km from the coast. The selected regions are located at seasonal upwelling areas, at the mouth of terrestrial discharge from the Guadiana and Arade Rivers (the two main rivers), and near a coastal lagoon. From west to east, the stations are named: Station 1 (off Aljezur), Station 2 (off Sagres), Station 3 (off Portimão), Station 4 (off Ria Formosa) and Station 5 (off Guadiana Estuary), as shown in (Fig. 3.1).

The first station is located off the coast of **Aljezur** (37.34º N, -8.95º E). This station is part of the Eastern North Atlantic Upwelling system (Cristina et al., 2015; Goela et al., 2014; Relvas & Barton, 2005), and it is characterised by a well-defined seasonal upwelling during summer (March to September) in response to northerly wind along the western coast (Leitão et al., 2019; Ramos et al., 2013; Relvas et al., 2009).

The second station is located (36.96°N, -8.86°E) off the coast of **Sagres**, in the SW transition zone of the Algarve. It is characterised by the seasonal upwelling induced by northerly winds along the west coast, with cold and nutrient upwelled waters flowing counter clockwise around CSV and eastward along the southern continental shelf (Relvas & Barton, 2002). This seasonal upwelling occurs mostly during early spring to late summer. This event is the main source of nutrients since there are no permanent rivers in the area (Goela et al., 2016). The area is also well known for its economic activity of offshore aquaculture.

The third station selected is located (37.05°N, -8.55°E) off the coast of **Portimão**. This area is near the Arade River outflow and from the Portimão Canyon (Loureiro et al., 2005; Marchès et al., 2007). Waters off coast of Portimão are subjected to the input of suspended matter from different sources that will cause changes in the salinity, nutrients and Chl-*a* that can be observed during high flow discharges from Arade River. Under small river discharges, mainly during the summer season, or in years of drought, the inputs are mainly governed by upwelling events and relaxation regimes that trigger coastal counter currents (CCCs) that are characterised by warmer and saltier waters (Júnior et al., 2021; Cardeira et al., 2013).

The fourth station located (36.93°N, -7.82°E) is close to the **Ria Formosa** coastal lagoon, one of the most important wetlands along the south coast of Portugal. This area has narrow and elongated morphosedimentary features that diverge North-West and North-East oriented from the city of Faro, enabling the exchange of water, sediments, nutrients, and other chemical elements between the lagoon and the ocean (Cristina *et al.* 2019, Moura *et al.* 2019). The fluctuations in currents along the coast also promote changes in the constituents of the waters (Loureiro et al., 2006). When the winds are favourable, the upwelling events extend along the south coast until the Cape Santa Maria (CSM). These events are more sporadic and weaker in this station and alternate with periods of relaxation that promote the CCC (Cardeira et al., 2013; Loureiro et al., 2006).

The fifth station is located off **Guadiana Estuary** (37.06°N, -7.39°E) near the southern border between Spain and Portugal in the lower estuary mouth. The water circulation within the estuary is restricted in the narrow Guadiana River channel, which connects directly to the ocean surface and brings water rich in nutrients and sediments (Garel *et al.* 2009). In addition, it influences the adjacent coastal waters until about 10 km from the coast during periods of high precipitation levels (Cardeira et al., 2013; Cravo et al., 2006).


**Fig. 3.1.** Geographic location of the five study stations in the south coast of Portugal (main image contains Sentinel-2B Level 2A data [2020], processed by ESA; overview image contains water colour enhanced ML Sentinel-3 OLCI [1-03-2016], processed by ESA), where CSV is Cape São Vicente, and CSM is Cape Santa Maria.

## 3.2 Data Sources

### 3.2.1 Chlorophyll-a Concentration

The Chl-*a* data were downloaded from the E.U. Copernicus Marine Service (CMEMS-https://resources.marine.copernicus.eu/product) on regional domains of Iberian-Biscay-Ireland (IBI) Reginal Sea (*OCEANCOLOUR_ATL_CHL_L4_REP_OBSERVATIONS_009_091*). For this region, the ESA OC-CCI programme merged and bias-corrected the Remote Sensing Reflectance ($R_{rs}$) data from multiple ocean colour sensors (SeaWiFS, MODIS-Aqua, MERIS, VIIRS and OLCI-3A) to compute surface Chl-*a* (mg $m^{-3}$, 1 km resolution) using the regional OC5 Chl-*a* algorithm (Baladrón *et al.* 2020). The Chl-*a* data were obtained as Level 4 (L4) product with a monthly-mean temporal resolution. Moreover, the L4 product already gives us a complete dataset where the missing data was inputted using interpolation (Volpe *et al.* 2019). For this study, a temporal coverage from 2002 to 2019, ranging over 17 years of data, was used.

### 3.2.2 Sea Surface Temperature

Monthly-mean sea surface temperature **(**SST) product was downloaded from CMEMS. The SST was obtained from the IBI ocean physics reanalysis 3D numerical model reprocessed to L4 product and has a 0.083° × 0.083° spatial resolution (*IBI_MULTIYEAR_PHY_005_002*). The IBI model numerical core is based on the NEMO v3.6 ocean general circulation model run at 1/12° horizontal resolution (Levier *et al.* 2021). The original SST time series covers from 1993 to 2019. However, to be consistent with the data on Chl-*a*, only the period between 2002 and 2019 was extracted.

### 3.2.3 Nutrient

In order to research the nutrient conditions in the study area, the data were gathered from the numerical biogeochemical model PISCES and NEMO-v3.4 ocean general circulation model run at a horizontal resolution $1/12^0$ to generate biogeochemical forecast L4 product downloaded from the CMEMS (McGovern *et al.* 2020). The database *IBI_MULTIYEAR_BGC_005_003*, comprises monthly ocean field variables, such as nitrate ($NO_3^-$), ammonium ($NH_4^+$), phosphate ($PO_4^{-3}$), and silicate ($SiO_4^{-4}$). The grided forecast product has been covered since 1993 with 0.083° × 0.083° spatial resolution. The time horizon considered for the study period was 2002-2019, the same as Chl-*a*.

### 3.2.4 Processing the data from the Copernicus Marine Service

The monthly Chl-*a*, SST, Nutrients ($NO_3^-$, $NH_4^+$, $PO_4^{-3}$, and $SiO_4^{-4}$) parameters for the selected stations downloaded from the CMEMS (https://resources.marine.copernicus.eu/products) between 2002 and 2019 were extracted using Sentinel Application Platform (SNAP) toolbox version 8.05. Based on the coordinates of each station a 3 by 3-pixel matrices were extracted at 5 km from the coast to avoid the influence of the land.

## 3.3 Statistical Approaches

Descriptive statistical measures, tables, and graphical approaches, such as time series plots and boxplots, are the primary statistical approaches used to explore and analyse the data. The boxplot is a valuable graph that detects unusual observations, also called outliers (Shahbaba 2009). Statistical descriptive measures such as median, interquartile range (IQR), maximum (Max), and minimum (Min) observed values were used to interpret the data. The sample median is a measure of central location, corresponding to the middle in a sequence of observations ordered from smallest to largest. The IQR is a measure of dispersion, the difference between the third quartile ($Q_3$) and the first quartile ($Q_1$). Median and IQR, are robust measures used in the presence of outliers in the sample (Shahbaba 2009).

The data analysed in this case study are a sequence of observations collected over time, designated as time series and represented by $\{Y_1, Y_2, \ldots, Y_T\}$(Chatfield 2004). Time series graphs allow visualisation of the data, such as detecting patterns, unusual observations, and any change over time. In a time series, trends can be observed, and repetitive patterns when the data are affected by seasonal factors at any time of the year, the month, or the day of the week (Hyndman & Athanasopoulos 2018). Seasonality is always of a fixed and known frequency.

The autocorrelation plots are commonly used to check randomness (if there is no time dependence), trend, seasonal fluctuation, and outliers in time series (Chatfield 2004). Autocorrelation is a correlation between an observation at time t and t-k, say, $Y_t$ and $Y_{t-k}$ (Shumway & Stoffer 2011). It will give us a better understanding of how the data observations in a time series are associated with previous time steps of observation value. The time steps at those previous times are referred to as lags. The autocorrelation is denoted by $r_k$ or ACF(k), and it is determined by:

$$r_k = \frac{\sum_{t=k+1}^{T}(Y_t-\bar{Y})(Y_{t-k}-\bar{Y})}{\sum_{t=1}^{T}(Y_t-\bar{Y})^2} \qquad (1)$$

where $r_k$ is the autocorrelation coefficient at lag k (k = 0, 1, 2, 3, ...), $Y_t$ is the observation at time t, $\bar{Y}$ is the mean, and T is the length of the time horizon. If the ACF turns out to be near one or significantly non-zero, it will be non-random, and if the ACF be near zero for all time-lag separation, it will be random (Hyndman & Athanasopoulos 2018). If the time series contains a trend, then the ACF for small lags tend to be significant and positive. If there is seasonality, the ACF will be larger at the seasonal lags i.e., at multiples of the seasonal frequency (Hyndman & Athanasopoulos 2018). In addition, the ACF plot presents also the 95% confidence interval of significance limits. If the ACF coefficient values fall outside the confidence limits, the time series observations are very likely to correlate to the previous time steps of observation value.

The time series used in the case study have different units and scales, therefore, the min-max normalisation (Eq. (2)) was applied in order to have the same scale feature so that each variable could be easily compared. The min-max normalisation is given by:

$$Y_t^{norm} = \frac{Y_t - \min(Y)}{\max(Y) - \min(Y)} \quad , t= 1,..,T, \qquad (2)$$

where $Y_t^{norm}$ is the normalised value at time t, Y is the raw data and $Y_t$ is the observation at time t. This transformation rescales the data to a fixed range [0,1] by preserving the original data distribution (Dalwinder & Birmohan 2022).

To investigate the existence of any relationships between the variables, the nonparametric Spearman's correlation coefficient ($r_s$) was used. This coefficient is defined as the Pearson correlation coefficient but computed over the rank of the observations (Wunderlin *et al.* 2001). This rank-order computing is the powerful benefit of Spearman's (Bishara & Hittner 2012). For this reason, Spearman is the appropriate measure than Pearson's in case of the existence of outliers (Ángel *et al.* 2006). This association have properties depending on the direction and strength of association between the variables. Regarding direction, it could be positive when both variables move in the same direction (as one variable increases/decreases, the other variable also increases/decreases; or it could be negative, when the variables move in the opposite direction (as one variable increases/decreases the other variable decreases/increases) (Shahbaba 2009). If the coefficient value is close to ±1, it means that the strength of the relationship is strong; in case the correlation coefficient is close to zero it means that there is no relationship between the variables (Shahbaba 2009). The scatterplot is a helpful graph that shows the relationship between two variables.

The Spearman's rank correlation at a significance level (α) is statistically significant when the p-value is less than α. In this case the null hypothesis (no relation) is rejected, meaning that there is an association between the two variables. For this study a α = 5% was considered.

All the statistical analyses were performed in R version 4.1.2 (R Core Team 2021) and the packages ggplot2 (Wickham 2016), tidyverse (Wickham *et al*. 2019), officer (Gohel 2021), rvg (Gohel 2020), viridis (Simon *et.al*. 2021), ggpubr (Kassambara 2020), Rcmdr (Fox and Bouchet-Valat 2020), and readxl (Wickham and Bryan 2019) were used for analyses.

# Chapter 4: Results

## 4.1 Characterization of Station 1 (off Aljezur)

### 1.1.1 Chlorophyll-a Concentration

Monthly time series of Chl-*a* (mg $m^{-3}$), Fig. 4.1(a), exhibit seasonal behaviour. Fig. 4.1.(c) shows the seasonal period of Chl-*a* can be characterised by an increase from January until July, with higher values in summer, and then decreased until December, the wintertime. There was no significant increase or decrease of the Chl-*a* along the time horizon; however, there was a slight decreasing trend between 2002-2007 and 2009-2011.

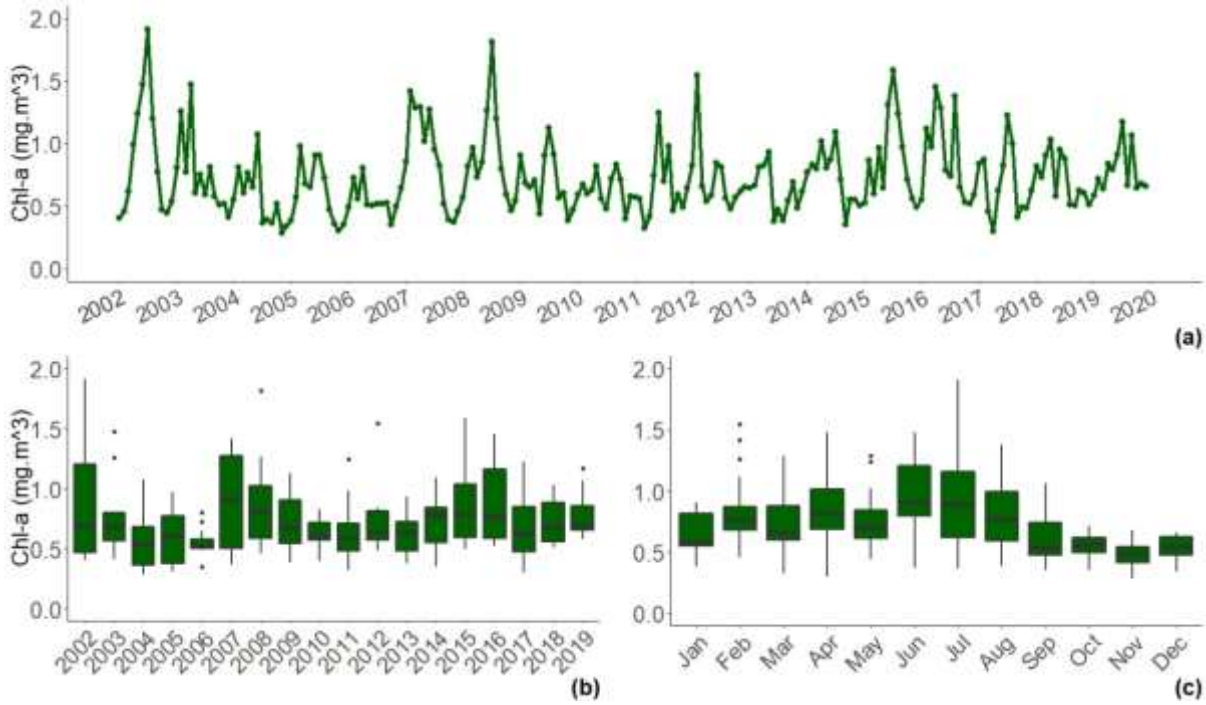


**Fig. 4.1.** *Monthly chlorophyll-a concentration (Chl-a mg $m^{-3}$) concentration: (a) the time series plot; the boxplot (b) by year, and (c) by month for Station 1 (off Aljezur).*

The annual and monthly variability of Chl-*a* are presented in Fig.4.1(b) and Fig.4.1(c), respectively. By merging this graphical information, the minimum and the maximum values of the Chl-*a* were identified in November 2004 (0.28 mg $m^{-3}$) and in July 2002 (1.91 mg $m^{-3}$).

The comparison of Chl-*a* using the descriptive measure median (due to the presence of outliers) shows that half of the data in 2007 are greater than 0.91 mg $m^{-3}$, as seen in Fig. 4.1(b) and Table 4.1; however, it is 2002 that shows the biggest range, from 0.41-1.91 mg $m^{-3}$. Concerning the dispersion of the data, the IQR was high in 2007 (0.77 mg $m^{-3}$), with 50% of

the data between 0.5-1.28 mg $m^{-3}$. The year with the smallest dispersion is 2006 (IQR=0.07 mg $m^{-3}$), with 25% of Chl-*a* values above 0.58 mg $m^{-3}$ and below 0.5 mg $m^{-3}$.

***Table 4.1.*** *Statistical descriptive measures of Chl-a (mg $m^{-3}$) by year Station 1 (off Aljezur).*

| Year | IQR | Min | $Q_1$ | Median | $Q_3$ | Max |
|---|---|---|---|---|---|---|
| **2002** | 0.74 | 0.41 | 0.47 | 0.69 | 1.21 | 1.91 |
| **2003** | 0.24 | 0.41 | 0.56 | 0.68 | 0.80 | 1.47 |
| **2004** | 0.31 | 0.28 | 0.37 | 0.53 | 0.68 | 1.07 |
| **2005** | 0.40 | 0.31 | 0.38 | 0.61 | 0.77 | 0.98 |
| **2006** | 0.07 | 0.35 | 0.50 | 0.52 | 0.58 | 0.80 |
| **2007** | 0.77 | 0.37 | 0.50 | 0.91 | 1.28 | 1.42 |
| **2008** | 0.44 | 0.46 | 0.59 | 0.81 | 1.02 | 1.81 |
| **2009** | 0.36 | 0.38 | 0.54 | 0.67 | 0.90 | 1.13 |
| **2010** | 0.14 | 0.40 | 0.57 | 0.61 | 0.72 | 0.83 |
| **2011** | 0.22 | 0.32 | 0.48 | 0.58 | 0.71 | 1.25 |
| **2012** | 0.25 | 0.48 | 0.57 | 0.64 | 0.82 | 1.54 |
| **2013** | 0.24 | 0.37 | 0.48 | 0.63 | 0.72 | 0.93 |
| **2014** | 0.29 | 0.35 | 0.55 | 0.79 | 0.84 | 1.09 |
| **2015** | 0.45 | 0.49 | 0.59 | 0.79 | 1.03 | 1.58 |
| **2016** | 0.58 | 0.52 | 0.58 | 0.76 | 1.16 | 1.45 |
| **2017** | 0.37 | 0.30 | 0.48 | 0.62 | 0.85 | 1.22 |
| **2018** | 0.32 | 0.51 | 0.56 | 0.68 | 0.88 | 1.03 |
| **2019** | 0.20 | 0.58 | 0.65 | 0.70 | 0.85 | 1.17 |

In terms of months (Fig. 4.1(c) and Table 4.2), 50% of the Chl-*a* values in June and July were at least 0.9 and 0.89 mg $m^{-3}$, respectively.

***Table 4.2.*** *Statistical descriptive measures of Chl-a (mg $m^{-3}$) by month Station 1 (off Aljezur).*

| Month | IQR | Min | $Q_1$ | Median | $Q_3$ | Max |
|---|---|---|---|---|---|---|
| **Jan** | 0.26 | 0.38 | 0.55 | 0.59 | 0.81 | 0.90 |
| **Feb** | 0.19 | 0.46 | 0.68 | 0.77 | 0.87 | 1.54 |
| **Mar** | 0.28 | 0.32 | 0.60 | 0.66 | 0.88 | 1.29 |
| **Apr** | 0.33 | 0.30 | 0.68 | 0.81 | 1.01 | 1.47 |
| **May** | 0.23 | 0.44 | 0.61 | 0.70 | 0.84 | 1.29 |
| **Jun** | 0.41 | 0.37 | 0.80 | 0.90 | 1.20 | 1.47 |
| **Jul** | 0.54 | 0.37 | 0.62 | 0.89 | 1.16 | 1.91 |
| **Aug** | 0.40 | 0.39 | 0.59 | 0.77 | 0.99 | 1.38 |
| **Sep** | 0.27 | 0.35 | 0.47 | 0.54 | 0.74 | 1.06 |
| **Oct** | 0.12 | 0.35 | 0.50 | 0.56 | 0.62 | 0.71 |
| **Nov** | 0.13 | 0.28 | 0.41 | 0.49 | 0.55 | 0.68 |
| **Dec** | 0.15 | 0.34 | 0.48 | 0.54 | 0.62 | 0.66 |

In July, the variability is bigger, ranging between 0.37 and 1.91 mg $m^{-3}$. Also, in July, the dispersion presents the highest IQR value (0.54 mg $m^{-3}$), with 50% of the Chl-*a* (mg $m^{-3}$) values

falling within the interval [0.62, 1.16]. Conversely, the lower dispersion was noted in October (IQR=0.12 mg $m^{-3}$), with half the values falling within [0.5, 0.62 mg $m^{-3}$].

The ACF for Chl-*a* time series data was applied and displayed in Fig.4.2. The ACF shows some significant peak autocorrelation at lags 12, 24, and so on. This indicates the presence of a seasonality pattern in the data with a length of 12 months, as was also shown in Fig. 4.1(a). More so, the ACF showed positive and large values for small lags, this might indicate a slowly declining trend at the beginning of the data. This indication supports the initial statement given in the timeseries plot, the data is considered to have a slightly decreasing trend between 2002-2007 and 2009-2011.

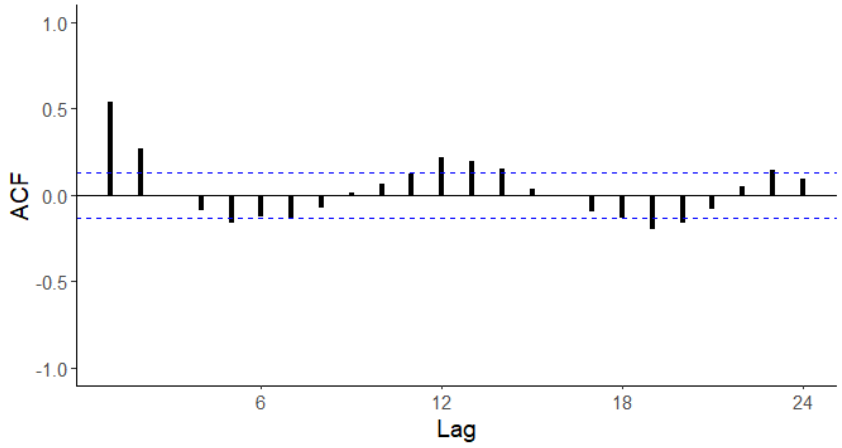


***Fig. 4.2.*** *ACF for chlorophyll-a concentration (Chl-a mg m-3) time series for Station 1 (off Aljezur).*

### 4.1.1 Sea Surface Temperature

The data in Fig. 4.3 shows a monthly SST measured value in degrees centigrade for the years between 2002 and 2019. A constant seasonal amplitude and patterns revealed over the time series in Fig. 4.3(a), showing a stable annual cycle. The seasonal pattern presented in Fig.4.3(c) shows the SST are at a minimum in February, steadily increases until September and then begins declining until February. In general, SST show the higher values in summer and first autumn months and lower values during the winter months (Fig.4.3(c) and Table 4.3).

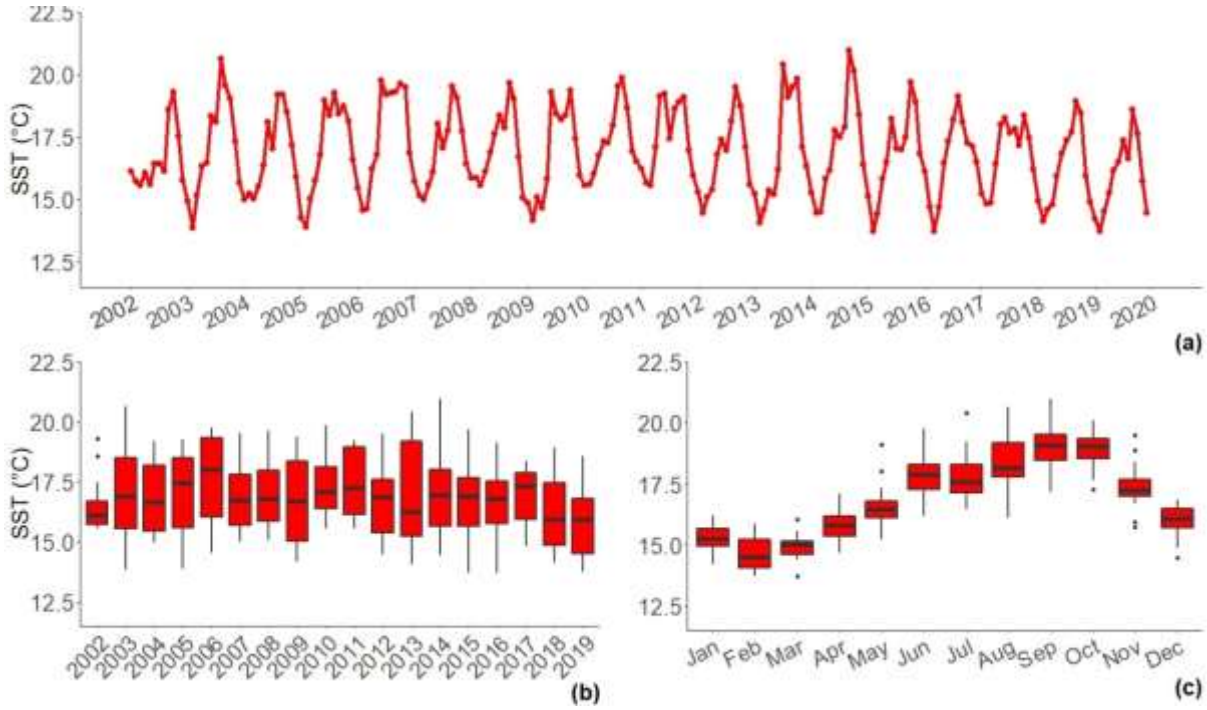


***Fig. 4.3.*** *Monthly time series of sea surface temperature (SST-ºC): (a) the time series plot; the boxplot (b) by year, and (c) by month for Station 1 (off Aljezur).*

According to what is shown in Fig.4.3(b), Fig.4.3(c), Table 4.3 and Table 4.4, the minimum and the maximum values of the SST are recorded in February 2015 (13.7 ºC) and in September 2014 (21.0 ºC), respectively. The highest median value of the dataset was found in the year 2006 (18.0 ºC). The dispersion of the data (IQR) was high in 2013 (4.0 ºC), with 50% of the data found between 15.2-19.2 ºC, while the smallest dispersion was found in 2002 (IQR=0.97 ºC), falling within [15.7, 16.7 ºC] interval.

Monthly variability of SST (Fig. 4.2a (c) and Table 2b), displays the highest median value in September (19.1 ºC), with the data values ranging between 17.2 and 21.0 ºC. The highest dispersion was observed in August, with an IQR = 1.41 ºC and 50% of the SST values falling within the interval [17.8, 19.2 ºC]. Alternatively, the smallest dispersion was noted in November (IQR=0.68 ºC), with 25% of values being above 17.0 ºC and below 17.7 ºC.

***Table 4.3.*** *Statistical descriptive measures of sea surface temperature (SST-ºC) by year for Station 1 (off Aljezur).*

| Year | IQR | Min | $Q_1$ | Median | $Q_3$ | Max |
|---|---|---|---|---|---|---|
| **2002** | 1.0 | 15.6 | 15.7 | 16.1 | 16.7 | 19.3 |
| **2003** | 3.0 | 13.8 | 15.5 | 16.9 | 18.5 | 20.6 |
| **2004** | 2.7 | 15.0 | 15.5 | 16.7 | 18.2 | 19.2 |
| **2005** | 2.9 | 13.9 | 15.6 | 17.5 | 18.5 | 19.3 |
| **2006** | 3.3 | 14.6 | 16.0 | 18.0 | 19.3 | 19.7 |
| **2007** | 2.1 | 15.0 | 15.7 | 16.7 | 17.8 | 19.5 |
| **2008** | 2.1 | 15.1 | 15.9 | 16.8 | 18.0 | 19.7 |
| **2009** | 3.4 | 14.2 | 15.0 | 16.7 | 18.4 | 19.4 |
| **2010** | 1.7 | 15.6 | 16.4 | 17.1 | 18.1 | 19.9 |
| **2011** | 2.8 | 15.5 | 16.1 | 17.2 | 18.9 | 19.2 |
| **2012** | 2.2 | 14.5 | 15.4 | 16.9 | 17.6 | 19.5 |
| **2013** | 4.0 | 14.0 | 15.2 | 16.2 | 19.2 | 20.4 |
| **2014** | 2.3 | 14.4 | 15.7 | 16.9 | 18.0 | 21.0 |
| **2015** | 2.0 | 13.7 | 15.6 | 16.9 | 17.7 | 19.7 |
| **2016** | 1.8 | 13.7 | 15.8 | 16.8 | 17.5 | 19.1 |
| **2017** | 1.9 | 14.8 | 15.9 | 17.3 | 17.9 | 18.4 |
| **2018** | 2.6 | 14.1 | 14.9 | 15.9 | 17.4 | 18.9 |
| **2019** | 2.3 | 13.7 | 14.5 | 15.9 | 16.8 | 18.6 |

***Table 4.4.*** *Statistical descriptive measures of sea surface temperature (SST-ºC) by month for Station 1 (off Aljezur).*

| Month | IQR | Min | $Q_1$ | Median | $Q_3$ | Max |
|---|---|---|---|---|---|---|
| **Jan** | 0.7 | 14.2 | 14.9 | 15.2 | 15.7 | 16.2 |
| **Feb** | 1.1 | 13.7 | 14.1 | 14.5 | 15.2 | 15.9 |
| **Mar** | 0.6 | 13.7 | 14.6 | 15.0 | 15.1 | 16.0 |
| **Apr** | 0.8 | 14.7 | 15.4 | 15.8 | 16.2 | 17.1 |
| **May** | 0.7 | 15.2 | 16.1 | 16.5 | 16.8 | 19.1 |
| **Jun** | 1.0 | 16.2 | 17.3 | 17.9 | 18.3 | 19.7 |
| **Jul** | 1.2 | 16.4 | 17.1 | 17.6 | 18.3 | 20.4 |
| **Aug** | 1.4 | 16.1 | 17.8 | 18.2 | 19.2 | 20.6 |
| **Sep** | 1.1 | 17.2 | 18.5 | 19.1 | 19.5 | 21.0 |
| **Oct** | 0.8 | 17.3 | 18.5 | 19.0 | 19.3 | 20.1 |
| **Nov** | 0.7 | 15.7 | 17.0 | 17.2 | 17.7 | 19.5 |
| **Dec** | 0.8 | 14.5 | 15.7 | 16.1 | 16.5 | 16.8 |

The ACF applied for SST shown in Fig. 4.4., reflected a consistent pattern in the autocorrelations. This indicates that the SST has a strong significant autocorrelation value at the lags 12, 24, and so on which indicates the presence of seasonality.

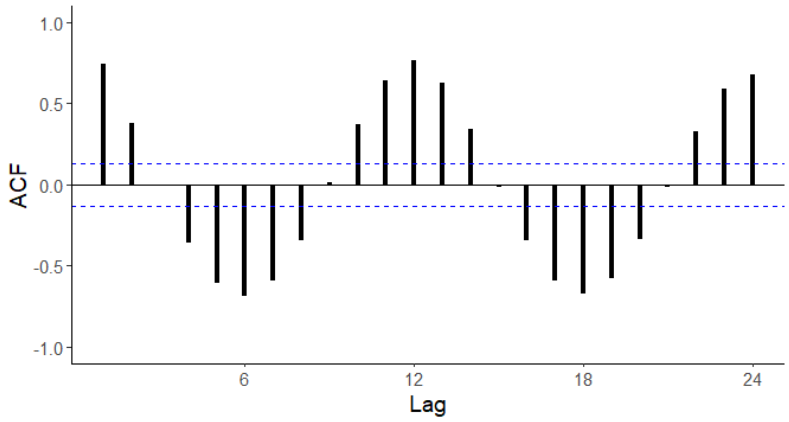


**Fig. 4.4.** ACF for sea surface temperature (SST-ºC) of time series for Station 1 (off Aljezur).

### 4.1.2 Nutrients

The monthly mean time series data plot for nutrient (nitrates $NO_3^-$, ammonia ($NH_4^+$), phosphates ($PO_4^{-3}$), and silicates ($SiO_4^{-4}$)) from 2002 to 2019 has been explored in Fig. 4.5(a–c). With time series plot (Fig. 4.5(a)), for three nutrients ($NH_4^+$, $PO_4^{-3}$, and $SiO_4^{-4}$) the seasonal amplitude and patterns are constant over the time. For $NO_3^-$ the seasonal pattern shows a tendency to increase between 2013 and 2016.

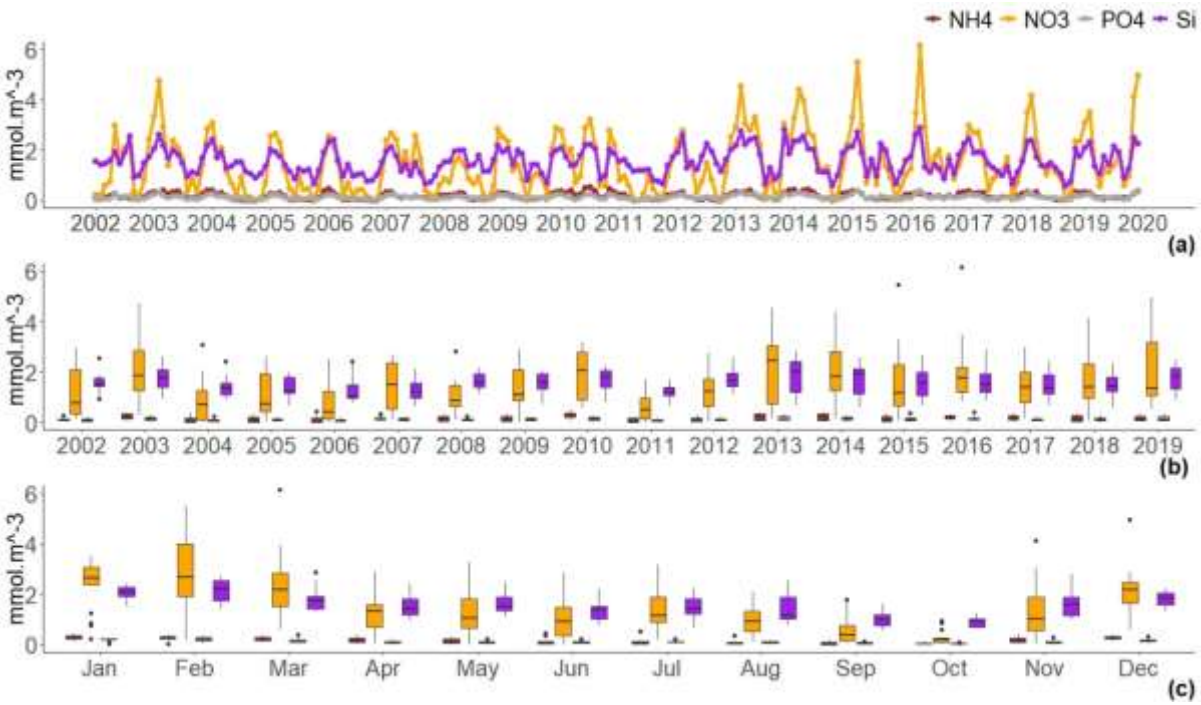


***Fig. 4.5.****Monthly time series of ($NH_4^+$, $NO_3^-$, $PO_4^{-3}$, and $SiO_4^{-4}$): (a) the time series plot; the boxplot (b) by year, and (c) by month.*

The three nutrients $NO_3^-$, $PO_4^{-3}$ and $SiO_4^{-4}$ (Fig. 4.5(a–c); Table (4.5 and 4.6)) revealed with the maximum values in March 2016, with 6.15, 0.39, and 2.87 $mmol.m^{-3}$ of concentration

values, respectively. $NH_4^+$ exhibited the maximum concentration value in July 2010 with 5.15 mmol.m$^{-3}$. The minimum concentration values for $NH_4^+$ and $PO_4^{-3}$ were detected in May 2004 and 2016, respectively. Likewise, the $NO_3^-$ showed the minimum values in June 2011 at 0.01 mmol.m$^{-3}$, and $SiO_4^{-4}$ was revealed in September 2018 at 0.56 mmol.m$^{-3}$.

The comparison of nutrients using the descriptive measure median in Fig. 4.5 (b) and Table 4.5 shows that the highest median was found in 2013 for three nutrients $NO_3^-$, $PO_4^{-3}$, and $SiO_4^{-4}$ with values of 2.45, 0.19 and 2.1 mmol.m$^{-3}$, respectively. While $NH4^+$, indicated the highest median value in 2010 (>0.34 mmol.m$^{-3}$) (Fig. 4.5 (b)).

Table 4.5 show that the IQR was high in 2013 for $PO_4^{-3}$ and $SiO_4^{-4}$ with 0.5 and 1.21 mmol.m$^{-3}$, respectively. Similarly, the IQR was high in 2014 (0.26 mmol.m$^{-3}$) for $NH_4^+$ and in 2019 (2.1 mmol.m$^{-3}$) for $NO_3^-$. The lowest IQR value for $NH_4^+$ and $SiO_4^{-4}$ was found in 2002 at 0.06 and 0.33 mmol.m$^{-3}$, respectively. For $NO_3^-$ and $PO_4^{-3}$ the lowest IQR values were found in 2011 with 0.82 and 0.06 mmol.m$^{-3}$, correspondingly. For higher dispersion, 50% of all nutrient data values were found between 0.08 and 3.2 mmol.m$^{-3}$, while the smallest dispersion falls within [0.03, 1.76 mmol.m$^{-3}$].

Monthly variability (Fig. 4.5 (b-c) and Table 4.6) revealed the highest median value for two targeted nutrients $NH_4^+$ and $PO_4^{-3,}$ in January with 0.31 and 0.21 mmol.m$^{-3}$, respectively. While $NO_3^-$ and $SiO_4^{-4}$ indicated the highest median value in February with 2.68 and 2.21 mmol.m$^{-3}$, correspondingly. In October, the dispersion presents the lowest IQR value for all nutrients. In this lowest dispersion, 25% of nutrients data values were above 0.01 and below 1.04 mmol.m$^{-3}$. Conversely, the highest dispersion was noted in February for $NO_3^-$ and $PO_4^{-3}$, with half the values falling within [1.91, 3.98] and [0.15,0.28] mmol.m$^{-3}$ interval, respectively. In May, the dispersion presents the highest IQR value (0.17 mmol.m$^{-3}$), with 25% of $NH_4^+$ data values were found to be above 0.06 and below 0.22 mmol.m$^{-3}$. Also, the highest dispersion value of $SiO_4^{-4}$ was noted in August (IQR=0.045 mmol.m$^{-3}$), with half the values falling within [1. 03, 1.86 mmol.m$^{-3}$] interval.

The ACF plotted for all nutrients in Fig. 4.6 showed the presence of a seasonality pattern as the Chl-*a* and SST for Station 1.

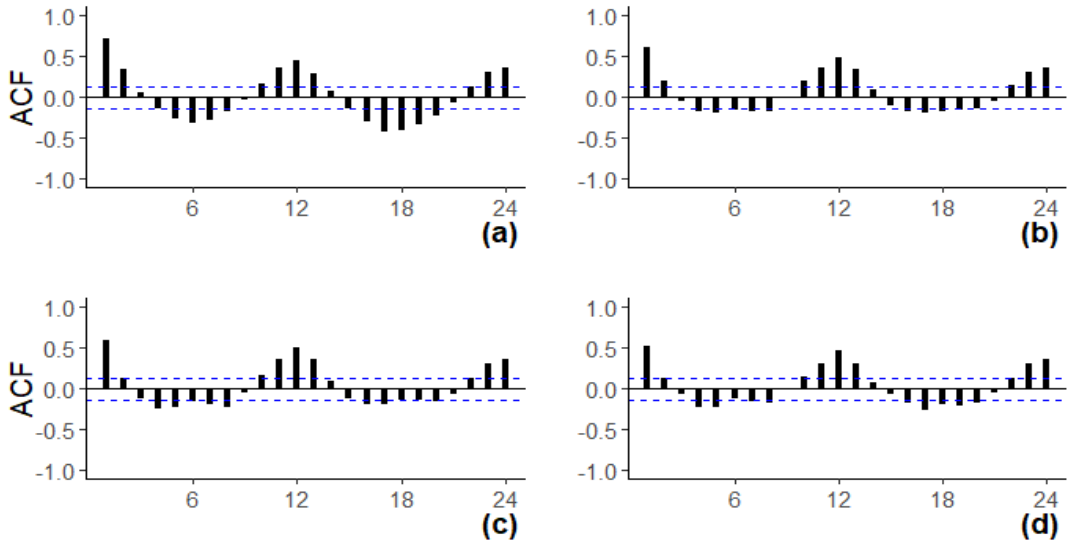


***Fig. 4.6.*** *ACF plots of time series for (a) $NH_4^+$, (b) $NO_3^-$ (c) $PO_4^+$ and (d) $SiO_4^{-4}$ for Station 1 (off Aljezur)*

***Table 4.5.*** *Statistical descriptive measures of Nutrients ($NH_4^+$, $NO_3^-$, $PO_4^{-3}$, and $SiO_4^{-4}$) $mmol.m^{-3}$ by year for Station 1(off Aljezur). *Bold values are higher values of each statistical measures*

| Year | $NH_4^+$ | $NO_3^-$ | $PO_4^{-3}$ | $SiO_4^{-4}$ | $NH_4^+$ | $NO_3^-$ | $PO_4^{-3}$ | $SiO_4^{-4}$ | $NH_4^+$ | $NO_3^-$ | $PO_4^{-3}$ | $SiO_4^{-4}$ | $NH_4^+$ | $NO_3^-$ | $PO_4^{-3}$ | $SiO_4^{-4}$ | $NH_4^+$ | $NO_3^-$ | $PO_4^{-3}$ | $SiO_4^{-4}$ | $NH_4^+$ | $NO_3^-$ | $PO_4^{-3}$ | $SiO_4^{-4}$ |
|---|---|---|---|---|---|---|---|---|---|---|---|---|---|---|---|---|---|---|---|---|---|---|---|---|
| | **IQR** | | | | **Min** | | | | **$Q_1$** | | | | **Median** | | | | **$Q_3$** | | | | **Max** | | | |
| **2002** | 0.06 | 1.75 | 0.12 | 0.33 | 0.03 | 0.15 | 0.01 | 0.93 | 0.08 | 0.33 | 0.03 | 1.43 | 0.11 | 0.77 | 0.06 | 1.52 | 0.14 | 2.08 | 0.15 | 1.76 | 0.27 | 2.96 | 0.22 | 2.54 |
| **2003** | 0.18 | 1.60 | 0.12 | 0.70 | 0.09 | 0.31 | 0.02 | 0.94 | 0.15 | 1.25 | 0.09 | 1.38 | 0.29 | 1.86 | 0.14 | 1.75 | 0.32 | 2.85 | 0.20 | 2.08 | 0.39 | 4.74 | 0.32 | 2.62 |
| **2004** | 0.17 | 1.17 | 0.08 | 0.45 | < 0.01 | 0.02 | 0.01 | 0.89 | 0.01 | 0.11 | 0.04 | 1.11 | 0.04 | 0.71 | 0.07 | 1.35 | 0.17 | 1.28 | 0.12 | 1.56 | 0.38 | 3.07 | 0.24 | 2.41 |
| **2005** | 0.20 | 1.49 | 0.10 | 0.63 | < 0.01 | 0.05 | 0.02 | 0.67 | 0.02 | 0.44 | 0.06 | 1.15 | 0.08 | 0.73 | 0.08 | 1.23 | 0.22 | 1.94 | 0.16 | 1.79 | 0.35 | 2.63 | 0.20 | 2.01 |
| **2006** | 0.15 | 1.10 | 0.08 | 0.56 | < 0.01 | 0.02 | 0.01 | 0.76 | 0.01 | 0.15 | 0.04 | 0.95 | 0.02 | 0.40 | 0.06 | 1.03 | 0.16 | 1.24 | 0.11 | 1.51 | 0.45 | 2.53 | 0.21 | 2.41 |
| **2007** | 0.08 | 1.82 | 0.12 | 0.57 | 0.03 | 0.16 | 0.02 | 0.64 | 0.10 | 0.55 | 0.06 | 0.98 | 0.15 | 1.48 | 0.12 | 1.23 | 0.18 | 2.37 | 0.18 | 1.55 | 0.33 | 2.68 | 0.22 | 2.11 |
| **2008** | 0.19 | 0.84 | 0.06 | 0.54 | 0.01 | 0.10 | 0.03 | 1.14 | 0.04 | 0.63 | 0.08 | 1.40 | 0.15 | 0.86 | 0.09 | 1.57 | 0.23 | 1.47 | 0.14 | 1.94 | 0.29 | 2.83 | 0.23 | 2.17 |
| **2009** | 0.19 | 1.24 | 0.07 | 0.61 | < 0.01 | 0.01 | 0.03 | 0.70 | 0.06 | 0.86 | 0.09 | 1.32 | 0.10 | 1.11 | 0.10 | 1.61 | 0.25 | 2.10 | 0.16 | 1.92 | 0.33 | 2.87 | 0.21 | 2.05 |
| **2010** | 0.18 | 1.88 | 0.14 | 0.64 | 0.07 | 0.58 | 0.02 | 0.81 | 0.21 | 0.89 | 0.07 | 1.41 | **0.34** | 2.05 | 0.15 | 1.80 | 0.39 | 2.77 | 0.21 | 2.05 | **0.52** | 3.18 | 0.23 | 2.22 |
| **2011** | 0.17 | 0.82 | 0.06 | 0.35 | < 0.01 | 0.01 | 0.00 | 0.67 | 0.02 | 0.15 | 0.03 | 1.06 | 0.04 | 0.50 | 0.06 | 1.19 | 0.19 | 0.97 | 0.09 | 1.41 | 0.22 | 1.72 | 0.16 | 1.69 |
| **2012** | 0.15 | 1.09 | 0.07 | 0.53 | < 0.01 | 0.05 | 0.01 | 1.15 | 0.03 | 0.65 | 0.08 | 1.42 | 0.10 | 1.22 | 0.11 | 1.67 | 0.18 | 1.74 | 0.15 | 1.95 | 0.32 | 2.75 | 0.23 | 2.60 |
| **2013** | 0.25 | **2.32** | **0.15** | **1.21** | 0.03 | 0.18 | 0.03 | 0.67 | 0.08 | 0.72 | 0.08 | 1.21 | 0.27 | **2.47** | **0.20** | **2.01** | 0.33 | 3.04 | 0.23 | 2.42 | 0.38 | 4.53 | 0.32 | 2.81 |
| **2014** | **0.26** | 1.57 | 0.11 | 1.01 | 0.01 | 0.13 | 0.01 | 0.60 | 0.08 | 1.26 | 0.10 | 1.12 | 0.27 | 1.81 | 0.14 | 1.94 | 0.34 | 2.83 | 0.20 | 2.13 | 0.41 | 4.37 | 0.30 | 2.55 |
| **2015** | 0.17 | 1.63 | 0.11 | 0.92 | 0.03 | 0.07 | 0.01 | 0.66 | 0.06 | 0.67 | 0.07 | 1.08 | 0.08 | 1.17 | 0.11 | 1.58 | 0.23 | 2.30 | 0.18 | 2.01 | 0.38 | 5.47 | 0.37 | 2.70 |
| **2016** | 0.12 | 0.98 | 0.07 | 0.72 | 0.09 | 0.85 | 0.06 | 0.86 | 0.15 | 1.22 | 0.10 | 1.21 | 0.20 | 1.76 | 0.13 | 1.50 | 0.27 | 2.20 | 0.16 | 1.92 | 0.31 | **6.15** | **0.39** | **2.87** |
| **2017** | 0.17 | 1.18 | 0.08 | 0.74 | 0.02 | 0.18 | 0.03 | 0.66 | 0.10 | 0.81 | 0.07 | 1.14 | 0.14 | 1.41 | 0.11 | 1.38 | 0.27 | 1.99 | 0.15 | 1.88 | 0.36 | 2.98 | 0.23 | 2.44 |
| **2018** | 0.24 | 1.36 | 0.10 | 0.58 | 0.01 | 0.07 | 0.01 | 0.56 | 0.05 | 0.97 | 0.08 | 1.23 | 0.11 | 1.41 | 0.11 | 1.43 | 0.29 | 2.33 | 0.17 | 1.81 | 0.33 | 4.15 | 0.29 | 2.36 |
| **2019** | 0.17 | 2.11 | 0.14 | 0.85 | 0.07 | 0.55 | 0.03 | 0.87 | 0.08 | 1.06 | 0.09 | 1.32 | 0.09 | 1.37 | 0.11 | 1.82 | 0.25 | 3.18 | 0.23 | 2.17 | 0.37 | 4.96 | 0.33 | 2.48 |

***Table 4.6.*** *Statistical descriptive measures of Nutrients ($NH_4^+$, $NO_3^-$, $PO_4^{-3}$, and $SiO_4^{-4}$) $mmol.m^{-3}$ by month for Station 1 (off Aljezur). *Bold values are higher values of each statistical measures*

| Month | $NH_4^+$ | $NO_3^-$ | $PO_4^{-3}$ | $SiO_4^{-4}$ | $NH_4^+$ | $NO_3^-$ | $PO_4^{-3}$ | $SiO_4^{-4}$ | $NH_4^+$ | $NO_3^-$ | $PO_4^{-3}$ | $SiO_4^{-4}$ | $NH_4^+$ | $NO_3^-$ | $PO_4^{-3}$ | $SiO_4^{-4}$ | $NH_4^+$ | $NO_3^-$ | $PO_4^{-3}$ | $SiO_4^{-4}$ | $NH_4^+$ | $NO_3^-$ | $PO_4^{-3}$ | $SiO_4^{-4}$ |
|---|---|---|---|---|---|---|---|---|---|---|---|---|---|---|---|---|---|---|---|---|---|---|---|---|
| | **IQR** | | | | **Min** | | | | **$Q_1$** | | | | **Median** | | | | **$Q_3$** | | | | **Max** | | | |
| **Jan** | 0.11 | 0.70 | 0.04 | 0.38 | 0.11 | 0.23 | 0.03 | 1.53 | 0.24 | 2.37 | 0.19 | 1.91 | **0.31** | 2.65 | 0.21 | 2.07 | **0.35** | 3.07 | 0.23 | 2.29 | 0.45 | 3.51 | 0.27 | 2.44 |
| **Feb** | 0.07 | **2.07** | **0.13** | 0.78 | 0.03 | 0.20 | 0.03 | 1.40 | 0.24 | 1.91 | 0.15 | 1.76 | 0.28 | **2.68** | **0.21** | **2.21** | 0.31 | **3.98** | **0.28** | **2.54** | 0.38 | 5.47 | 0.37 | 2.72 |
| **Mar** | 0.15 | 1.33 | 0.09 | 0.51 | 0.09 | 0.58 | 0.05 | 1.29 | 0.16 | 1.52 | 0.11 | 1.42 | 0.27 | 2.18 | 0.17 | 1.74 | 0.31 | 2.85 | 0.20 | 1.93 | 0.39 | **6.15** | **0.39** | **2.87** |
| **Apr** | 0.14 | 0.90 | 0.08 | 0.64 | < 0.01 | 0.07 | 0.01 | 0.95 | 0.11 | 0.69 | 0.06 | 1.18 | 0.15 | 1.33 | 0.11 | 1.41 | 0.25 | 1.60 | 0.14 | 1.83 | 0.41 | 2.91 | 0.21 | 2.40 |
| **May** | **0.17** | 1.13 | 0.06 | 0.54 | < 0.01 | 0.01 | 0.00 | 1.11 | 0.06 | 0.67 | 0.08 | 1.35 | 0.10 | 1.06 | 0.09 | 1.52 | 0.22 | 1.80 | 0.14 | 1.89 | 0.32 | 3.28 | 0.24 | 2.47 |
| **Jun** | 0.09 | 1.14 | 0.06 | 0.48 | < 0.001 | 0.01 | 0.03 | 0.77 | 0.02 | 0.35 | 0.06 | 1.02 | 0.08 | 0.92 | 0.09 | 1.37 | 0.11 | 1.49 | 0.12 | 1.50 | 0.47 | 2.85 | 0.22 | 2.22 |
| **Jul** | 0.07 | 0.98 | 0.05 | 0.60 | 0.01 | 0.18 | 0.03 | 0.67 | 0.04 | 0.90 | 0.08 | 1.21 | 0.07 | 1.14 | 0.10 | 1.42 | 0.11 | 1.89 | 0.13 | 1.81 | **0.52** | 3.18 | 0.23 | 2.25 |
| **Aug** | 0.06 | 0.82 | 0.05 | **0.83** | < 0.01 | 0.11 | 0.02 | 0.79 | 0.04 | 0.52 | 0.06 | 1.04 | 0.07 | 0.91 | 0.09 | 1.14 | 0.09 | 1.33 | 0.11 | 1.86 | 0.36 | 2.08 | 0.16 | 2.54 |
| **Sep** | 0.08 | 0.62 | 0.04 | 0.41 | < 0.01 | 0.07 | 0.01 | 0.56 | 0.01 | 0.15 | 0.03 | 0.77 | 0.04 | 0.38 | 0.05 | 0.98 | 0.09 | 0.77 | 0.07 | 1.19 | 0.18 | 1.79 | 0.14 | 1.60 |
| **Oct** | 0.05 | 0.19 | 0.02 | 0.33 | < 0.01 | 0.02 | 0.01 | 0.66 | 0.02 | 0.08 | 0.01 | 0.70 | 0.04 | 0.19 | 0.03 | 0.93 | 0.06 | 0.27 | 0.03 | 1.04 | 0.12 | 0.95 | 0.08 | 1.23 |
| **Nov** | 0.15 | 1.32 | 0.09 | 0.73 | < 0.01 | 0.02 | 0.01 | 0.98 | 0.10 | 0.56 | 0.05 | 1.14 | 0.17 | 1.04 | 0.09 | 1.60 | 0.25 | 1.87 | 0.14 | 1.87 | 0.44 | 4.12 | 0.28 | 2.81 |
| **Dec** | 0.11 | 0.82 | 0.06 | 0.45 | 0.13 | 0.61 | 0.06 | 1.31 | 0.22 | 1.66 | 0.14 | 1.60 | 0.29 | 2.17 | 0.16 | 1.85 | 0.33 | 2.48 | 0.20 | 2.05 | 0.39 | 4.96 | 0.33 | 2.25 |

## 4.2 Characterization of Station 2 (off Sagres)

### 4.2.1 Chlorophyll-a Concentration

Fig. 4.7(a-b) illustrates the temporal variability of Chl-*a* from 2012-2019 for Station 2 (off Sagres). With the time series plot (Fig. 4.7(a)), the seasonal amplitude and patterns showed a gradually decreasing trend between 2002-2006 and 2007-2012. It's also noted in Fig. 4.7(c), that the seasonal behaviour with a peak during the summer of the months and a lower concentration value in the wintertime.

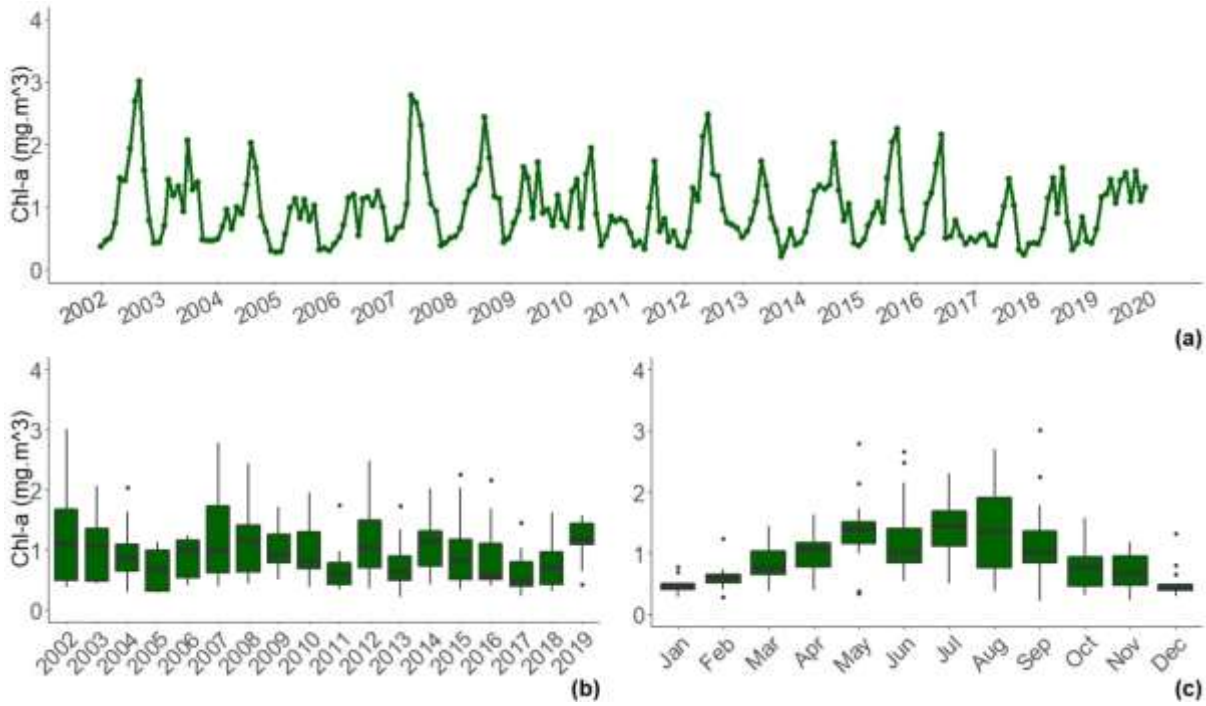


***Fig. 4.7.****Monthly chlorophyll-a concentration (Chl-a mg m$^{-3}$) concentration: (a) the time series plot; the boxplot (b) by year, and (c) by month for Station 2 (off Sagres).*

The Chl-*a* value were at a minimum in September 2013 and November 2017 and a maximum in September 2002 (Fig. 4.7(b-c) and Table 4.7). The highest median value was identified in 2007 and 2019 (Table 4.7). The highest dispersion of the data was discovered in 2002 (IQR=1.2 mg m$^{-3}$), with 50% of the data values falling between 0.5 and 1.7 mg m$^{-3}$. The year with the smallest dispersion was in 2019 (IQR=0.3 mg m$^{-3}$), with 25% of Chl-*a* values above 1.4 mg m$^{-3}$ and below 1.1 mg m$^{-3}$.

***Table 4.7.*** *Statistical descriptive measures of chlorophyll-a concentration (Chl-a mg $m^{-3}$) by year for Station 2 (off Sagres).*

| Year | IQR | Min | $Q_1$ | Median | $Q_3$ | Max |
|---|---|---|---|---|---|---|
| **2002** | 1.18 | 0.37 | 0.49 | 1.11 | 1.67 | 3.01 |
| **2003** | 0.88 | 0.44 | 0.47 | 1.06 | 1.35 | 2.06 |
| **2004** | 0.45 | 0.30 | 0.64 | 0.87 | 1.09 | 2.03 |
| **2005** | 0.68 | 0.28 | 0.31 | 0.67 | 0.99 | 1.13 |
| **2006** | 0.62 | 0.41 | 0.53 | 1.01 | 1.15 | 1.24 |
| **2007** | 1.11 | 0.39 | 0.62 | 0.99 | 1.72 | 2.79 |
| **2008** | 0.77 | 0.44 | 0.63 | 1.15 | 1.40 | 2.43 |
| **2009** | 0.47 | 0.50 | 0.79 | 0.93 | 1.25 | 1.72 |
| **2010** | 0.61 | 0.38 | 0.69 | 0.83 | 1.29 | 1.95 |
| **2011** | 0.35 | 0.33 | 0.43 | 0.60 | 0.78 | 1.73 |
| **2012** | 0.79 | 0.36 | 0.70 | 1.03 | 1.49 | 2.48 |
| **2013** | 0.40 | 0.21 | 0.49 | 0.63 | 0.89 | 1.73 |
| **2014** | 0.58 | 0.42 | 0.73 | 1.15 | 1.31 | 2.02 |
| **2015** | 0.66 | 0.33 | 0.51 | 0.83 | 1.17 | 2.25 |
| **2016** | 0.60 | 0.41 | 0.50 | 0.56 | 1.09 | 2.15 |
| **2017** | 0.40 | 0.23 | 0.39 | 0.49 | 0.80 | 1.45 |
| **2018** | 0.54 | 0.31 | 0.42 | 0.70 | 0.96 | 1.62 |
| **2019** | 0.34 | 0.42 | 1.08 | 1.18 | 1.43 | 1.57 |

The highest median value as shown in Fig. 4.7(c) and Table 4.8 found in three months, May, July, and August, with a value of 1.4 mg $m^{-3}$. In August, the dispersion presents the highest IQR value (1.1 mg $m^{-3}$), with 50% of the Chl-*a* values falling within the interval [0.8, 1.9]. The smallest dispersion was noted in wintertime (December to February) (IQR=0.1 mg $m^{-3}$), with half the values falling within [0.4 mg $m^{-3}$, 0.5 mg $m^{-3}$].

***Table 4.8.*** *Statistical descriptive measures of chlorophyll-a concentration (Chl-a mg $m^{-3}$)by month for Station 2 (off Sagres).*

| Month | IQR | Min | $Q_1$ | Median | $Q_3$ | Max |
|---|---|---|---|---|---|---|
| **Jan** | 0.09 | 0.28 | 0.41 | 0.44 | 0.50 | 0.77 |
| **Feb** | 0.14 | 0.29 | 0.52 | 0.59 | 0.66 | 1.24 |
| **Mar** | 0.38 | 0.38 | 0.65 | 0.76 | 1.03 | 1.44 |
| **Apr** | 0.39 | 0.40 | 0.78 | 1.08 | 1.17 | 1.63 |
| **May** | 0.36 | 0.33 | 1.15 | 1.39 | 1.51 | 2.79 |
| **Jun** | 0.56 | 0.54 | 0.84 | 1.02 | 1.40 | 2.66 |
| **Jul** | 0.57 | 0.50 | 1.12 | 1.44 | 1.69 | 2.30 |
| **Aug** | 1.14 | 0.38 | 0.76 | 1.37 | 1.90 | 2.69 |
| **Sep** | 0.53 | 0.21 | 0.84 | 1.02 | 1.37 | 3.01 |
| **Oct** | 0.47 | 0.31 | 0.46 | 0.77 | 0.94 | 1.58 |
| **Nov** | 0.48 | 0.23 | 0.48 | 0.68 | 0.95 | 1.18 |
| **Dec** | 0.10 | 0.30 | 0.39 | 0.43 | 0.49 | 1.32 |

The ACF was also applied to Sation-2 (Appendix A in Fig.A.1) and also revealed 12 months seasonality pattern for Chl-*a* time series data.

### 4.2.2 Sea Surface Temperature

Fig. 4.8(a-c) displays a monthly time series data of SST for Station 2 . As Fig. 4.8(a) shows, constant seasonal amplitude and patterns revealed over the time series data that is in line with the results from the ACF (See Fig.A.1. at Appendix A). Generally, the seasonal period of SST (Fig. 4.8(c)) can be characterised by higher values in summer and autumn and lower values in winter.

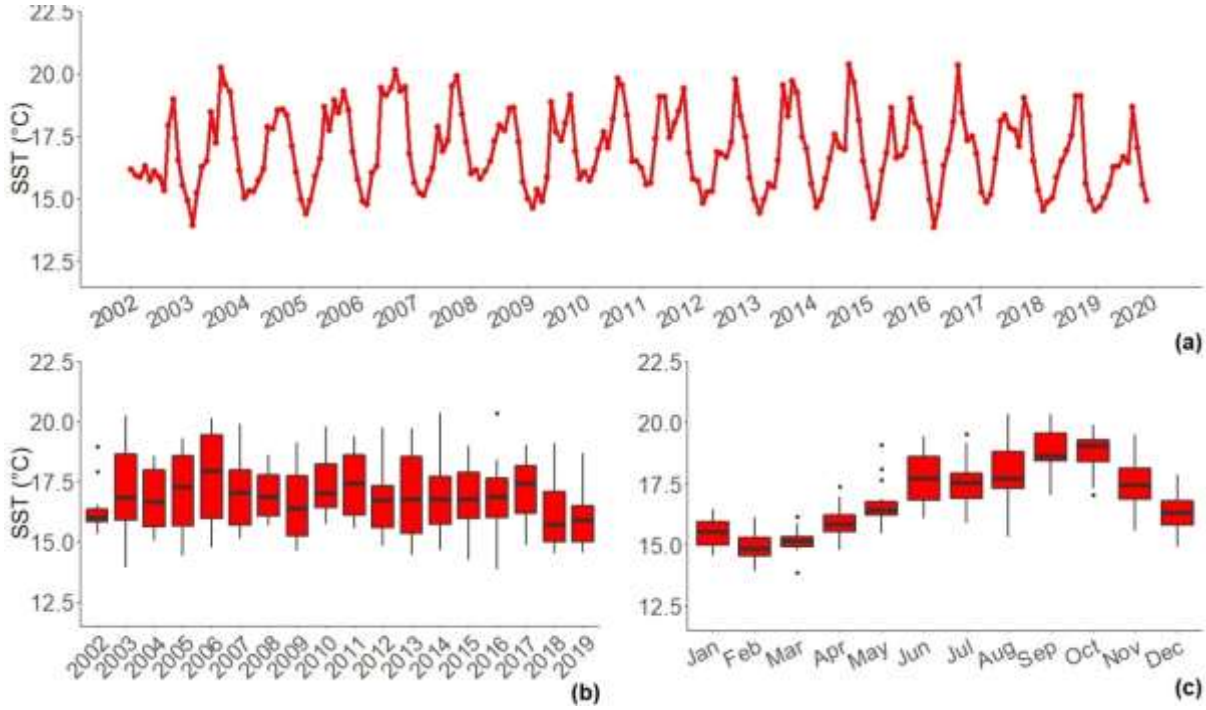


***Fig. 4.8.*** *Monthly time series of sea surface temperature (SST-ºC): (a) the time series plot; the boxplot (b) by year, and (c) by month for Station 2 (off Sagres).*

In Table 4.9. the minimum SST values were detected in March 2003 and February 2016 with values of 13.9 ºC. The maximum values of the SST are recorded in September 2014 (20.4 ºC). The highest median value of the dataset was found in the year 2006 (18.0 ºC), with the data values ranging between 14.8 and 19.4 ºC. Also, for this year the dispersion of the data was high (IQR=3.5 ºC), with 50% of the data found between 16.0 and 19.4 ºC. The year with the smallest dispersion was found in 2002 (IQR=0.5 ºC), the data values falling within [15.8 ºC, 16.3 ºC] interval.

***Table 4.9.*** *Statistical descriptive measures of sea surface temperature (SST-ºC) by year for Station 2 (off Sagres).*

| Year | IQR | Min | $Q_1$ | Median | $Q_3$ | Max |
|---|---|---|---|---|---|---|
| **2002** | 0.5 | 15.3 | 15.8 | 16.0 | 16.3 | 18.9 |
| **2003** | 2.7 | 13.9 | 15.9 | 16.9 | 18.6 | 20.2 |
| **2004** | 2.4 | 15.0 | 15.6 | 16.6 | 18.0 | 18.6 |
| **2005** | 2.9 | 14.4 | 15.6 | 17.3 | 18.6 | 19.3 |
| **2006** | 3.5 | 14.8 | 16.0 | 18.0 | 19.4 | 20.1 |
| **2007** | 2.3 | 15.1 | 15.7 | 17.1 | 18.0 | 19.9 |
| **2008** | 1.7 | 15.6 | 16.1 | 16.9 | 17.8 | 18.6 |
| **2009** | 2.5 | 14.6 | 15.3 | 16.4 | 17.7 | 19.1 |
| **2010** | 1.8 | 15.7 | 16.4 | 17.0 | 18.2 | 19.8 |
| **2011** | 2.5 | 15.6 | 16.1 | 17.4 | 18.6 | 19.4 |
| **2012** | 1.7 | 14.8 | 15.6 | 16.7 | 17.3 | 19.7 |
| **2013** | 3.2 | 14.4 | 15.3 | 16.7 | 18.5 | 19.7 |
| **2014** | 2.0 | 14.7 | 15.7 | 16.8 | 17.7 | 20.4 |
| **2015** | 1.9 | 14.2 | 16.0 | 16.8 | 17.9 | 19.0 |
| **2016** | 1.6 | 13.9 | 16.0 | 16.9 | 17.6 | 20.3 |
| **2017** | 2.0 | 14.9 | 16.2 | 17.4 | 18.2 | 19.0 |
| **2018** | 2.1 | 14.5 | 15.0 | 15.7 | 17.1 | 19.1 |
| **2019** | 1.5 | 14.5 | 15.0 | 15.9 | 16.5 | 18.7 |

Fig. 4.8(c) and Table 4.10 illustrate the monthly variability of SST for Station 2 . The highest median value was shown in October (19.1 ºC), with the data values ranging between 17.0 and 19.3 ºC. The highest dispersion was observed in June (IQR = 1.8 ºC), and 50% of these values fell within the interval [16.8, 18.6]. The smallest dispersion was observed in March (IQR=0.4 ºC), with 25% of values being above 14.9 ºC and below 15.3 ºC.

***Table 4.10.*** *Statistical descriptive measures of sea surface temperature (SST-ºC) by month for Station 2 (off Sagres).*

| Month | IQR | Min | $Q_1$ | Median | $Q_3$ | Max |
|---|---|---|---|---|---|---|
| **Jan** | 0.9 | 14.5 | 15.0 | 15.5 | 15.9 | 16.5 |
| **Feb** | 0.7 | 13.9 | 14.5 | 14.8 | 15.3 | 16.1 |
| **Mar** | 0.4 | 13.9 | 14.9 | 15.1 | 15.3 | 16.1 |
| **Apr** | 0.7 | 14.8 | 15.5 | 15.8 | 16.2 | 17.4 |
| **May** | 0.6 | 15.5 | 16.2 | 16.4 | 16.8 | 19.1 |
| **Jun** | 1.8 | 16.1 | 16.8 | 17.7 | 18.6 | 19.4 |
| **Jul** | 1.0 | 15.9 | 16.9 | 17.5 | 17.9 | 19.5 |
| **Aug** | 1.5 | 15.3 | 17.3 | 17.7 | 18.8 | 20.3 |
| **Sep** | 1.1 | 17.0 | 18.4 | 18.6 | 19.6 | 20.4 |
| **Oct** | 0.9 | 17.0 | 18.4 | 19.1 | 19.3 | 19.9 |
| **Nov** | 1.3 | 15.5 | 16.8 | 17.4 | 18.1 | 19.5 |
| **Dec** | 1.0 | 14.9 | 15.8 | 16.3 | 16.8 | 17.8 |

### 4.2.3 Nutrients

Nutrients ($NH_4^+$, $NO_3^-$, $PO_4^{-3}$, and $SiO_4^{-4}$) monthly time series data for 19 years has been explored in Fig. 4.9(a–c). The time series plot (Fig. 4.9(a)) depicted a seasonal amplitude pattern for three nutrients ($NH_4^+$, $PO_4^{-3}$, and $SiO_4^{-4}$) over time; however, for $NO_3^-$ the seasonal pattern showed a trend increase between 2004-2016.

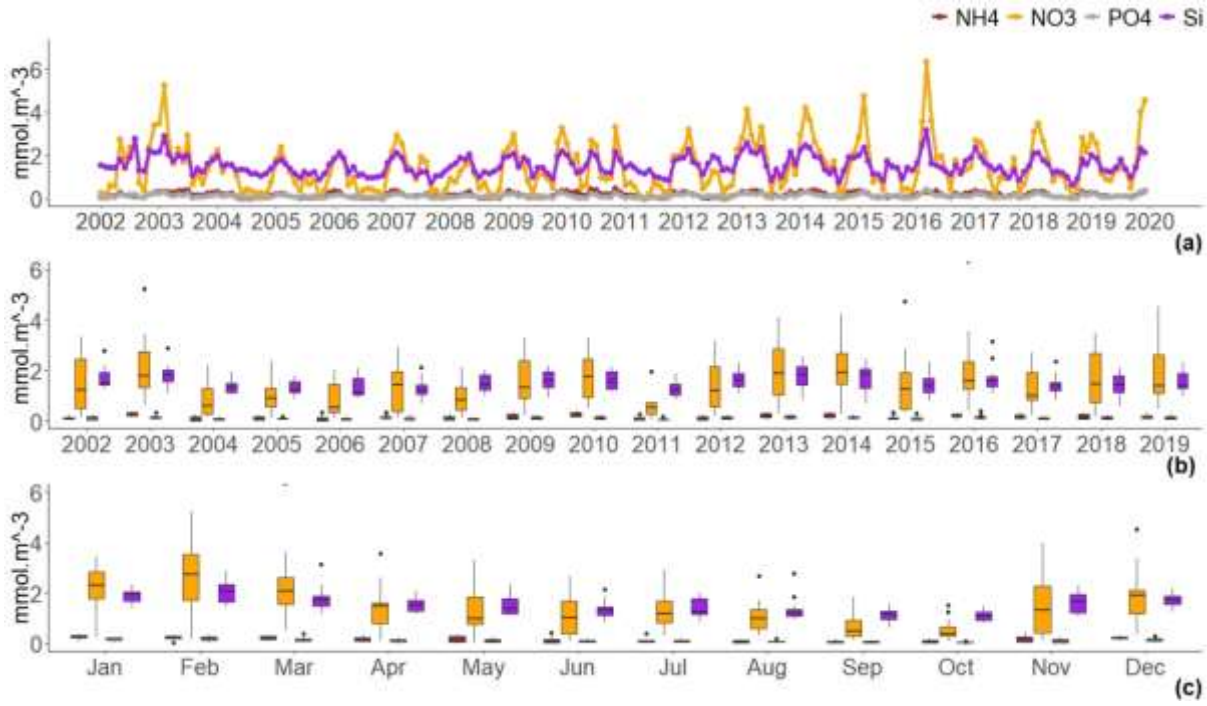


***Fig. 4.9.*** *Monthly time series of nutrients ($NH_4^+$, $NO_3^-$, $PO_4^{-3}$, and $SiO_4^{-4}$): (a) the time series plot; the boxplot (b) by year, and (c) by month for Station 2 (off Sagres).*

The three nutrients $NO_3^-$, $PO_4^{-3}$ and $SiO_4^{-4}$ (Fig. 4.9(a–c); Table (4.11 and 4.12)) revealed maximum values in March 2016, with 6.3, 0.41, and 3.13 mmol.m$^{-3}$ of concentration values, respectively. $NH_4^+$ exhibited the maximum concentration value in November 2010 with 0.45 mmol.m$^{-3}$. The minimum concentration values for $NH_4^+$ discovered in June 2011 (0.01 mmol.m$^{-3}$) and for $NO_3^-$ found in May 2011 (0.04 mmol.m$^{-3}$). For both $SiO_4^{-4}$ and $PO_4^{-3}$ the minimum values discovered in September 2018 at 0.01 and 0.62 mmol.m$^{-3}$, respectively.

The highest median was found in 2014 for two nutrients $NO_3^-$ and $SiO_4^{-4}$ with values of 1.91 mmol.m$^{-3}$, respectively. For $NH4^+$ and $PO_4^{-3}$ the highest median value found in 2003 (0.3 mmol.m$^{-3}$) and (0.2 mmol.m$^{-3}$), respectively (Fig. 4.9 (b)).

The highest IQR value for $NO_3^-$ and $PO_4^{-3}$ was identified in 2002 with 1.95 and 0.14 mmol.m$^{-3}$, respectively (Table 4.11). Also, both showed the lowest IQR value in 2011 with 0.48 and 0.03 mmol.m$^{-3}$, respectively. The higher dispersion for $NO_3^-$ showed half of the data

between 0.51 and 2.5 mmol.m$^{-3}$, while the smallest dispersion falls within [0.3 mmol.m$^{-3}$, 0.74 mmol.m$^{-3}$]. $PO_4^{-3}$ showed 50% of the data value for higher dispersion between 0.05 and 0.18 mmol.m$^{-3}$ and for smallest dispersion between 0.03 mmol.m$^{-3}$ and 0.07 mmol.m$^{-3}$.

The highest IQR for $NH_4^+$ was found in 2018 (0.22 mmol.m$^{-3}$) and lowest in 2015 (0.07 mmol.m$^{-3}$). Half of the $NH_4^+$ data for higher dispersion was found between 0.07 and 0.28 mmol.m$^{-3}$ and for smallest dispersion falls within [0.08, 0.15]. The highest IQR for $SiO_4^{-4}$ was found in 2014(0.73 mmol.m$^{-3}$) and the lowest in 2017 (0.33 mmol.m$^{-3}$). Half of the data for higher dispersion was found between 1.31 and 2.04 mmol.m$^{-3}$ and for smallest dispersion falls within [1.22, 1.54 mmol.m$^{-3}$].

Fig. 4.9 (b) and Table 4.12 illustrate nutrients monthly variability. The highest median value for three targeted nutrients $NO_3^-$ , $PO_4^{-3}$ and $SiO_4^{-4}$ were found in February. The highest median value for $NH_4^+$ was found in January with 0.31 mmol.m$^{-3}$. In November, the dispersion presents the highest IQR value for $NO_3^-$ , $PO_4^{-3}$ and $SiO_4^{-4}$. For the highest dispersion, 25% of $NO_3^-$ data values were found to be above 0.4 and below 2.3 mmol.m$^{-3}$. For this month half of the $PO_4^{-3}$ data values were found between 0.04 and 0.2 mmol.m$^{-3}$ and for $SiO_4^{-4}$ within [1.23, 1.93]. In October, the dispersion presents the lowest IQR value for $NO_3^-$ and $PO_4^{-3}$ with 0.37 and 0.0.02 mmol.m$^{-3}$, respectively. Half of the data for this dispersion was found between 0.3 and 0.67 mmol.m$^{-3}$ for $NO_3^-$ and for $PO_4^{-3}$ falls within [0.03, 0.1]. August indicated the lowest IQR value for $SiO_4^{-4}$ (0.27 mmol.m$^{-3}$) with half the values falling within [1.1, 1.4]. $NH_4^+$ showed the highest IQR value in May (0.23 mmol.m$^{-3}$) with 50% values falls within [1.91, 3.98] and lowest value in July (0.1 mmol.m$^{-3}$) with 25% of data values above 0.06 and below 0.11 mmol.m$^{-3}$.

The ACF for all nutrients applied Appendix A in Fig. A.2. (a-d) showed a length of 12 months seasonality pattern in the nutrients data and a significant autocorrelation at multiples of lag 12, 24, and so on.

***Table 4.11.*** *Statistical descriptive measures of Nutrients ($NH_4^+$, $NO_3^-$, $PO_4^{-3}$, and $SiO_4^{-4}$) mmol.$m^{-3}$ by year for Station 2 (off Sagres). *Bold values are higher values of each statistical measures*

| Year | $NH_4^+$ | $NO_3^-$ | $PO_4^{-3}$ | $SiO_4^-$ | $NH_4^+$ | $NO_3^-$ | $PO_4^{-3}$ | $SiO_4^-$ | $NH_4^+$ | $NO_3^-$ | $PO_4^{-3}$ | $SiO_4^-$ | $NH_4^+$ | $NO_3^-$ | $PO_4^{-3}$ | $SiO_4^-$ | $NH_4^+$ | $NO_3^-$ | $PO_4^{-3}$ | $SiO_4^-$ | $NH_4^+$ | $NO_3^-$ | $PO_4^{-3}$ | $SiO_4^-$ |
|---|---|---|---|---|---|---|---|---|---|---|---|---|---|---|---|---|---|---|---|---|---|---|---|---|
| | **IQR** | | | | **Min** | | | | **$Q_1$** | | | | **Median** | | | | **$Q_3$** | | | | **Max** | | | |
| **2002** | 0.08 | **1.95** | **0.14** | 0.52 | 0.02 | 0.19 | 0.03 | 1.26 | 0.06 | 0.51 | 0.05 | 1.42 | 0.1 | 1.23 | 0.1 | 1.49 | 0.14 | 2.47 | 0.18 | 1.94 | 0.25 | 3.36 | 0.24 | 2.78 |
| **2003** | 0.12 | 1.44 | 0.09 | 0.45 | 0.12 | 0.64 | 0.04 | 1.09 | 0.21 | 1.32 | 0.11 | 1.56 | **0.29** | 1.78 | 0.14 | 1.82 | 0.33 | 2.76 | 0.19 | 2.02 | 0.39 | 5.23 | 0.35 | 2.88 |
| **2004** | 0.16 | 1.04 | 0.07 | 0.35 | 0 | 0.19 | 0.03 | 1.02 | 0.02 | 0.27 | 0.04 | 1.14 | 0.06 | 0.59 | 0.07 | 1.32 | 0.18 | 1.31 | 0.11 | 1.5 | 0.29 | 2.21 | 0.17 | 1.97 |
| **2005** | 0.13 | 0.73 | 0.04 | 0.44 | 0.01 | 0.11 | 0.03 | 0.86 | 0.05 | 0.58 | 0.07 | 1.13 | 0.07 | 0.9 | 0.09 | 1.23 | 0.18 | 1.31 | 0.11 | 1.57 | 0.25 | 2.4 | 0.18 | 1.78 |
| **2006** | 0.13 | 1.11 | 0.08 | 0.64 | 0.01 | 0.11 | 0.02 | 0.94 | 0.02 | 0.35 | 0.05 | 1.04 | 0.04 | 0.53 | 0.06 | 1.13 | 0.15 | 1.45 | 0.13 | 1.68 | 0.35 | 2.01 | 0.17 | 2.09 |
| **2007** | 0.08 | 1.58 | 0.11 | 0.38 | 0.03 | 0.14 | 0.02 | 0.7 | 0.1 | 0.38 | 0.04 | 1.05 | 0.11 | 1.42 | 0.11 | 1.24 | 0.18 | 1.97 | 0.15 | 1.44 | 0.33 | 2.9 | 0.23 | 2.12 |
| **2008** | 0.13 | 0.88 | 0.07 | 0.58 | 0.01 | 0.14 | 0.04 | 1 | 0.04 | 0.45 | 0.05 | 1.24 | 0.12 | 0.85 | 0.08 | 1.45 | 0.17 | 1.33 | 0.12 | 1.83 | 0.3 | 2.11 | 0.17 | 2.04 |
| **2009** | 0.19 | 1.51 | 0.1 | 0.61 | 0.01 | 0.21 | 0.04 | 0.92 | 0.07 | 0.9 | 0.09 | 1.34 | 0.12 | 1.32 | 0.1 | 1.59 | 0.26 | 2.4 | 0.19 | 1.95 | 0.33 | 3.27 | 0.24 | 2.18 |
| **2010** | 0.16 | 1.52 | 0.12 | 0.7 | 0.15 | 0.5 | 0.01 | 1.16 | 0.18 | 0.94 | 0.06 | 1.26 | 0.25 | 1.77 | 0.09 | 1.56 | 0.34 | 2.46 | 0.18 | 1.96 | **0.45** | 3.31 | 0.26 | 2.15 |
| **2011** | 0.09 | 0.48 | 0.04 | 0.44 | < 0.01 | 0.04 | 0.01 | 0.84 | 0.03 | 0.26 | 0.03 | 1.02 | 0.05 | 0.54 | 0.05 | 1.25 | 0.13 | 0.74 | 0.07 | 1.46 | 0.29 | 1.96 | 0.18 | 1.84 |
| **2012** | 0.13 | 1.57 | 0.1 | 0.53 | < 0.01 | 0.2 | 0.04 | 1.11 | 0.04 | 0.58 | 0.06 | 1.36 | 0.09 | 1.21 | 0.11 | 1.64 | 0.17 | 2.14 | 0.17 | 1.89 | 0.28 | 3.17 | 0.24 | 2.28 |
| **2013** | 0.17 | 1.8 | 0.13 | **0.73** | 0.06 | 0.31 | 0.04 | 0.86 | 0.13 | 1.04 | 0.09 | 1.44 | 0.22 | 1.9 | **0.15** | 1.82 | 0.3 | 2.84 | 0.22 | 2.17 | 0.33 | 4.11 | 0.29 | 2.56 |
| **2014** | 0.18 | 1.21 | 0.08 | **0.73** | 0.03 | 0.29 | 0.03 | 0.72 | 0.14 | 1.47 | 0.11 | 1.31 | 0.27 | **1.91** | 0.14 | **1.87** | 0.32 | 2.68 | 0.19 | 2.04 | 0.37 | 4.2 | 0.29 | 2.44 |
| **2015** | 0.07 | 1.48 | 0.11 | 0.55 | 0.05 | 0.35 | 0.03 | 0.82 | 0.08 | 0.46 | 0.05 | 1.15 | 0.09 | 1.25 | 0.11 | 1.41 | 0.15 | 1.94 | 0.16 | 1.7 | 0.35 | 4.74 | 0.32 | 2.35 |
| **2016** | 0.09 | 1.1 | 0.06 | 0.4 | 0.05 | 0.41 | 0.03 | 1.1 | 0.17 | 1.26 | 0.11 | 1.36 | 0.22 | 1.6 | 0.13 | 1.58 | 0.26 | 2.36 | 0.16 | 1.77 | 0.33 | **6.33** | **0.41** | **3.13** |
| **2017** | 0.14 | 1.09 | 0.08 | 0.33 | 0.04 | 0.23 | 0.02 | 0.83 | 0.1 | 0.83 | 0.07 | 1.22 | 0.17 | 1.01 | 0.08 | 1.38 | 0.24 | 1.92 | 0.14 | 1.54 | 0.33 | 2.71 | 0.21 | 2.34 |
| **2018** | **0.22** | 1.94 | 0.13 | 0.63 | 0.03 | 0.16 | 0.01 | 0.62 | 0.07 | 0.74 | 0.06 | 1.15 | 0.13 | 1.45 | 0.11 | 1.42 | 0.28 | 2.68 | 0.19 | 1.78 | 0.3 | 3.47 | 0.25 | 2.12 |
| **2019** | 0.13 | 1.54 | 0.11 | 0.57 | 0.05 | 0.47 | 0.03 | 0.98 | 0.1 | 1.08 | 0.08 | 1.32 | 0.11 | 1.39 | 0.11 | 1.41 | 0.22 | 2.62 | 0.19 | 1.88 | 0.33 | 4.54 | 0.3 | 2.31 |

***Table 4.12.*** *Statistical descriptive measures of Nutrients ($NH_4^+$, $NO_3^-$, $PO_4^{-3}$, and $SiO_4^{-4}$) mmol.$m^{-3}$ by month for Station 2 (off Sagres).*

| Month | $NH_4^+$ | $NO_3^-$ | $PO_4^{-3}$ | $SiO_4^{-4}$ | $NH_4^+$ | $NO_3^-$ | $PO_4^{-3}$ | $SiO_4^{-4}$ | $NH_4^+$ | $NO_3^-$ | $PO_4^{-3}$ | $SiO_4^{-4}$ | $NH_4^+$ | $NO_3^-$ | $PO_4^{-3}$ | $SiO_4^{-4}$ | $NH_4^+$ | $NO_3^-$ | $PO_4^{-3}$ | $SiO_4^{-4}$ | $NH_4^+$ | $NO_3^-$ | $PO_4^{-3}$ | $SiO_4^{-4}$ |
|---|---|---|---|---|---|---|---|---|---|---|---|---|---|---|---|---|---|---|---|---|---|---|---|---|
| | IQR | | | | Min | | | | $Q_1$ | | | | Median | | | | $Q_3$ | | | | Max | | | |
| **Jan** | 0.11 | 1.04 | 0.07 | 0.35 | 0.06 | 0.27 | 0.04 | 1.42 | 0.22 | 1.80 | 0.14 | 1.69 | **0.30** | 2.29 | 0.19 | 1.96 | 0.32 | 2.83 | 0.21 | 2.04 | 0.35 | 3.44 | 0.24 | 2.34 |
| **Feb** | 0.07 | 1.82 | **0.13** | 0.69 | 0.02 | 0.19 | 0.03 | 1.44 | 0.21 | 1.71 | 0.13 | 1.64 | 0.26 | **2.74** | **0.20** | **2.08** | 0.28 | 3.53 | 0.25 | 2.33 | 0.33 | 5.23 | 0.35 | 2.88 |
| **Mar** | 0.15 | 1.07 | 0.07 | 0.41 | 0.09 | 0.52 | 0.03 | 1.20 | 0.16 | 1.55 | 0.11 | 1.49 | 0.20 | 2.07 | 0.16 | 1.71 | 0.30 | 2.62 | 0.19 | 1.89 | 0.34 | **6.33** | **0.41** | **3.13** |
| **Apr** | 0.12 | 0.84 | 0.07 | 0.43 | 0.02 | 0.13 | 0.01 | 1.15 | 0.11 | 0.77 | 0.07 | 1.28 | 0.16 | 1.50 | 0.12 | 1.50 | 0.23 | 1.61 | 0.14 | 1.71 | 0.37 | 3.56 | 0.23 | 2.07 |
| **May** | **0.23** | 1.10 | 0.08 | 0.59 | < 0.01 | 0.04 | 0.01 | 1.11 | 0.05 | 0.74 | 0.07 | 1.20 | 0.08 | 0.98 | 0.10 | 1.38 | 0.28 | 1.84 | 0.15 | 1.79 | 0.35 | 3.29 | 0.25 | 2.33 |
| **Jun** | 0.12 | 1.31 | 0.08 | 0.34 | < 0.01 | 0.11 | 0.03 | 0.82 | 0.04 | 0.38 | 0.05 | 1.11 | 0.09 | 1.02 | 0.09 | 1.33 | 0.16 | 1.69 | 0.12 | 1.45 | 0.41 | 2.69 | 0.21 | 2.15 |
| **Jul** | 0.05 | 0.88 | 0.06 | 0.62 | 0.02 | 0.31 | 0.04 | 0.86 | 0.06 | 0.81 | 0.07 | 1.15 | 0.08 | 1.18 | 0.10 | 1.24 | 0.11 | 1.69 | 0.13 | 1.77 | 0.39 | 2.93 | 0.22 | 2.00 |
| **Aug** | 0.08 | 0.78 | 0.05 | 0.27 | 0.01 | 0.33 | 0.03 | 0.95 | 0.04 | 0.58 | 0.06 | 1.09 | 0.08 | 0.98 | 0.08 | 1.22 | 0.12 | 1.36 | 0.11 | 1.35 | 0.17 | 2.69 | 0.20 | 2.78 |
| **Sep** | 0.09 | 0.63 | 0.05 | 0.35 | < 0.01 | 0.16 | 0.01 | 0.62 | 0.03 | 0.29 | 0.04 | 0.95 | 0.06 | 0.48 | 0.05 | 1.14 | 0.11 | 0.92 | 0.08 | 1.30 | 0.20 | 1.85 | 0.14 | 1.54 |
| **Oct** | 0.09 | 0.37 | 0.02 | 0.34 | 0.01 | 0.11 | 0.02 | 0.83 | 0.03 | 0.28 | 0.03 | 0.92 | 0.07 | 0.41 | 0.04 | 1.09 | 0.12 | 0.65 | 0.05 | 1.26 | 0.18 | 1.53 | 0.11 | 1.48 |
| **Nov** | 0.20 | **1.86** | 0.13 | **0.70** | 0.01 | 0.13 | 0.02 | 1.06 | 0.07 | 0.42 | 0.04 | 1.23 | 0.19 | 1.32 | 0.11 | 1.66 | 0.27 | 2.29 | 0.17 | 1.93 | **0.45** | 4.01 | 0.28 | 2.31 |
| **Dec** | 0.08 | 0.94 | 0.07 | 0.33 | 0.09 | 0.35 | 0.04 | 1.25 | 0.18 | 1.18 | 0.10 | 1.55 | 0.23 | 1.92 | 0.15 | 1.76 | 0.26 | 2.12 | 0.18 | 1.89 | 0.33 | 4.54 | 0.30 | 2.18 |

## 4.3 Characterization of Station 3 (off Portimão)

### 4.3.1 Chlorophyll-a Concentration

For the Station 3 the seasonal pattern is not so evident as seen in other stations, Chl-*a* tends to decrease between 2002-2005 (Fig. 4.10(a)). In general, the seasonal period of Chl-*a* can be characterised by an increase from January until July, with higher values in summer, and then decreased until January, the wintertime Fig. 4.10(c).

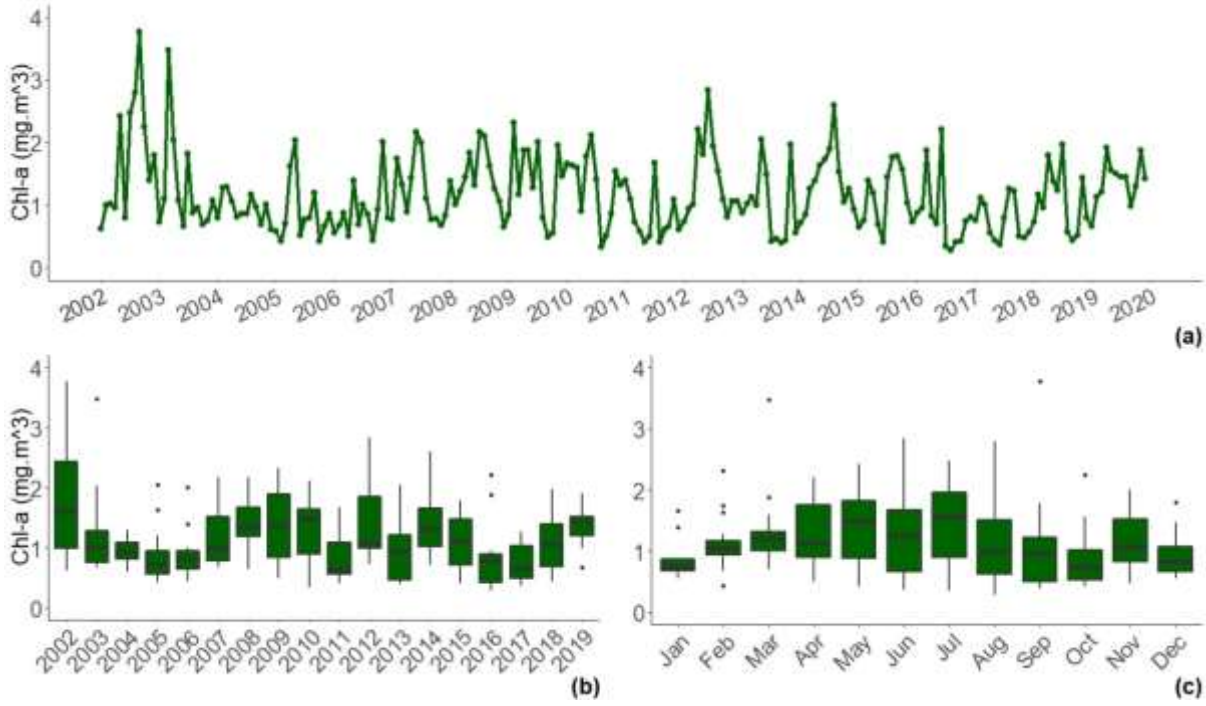


***Fig. 4.10.*** *Monthly chlorophyll-a concentration (Chl-a mg $m^{-3}$): (a) the time series plot; the boxplot (b) by year, and (c) by month for Station 3(off Portimão).*

The annual variability of Chl-*a* shown in Fig.4.10(b) and Table 4.13 revealed the maximum values in August 2002 (3.8 mg $m^{-3}$) and the minimum values in July 2010 and August 2016 with 0.3 mg $m^{-3}$, respectively. Table 4.13 indicated the highest median value in 2002 (1.6 mg $m^{-3}$). The highest IQR for Chl-*a* was found in 2002 (0.77 mg $m^{-3}$), with 25% of data values above 2.4 mg $m^{-3}$ and below 1.0 mg $m^{-3}$. The year with the smallest dispersion is 2004 and 2006 (IQR=0.3 mg $m^{-3}$), with 50% of the data values falling within [0.8, 1.1 mg $m^{-3}$] and [0.6, 0.9 mg $m^{-3}$], respectively.

***Table 4.13.*** *Statistical descriptive measures of chlorophyll-a concentration (Chl-a mg $m^{-3}$) by year for Station 3(off Portimão).*

| Year | IQR | Min | $Q_1$ | Median | $Q_3$ | Max |
|---|---|---|---|---|---|---|
| **2002** | 1.46 | 0.62 | 0.98 | 1.60 | 2.44 | 3.77 |
| **2003** | 0.54 | 0.67 | 0.75 | 1.02 | 1.29 | 3.47 |
| **2004** | 0.28 | 0.60 | 0.81 | 0.92 | 1.09 | 1.29 |
| **2005** | 0.38 | 0.43 | 0.57 | 0.73 | 0.95 | 2.04 |
| **2006** | 0.30 | 0.43 | 0.65 | 0.82 | 0.95 | 2.00 |
| **2007** | 0.73 | 0.67 | 0.78 | 1.00 | 1.51 | 2.17 |
| **2008** | 0.49 | 0.64 | 1.19 | 1.35 | 1.67 | 2.17 |
| **2009** | 1.06 | 0.49 | 0.84 | 1.37 | 1.89 | 2.32 |
| **2010** | 0.75 | 0.33 | 0.89 | 1.47 | 1.64 | 2.12 |
| **2011** | 0.53 | 0.40 | 0.56 | 0.63 | 1.09 | 1.67 |
| **2012** | 0.85 | 0.73 | 0.99 | 1.08 | 1.85 | 2.84 |
| **2013** | 0.76 | 0.40 | 0.46 | 0.94 | 1.21 | 2.05 |
| **2014** | 0.64 | 0.71 | 1.02 | 1.32 | 1.66 | 2.59 |
| **2015** | 0.76 | 0.41 | 0.71 | 1.12 | 1.48 | 1.78 |
| **2016** | 0.47 | 0.28 | 0.42 | 0.78 | 0.89 | 2.21 |
| **2017** | 0.54 | 0.37 | 0.49 | 0.66 | 1.03 | 1.26 |
| **2018** | 0.71 | 0.43 | 0.69 | 1.07 | 1.40 | 1.97 |
| **2019** | 0.32 | 0.67 | 1.19 | 1.43 | 1.52 | 1.91 |

Fig. 4.10(c) and Table 4.14 indicates that July is the month with the highest median value and the highest IQR for Chl-*a*, and the lowest IQR value of 0.2 mg m-3 was found in the months of January and February. For the highest dispersion, 50% of Chl-*a* values fell within the interval [0.9, 2.0 mg $m^{-3}$]. For the smallest dispersion, half of the Chl-*a* data values in January fell within [0.7, 0.9 mg $m^{-3}$] and in February found between 0.9 and 1.2 mg $m^{-3}$.

***Table 4.14.*** *Statistical descriptive measures of chlorophyll-a concentration (Chl-a mg $m^{-3}$) by month for Station 3(off Portimão).*

| Month | IQR | Min | $Q_1$ | Median | $Q_3$ | Max |
|---|---|---|---|---|---|---|
| **Jan** | 0.19 | 0.55 | 0.68 | 0.74 | 0.87 | 1.66 |
| **Feb** | 0.22 | 0.43 | 0.94 | 1.05 | 1.16 | 2.32 |
| **Mar** | 0.32 | 0.70 | 1.01 | 1.19 | 1.32 | 3.47 |
| **Apr** | 0.86 | 0.50 | 0.89 | 1.13 | 1.75 | 2.21 |
| **May** | 0.95 | 0.41 | 0.88 | 1.50 | 1.83 | 2.43 |
| **Jun** | 1.00 | 0.37 | 0.67 | 1.26 | 1.68 | 2.84 |
| **Jul** | 1.06 | 0.34 | 0.90 | 1.56 | 1.97 | 2.47 |
| **Aug** | 0.89 | 0.28 | 0.63 | 0.99 | 1.52 | 2.79 |
| **Sep** | 0.72 | 0.40 | 0.50 | 0.96 | 1.22 | 3.77 |
| **Oct** | 0.50 | 0.43 | 0.52 | 0.73 | 1.02 | 2.25 |
| **Nov** | 0.69 | 0.47 | 0.82 | 1.08 | 1.52 | 2.00 |
| **Dec** | 0.41 | 0.56 | 0.66 | 0.82 | 1.07 | 1.79 |

Appendix A in Fig. A.1., the ACF plot for Chl-*a* time series data shows positive and significant values for small lags, which might indicate a trend.

### 4.3.2 Sea Surface Temperature

A constant seasonal amplitude and patterns are revealed over the time series in Fig. 4.11(a). The seasonal pattern presented in Fig.4.11(c) shows that the SST are at a minimum in March, steadily increasing until August and then begins declining until March.

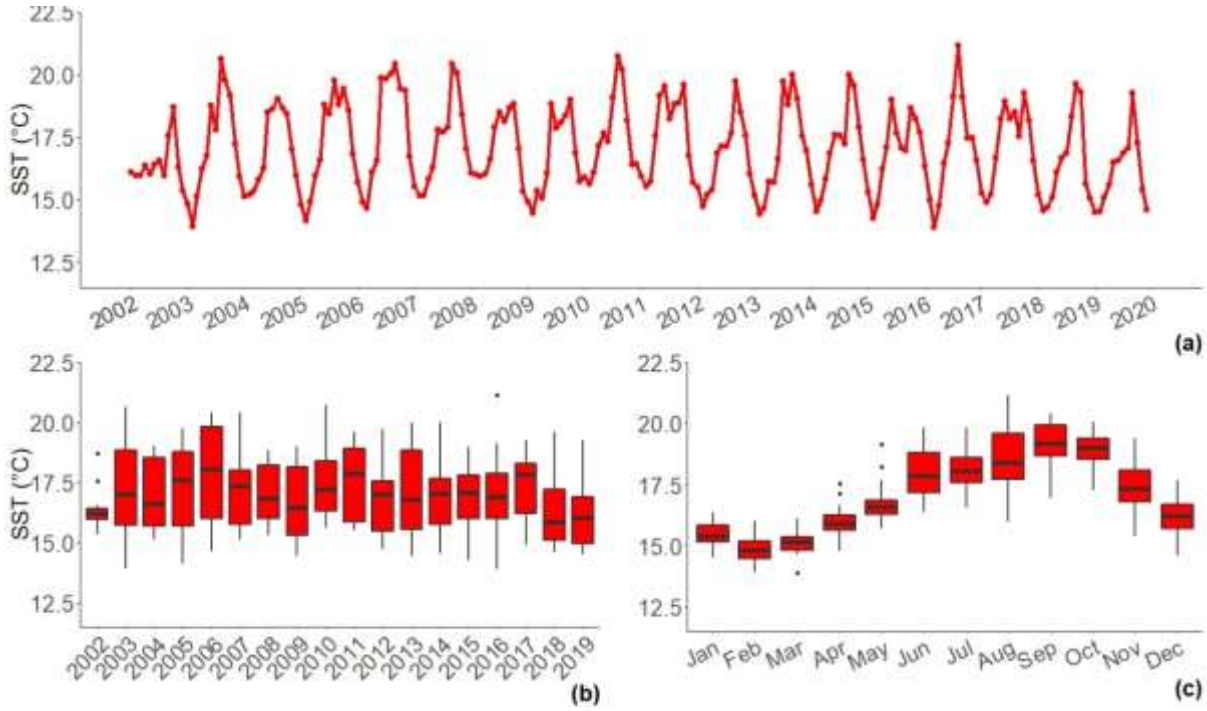


***Fig. 4.11.*** *Monthly time series of sea surface temperature (SST-ºC): (a) the time series plot; the boxplot (b) by year, and (c) by month for Station 3 (off Portimão).*

The annual variability of SST presented in Fig. 4.11 (b) and Table 4.15 displays the minimum and the maximum values of the SST in March 2003 (13.9 ºC) and in August 2016 (21.1 ºC), respectively. The highest median value of the dataset was found in the year 2006 (18.0 ºC). The dispersion of the data was high in 2006 (IQR =3.8 ºC) and low in 2002 (IQR=0.5 ºC). 50% of SST data value for higher dispersion was found between [16 ºC,19.8 ºC] and smallest dispersion fell between 16 and 16.4 ºC.

The monthly variability of SST (Fig. 4.11 (c) and Table 4.16), displays the highest median value in September (19.2 ºC). The highest dispersion was observed in August, with an IQR = 1.9 ºC and 50% of the SST values falling within the interval [17.7, 19.6]. Alternatively, the

smallest dispersion was noted in March (IQR=0.5 ºC), with 25% of values above 15.4 ºC and below 14.8 ºC.

***Table 4.15.*** *Statistical descriptive measures of sea surface temperature (SST-ºC) by year for Station 3 (off Portimão).*

| Year | IQR | Min | $Q_1$ | Median | $Q_3$ | Max |
|---|---|---|---|---|---|---|
| **2002** | 0.5 | 15.4 | 16.0 | 16.2 | 16.4 | 18.7 |
| **2003** | 3.1 | 13.9 | 15.7 | 17.0 | 18.9 | 20.6 |
| **2004** | 2.8 | 15.1 | 15.7 | 16.6 | 18.5 | 19.0 |
| **2005** | 3.1 | 14.1 | 15.7 | 17.6 | 18.8 | 19.8 |
| **2006** | 3.8 | 14.7 | 16.0 | 18.0 | 19.8 | 20.4 |
| **2007** | 2.3 | 15.1 | 15.8 | 17.4 | 18.0 | 20.4 |
| **2008** | 2.2 | 15.3 | 16.0 | 16.8 | 18.2 | 18.8 |
| **2009** | 2.9 | 14.4 | 15.3 | 16.5 | 18.2 | 19.0 |
| **2010** | 2.1 | 15.6 | 16.3 | 17.2 | 18.4 | 20.7 |
| **2011** | 3.1 | 15.5 | 15.9 | 17.9 | 18.9 | 19.6 |
| **2012** | 2.1 | 14.7 | 15.5 | 17.0 | 17.6 | 19.7 |
| **2013** | 3.3 | 14.4 | 15.6 | 16.8 | 18.9 | 20.0 |
| **2014** | 1.9 | 14.5 | 15.8 | 17.0 | 17.7 | 20.0 |
| **2015** | 1.8 | 14.3 | 16.0 | 17.1 | 17.8 | 19.0 |
| **2016** | 1.9 | 13.9 | 16.0 | 16.9 | 17.9 | 21.1 |
| **2017** | 2.1 | 14.9 | 16.2 | 17.8 | 18.3 | 19.3 |
| **2018** | 2.1 | 14.6 | 15.1 | 15.9 | 17.2 | 19.6 |
| **2019** | 2.0 | 14.5 | 15.0 | 16.0 | 16.9 | 19.3 |

***Table 4.16.*** *Statistical descriptive measures of sea surface temperature (SST-ºC) by month for Station 3 (off Portimão).*

| Month | IQR | Min | $Q_1$ | Median | $Q_3$ | Max |
|---|---|---|---|---|---|---|
| **Jan** | 0.7 | 14.5 | 15.1 | 15.4 | 15.8 | 16.3 |
| **Feb** | 0.7 | 13.9 | 14.5 | 14.8 | 15.2 | 16.0 |
| **Mar** | 0.5 | 13.9 | 14.8 | 15.1 | 15.4 | 16.1 |
| **Apr** | 0.6 | 14.8 | 15.6 | 15.9 | 16.2 | 17.5 |
| **May** | 0.6 | 15.7 | 16.3 | 16.6 | 16.9 | 19.2 |
| **Jun** | 1.7 | 16.4 | 17.2 | 17.9 | 18.8 | 19.8 |
| **Jul** | 1.0 | 16.6 | 17.6 | 18.0 | 18.6 | 19.8 |
| **Aug** | 1.9 | 16.0 | 17.7 | 18.4 | 19.6 | 21.1 |
| **Sep** | 1.3 | 17.0 | 18.7 | 19.2 | 19.9 | 20.4 |
| **Oct** | 0.9 | 17.3 | 18.5 | 19.0 | 19.4 | 20.1 |
| **Nov** | 1.3 | 15.4 | 16.8 | 17.3 | 18.1 | 19.4 |
| **Dec** | 1.0 | 14.6 | 15.7 | 16.2 | 16.7 | 17.7 |

The ACF in Fig. A.1. in Appendix A also clearly shows a seasonal pattern with respect to peaks lag at about 12, 24, and so on.

### 4.3.3 Nutrients

Fig. 4.12(a–c) shows the monthly mean time series data for nutrients at Station 3. With time series plot (Fig. 4.12(a)), for three nutrients $NH_4^+$, $PO_4^{-3}$, and $SiO_4^{-4}$ the seasonal amplitude and patterns are constant over time; however, for $NO_3^-$ the seasonal pattern showed increasing trend between 2004-2016.

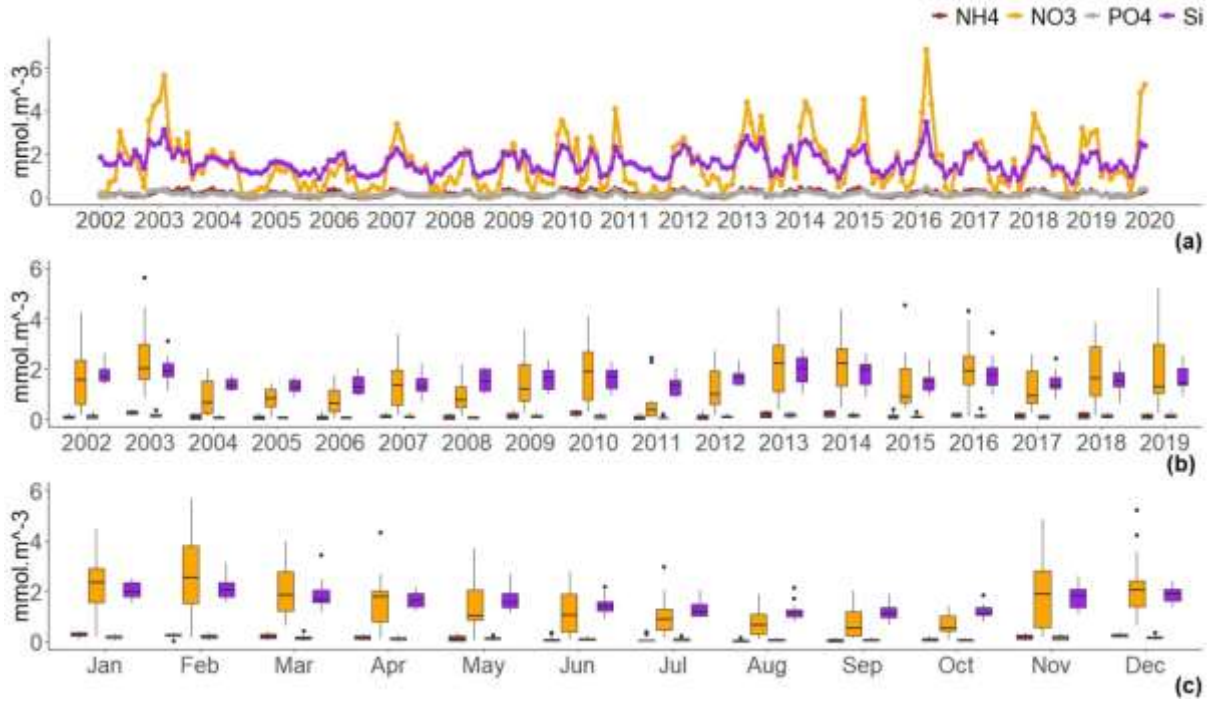


***Fig. 4.12.*** *Monthly time series of nutrients ($NH_4^+$, $NO_3^-$, $PO_4^{-3}$, and $SiO_4^{-4}$): (a) the time series plot; the boxplot (b) by year, and (c) by month for Station 3 (off Portimão).*

The three nutrients $NO_3^-$, $PO_4^{-3}$ and $SiO_4^{-4}$ revealed maximum values in March 2016, with 6.8, 0.44, and 3.44 mmol.m$^{-3}$ of concentration values, respectively (Fig. 4.12(a–c); Table (4.17 and 4.18)). $NH_4^+$ exhibited the maximum concentration value in January 2015 with 0.41 mmol.m$^{-3}$. The minimum concentration values for $NH_4^+$ and $NO_3^-$ found in June 2004 (0.01 mmol.m$^{-3}$) and June 2006 (0.1 mmol.m$^{-3}$), respectively. Then again, for $SiO_4^{-4}$ and $PO_4^{-3}$ the minimum values discovered in September 2018 at 0.01 and 0.7 mmol.m$^{-3}$, respectively.

The highest median was found in 2013 for three nutrients $NO_3^-$, $PO_4^{-3}$ and $SiO_4^{-4}$ with greater than 2.2, 0.2, and 2.02 mmol.m$^{-3}$, respectively (Fig. 4.12(b)). For $NH4^+$ the highest median value found in 2003 (0.3 mmol.m$^{-3}$). $PO_4^{-3}$ and $SiO_4^{-4}$ showed the highest IQR value in 2013 with 0.15 and 0.95 mmol.m$^{-3}$, respectively (Table 4.17). The lowest IQR value for $PO_4^{-3}$ was

revealed in 2011(0.03 mmol.m$^{-3}$) and for $SiO_4^{-4}$ in 2004 with 0.39 mmol.m$^{-3}$. The higher dispersion for $PO_4^{-3}$ showed half of the data between 0.1 and 0.24 mmol.m$^{-3}$, while the smallest dispersion falls within [0.03, 0.06 mmol.m$^{-3}$]. $SiO_4^{-4}$ showed 50% of the data value for higher dispersion between 1.5 and 2.44 mmol.m$^{-3}$ and for smallest dispersion between 1.2 mmol.m$^{-3}$ and 1.6 mmol.m$^{-3}$. The highest IQR for $NH_4^+$ was found in 2014 (0.25 mmol.m$^{-3}$) and lowest in 2002 (0.08 mmol.m$^{-3}$). Half of the data for higher dispersion was found between 0.09 and 0.34 mmol.m$^{-3}$ and for smallest dispersion falls within [0.05, 0.13]. The highest IQR for $NO_3^-$ was found in 2018(1.95 mmol.m$^{-3}$) and the lowest in 2011 (0.54 mmol.m$^{-3}$). Half of the data for higher dispersion was found between 0.93 and 2.9 mmol.m$^{-3}$, and for smallest dispersion falls within [0.14, 0.7 mmol.m$^{-3}$].

Fig. 4.12 (c) and Table 4.18 show the highest median value for $NO_3^-$ and $SiO_4^{-4}$ in February with 2.53 and 2.03 mmol.m$^{-3}$, respectively. The highest median value for $NH_4^+$ and $PO_4^{-3}$ was found in January, with a value of 0.31 and 0.2 mmol.m$^{-3}$, respectively. In November, the dispersion presents the highest IQR value for $PO_4^{-3}$ and $SiO_4^{-4}$ with 0.16 and 0.74 mmol.m$^{-3}$, respectively. For the highest dispersion, 50% of $PO_4^{-3}$ data values were found between 0.06 and 0.22 mmol.m$^{-3}$ and for $SiO_4^{-4}$ within [1.4, 2.1 mmol.m$^{-3}$]. In October, the dispersion presents the lowest IQR value for $NO_3^-$ and $PO_4^{-3}$ with 0.6 and 0.03 mmol.m$^{-3}$, respectively. Half of the data for this dispersion was found between 0.42 and 1.02 mmol.m$^{-3}$ for $NO_3^-$ and for $PO_4^{-3}$ falls within [0.04, 0.07 mmol.m$^{-3}$]. $NO_3^-$ showed the highest IQR value in February (2.3 mmol.m$^{-3}$) with 50% values falling within [1.5, 3.8 mmol.m$^{-3}$]. August indicated the lowest IQR value for $SiO_4^{-4}$ (0.3 mmol.m$^{-3}$) with half the values falling within [1, 1.3 mmol.m$^{-3}$]. $NH_4^+$ showed the highest IQR value in May (0.2 mmol.m$^{-3}$) with 50% values falling within [0.04, 0.24 mmol.m$^{-3}$] and lowest value in July (0.04 mmol.m$^{-3}$) with 25% of data values above 0.06 and below 0.02 mmol.m$^{-3}$.

***Table 4.17.*** *Statistical descriptive measures of nutrients ($NH_4^+$, $NO_3^-$, $PO_4^{-3}$, and $SiO_4^{-4}$) mmol.m$^{-3}$ by year for Station 3 (off Portimão).*

| Year | $NH_4^+$ | $NO_3^-$ | $PO_4^{-3}$ | $SiO_4^{-4}$ | $NH_4^+$ | $NO_3^-$ | $PO_4^{-3}$ | $SiO_4^{-4}$ | $NH_4^+$ | $NO_3^-$ | $PO_4^{-3}$ | $SiO_4^{-4}$ | $NH_4^+$ | $NO_3^-$ | $PO_4^{-3}$ | $SiO_4^{-4}$ | $NH_4^+$ | $NO_3^-$ | $PO_4^{-3}$ | $SiO_4^{-4}$ | $NH_4^+$ | $NO_3^-$ | $PO_4^{-3}$ | $SiO_4^{-4}$ |
|---|---|---|---|---|---|---|---|---|---|---|---|---|---|---|---|---|---|---|---|---|---|---|---|---|
| | IQR | | | | Min | | | | $Q_1$ | | | | Median | | | | $Q_3$ | | | | Max | | | |
| **2002** | 0.08 | 1.73 | 0.11 | 0.46 | 0.02 | 0.17 | 0.02 | 1.35 | 0.05 | 0.62 | 0.06 | 1.51 | 0.08 | 1.57 | 0.12 | 1.68 | 0.13 | 2.35 | 0.17 | 1.98 | 0.24 | 4.22 | 0.29 | 2.62 |
| **2003** | 0.14 | 1.39 | 0.09 | 0.51 | 0.13 | 0.87 | 0.06 | 1.12 | 0.22 | 1.60 | 0.12 | 1.71 | **0.31** | 2.03 | 0.16 | 1.93 | 0.36 | 2.99 | 0.20 | 2.21 | 0.39 | 5.63 | 0.38 | 3.11 |
| **2004** | 0.21 | 1.27 | 0.08 | 0.39 | < 0.01 | 0.12 | 0.03 | 1.11 | 0.00 | 0.25 | 0.04 | 1.20 | 0.08 | 0.68 | 0.07 | 1.32 | 0.21 | 1.52 | 0.12 | 1.58 | 0.24 | 2.03 | 0.16 | 1.75 |
| **2005** | 0.12 | 0.72 | 0.05 | 0.43 | < 0.01 | 0.06 | 0.03 | 0.88 | 0.02 | 0.50 | 0.05 | 1.12 | 0.07 | 0.82 | 0.08 | 1.27 | 0.14 | 1.21 | 0.10 | 1.56 | 0.28 | 1.43 | 0.11 | 1.69 |
| **2006** | 0.12 | 0.87 | 0.07 | 0.69 | < 0.01 | 0.05 | 0.02 | 0.93 | 0.01 | 0.29 | 0.04 | 1.02 | 0.04 | 0.64 | 0.06 | 1.27 | 0.13 | 1.16 | 0.11 | 1.71 | 0.32 | 1.77 | 0.16 | 2.04 |
| **2007** | 0.12 | 1.39 | 0.09 | 0.51 | 0.04 | 0.19 | 0.02 | 0.70 | 0.07 | 0.58 | 0.06 | 1.12 | 0.10 | 1.38 | 0.10 | 1.30 | 0.19 | 1.97 | 0.15 | 1.63 | 0.32 | 3.37 | 0.26 | 2.23 |
| **2008** | 0.17 | 0.83 | 0.06 | 0.85 | < 0.01 | 0.16 | 0.04 | 0.96 | 0.01 | 0.48 | 0.05 | 1.14 | 0.10 | 0.78 | 0.08 | 1.51 | 0.18 | 1.31 | 0.12 | 1.99 | 0.29 | 2.20 | 0.17 | 2.08 |
| **2009** | 0.21 | 1.45 | 0.11 | 0.78 | < 0.01 | 0.26 | 0.05 | 1.01 | 0.03 | 0.73 | 0.06 | 1.20 | 0.11 | 1.19 | 0.09 | 1.63 | 0.24 | 2.18 | 0.18 | 1.98 | 0.36 | 3.55 | 0.27 | 2.37 |
| **2010** | 0.15 | 1.93 | 0.15 | 0.73 | 0.03 | 0.31 | 0.01 | 0.94 | 0.18 | 0.76 | 0.04 | 1.24 | 0.30 | 1.88 | 0.12 | 1.70 | 0.33 | 2.70 | 0.19 | 1.97 | 0.39 | 4.08 | 0.30 | 2.30 |
| **2011** | 0.12 | 0.54 | 0.03 | 0.59 | < 0.01 | 0.06 | < 0.01 | 0.83 | 0.01 | 0.14 | 0.03 | 0.97 | 0.03 | 0.39 | 0.04 | 1.33 | 0.14 | 0.68 | 0.06 | 1.56 | 0.29 | 2.46 | 0.22 | 2.04 |
| **2012** | 0.16 | 1.32 | 0.08 | 0.43 | < 0.01 | 0.18 | 0.04 | 1.34 | 0.03 | 0.61 | 0.07 | 1.38 | 0.08 | 1.01 | 0.10 | 1.68 | 0.18 | 1.93 | 0.15 | 1.82 | 0.36 | 2.72 | 0.24 | 2.37 |
| **2013** | 0.21 | 1.86 | **0.15** | **0.95** | 0.06 | 0.36 | 0.04 | 0.99 | 0.09 | 1.11 | 0.09 | 1.49 | 0.24 | **2.23** | **0.17** | **2.02** | 0.30 | 2.96 | 0.24 | 2.44 | 0.39 | 4.40 | 0.32 | 2.80 |
| **2014** | **0.25** | 1.47 | 0.10 | 0.81 | 0.03 | 0.47 | 0.04 | 0.88 | 0.09 | 1.34 | 0.10 | 1.38 | 0.27 | 2.22 | 0.16 | 1.96 | 0.34 | 2.81 | 0.20 | 2.20 | 0.39 | 4.38 | 0.31 | 2.61 |
| **2015** | 0.12 | 1.37 | 0.10 | 0.48 | 0.01 | 0.41 | 0.04 | 0.94 | 0.05 | 0.66 | 0.06 | 1.18 | 0.08 | 0.92 | 0.09 | 1.48 | 0.18 | 2.02 | 0.16 | 1.66 | **0.41** | 4.55 | 0.32 | 2.38 |
| **2016** | 0.16 | 1.11 | 0.08 | 0.69 | 0.02 | 0.11 | 0.01 | 0.97 | 0.10 | 1.40 | 0.11 | 1.36 | 0.21 | 1.92 | 0.15 | 1.77 | 0.26 | 2.51 | 0.19 | 2.05 | 0.29 | **6.80** | **0.44** | **3.44** |
| **2017** | 0.20 | 1.27 | 0.11 | 0.44 | 0.03 | 0.23 | 0.02 | 0.80 | 0.05 | 0.64 | 0.05 | 1.23 | 0.14 | 0.95 | 0.08 | 1.35 | 0.24 | 1.91 | 0.16 | 1.67 | 0.31 | 2.59 | 0.20 | 2.43 |
| **2018** | 0.22 | **1.95** | 0.14 | 0.58 | < 0.01 | 0.14 | < 0.01 | 0.65 | 0.05 | 0.93 | 0.07 | 1.28 | 0.14 | 1.63 | 0.12 | 1.52 | 0.27 | 2.88 | 0.21 | 1.86 | 0.34 | 3.85 | 0.29 | 2.32 |
| **2019** | 0.17 | 1.94 | 0.14 | 0.68 | 0.01 | 0.23 | 0.01 | 0.95 | 0.05 | 1.04 | 0.08 | 1.35 | 0.08 | 1.29 | 0.10 | 1.44 | 0.22 | 2.98 | 0.22 | 2.04 | 0.31 | 5.20 | 0.36 | 2.51 |

***Table 4.18.*** *Statistical descriptive measures of nutrients ($NH_4^+$, $NO_3^-$, $PO_4^{-3}$, and $SiO_4^{-4}$) mmol.m$^{-3}$ by month for Station 3 (off Portimão).*

| Month | $NH_4^+$ | $NO_3^-$ | $PO_4^{-3}$ | $SiO_4^{-4}$ | $NH_4^+$ | $NO_3^-$ | $PO_4^{-3}$ | $SiO_4^{-4}$ | $NH_4^+$ | $NO_3^-$ | $PO_4^{-3}$ | $SiO_4^{-4}$ | $NH_4^+$ | $NO_3^-$ | $PO_4^{-3}$ | $SiO_4^{-4}$ | $NH_4^+$ | $NO_3^-$ | $PO_4^{-3}$ | $SiO_4^{-4}$ | $NH_4^+$ | $NO_3^-$ | $PO_4^{-3}$ | $SiO_4^{-4}$ |
|---|---|---|---|---|---|---|---|---|---|---|---|---|---|---|---|---|---|---|---|---|---|---|---|---|
| | IQR | | | | Min | | | | $Q_1$ | | | | Median | | | | $Q_3$ | | | | Max | | | |
| **Jan** | 0.14 | 1.37 | 0.12 | 0.59 | 0.05 | 0.17 | 0.03 | 1.51 | 0.22 | 1.54 | 0.12 | 1.77 | 0.31 | 2.36 | 0.19 | 1.99 | 0.35 | 2.91 | 0.24 | 2.35 | **0.41** | **0.41** | 4.44 | 0.30 |
| **Feb** | 0.08 | **2.28** | 0.15 | 0.55 | 0.02 | 0.18 | 0.02 | 1.54 | 0.22 | 1.52 | 0.12 | 1.79 | 0.26 | 2.53 | 0.19 | 2.04 | 0.30 | 3.80 | 0.27 | 2.35 | 0.35 | 0.35 | 5.63 | 0.38 |
| **Mar** | 0.18 | 1.56 | 0.11 | 0.49 | 0.08 | 0.62 | 0.03 | 1.20 | 0.13 | 1.20 | 0.09 | 1.54 | 0.19 | 1.85 | 0.14 | 1.69 | 0.31 | 2.77 | 0.20 | 2.03 | 0.39 | 0.39 | **6.80** | **0.44** |
| **Apr** | 0.13 | 1.23 | 0.09 | 0.54 | 0.03 | 0.12 | 0.00 | 1.23 | 0.10 | 0.78 | 0.07 | 1.38 | 0.15 | 1.79 | 0.13 | 1.60 | 0.22 | 2.01 | 0.16 | 1.91 | 0.31 | 0.31 | 4.31 | 0.28 |
| **May** | **0.20** | 1.18 | 0.07 | 0.55 | < 0.01 | 0.06 | 0.01 | 1.17 | 0.04 | 0.85 | 0.08 | 1.35 | 0.08 | 1.04 | 0.10 | 1.54 | 0.24 | 2.03 | 0.16 | 1.90 | 0.37 | 0.37 | 3.71 | 0.27 |
| **Jun** | 0.09 | 1.51 | 0.08 | 0.37 | < 0.01 | 0.05 | 0.02 | 0.94 | 0.02 | 0.39 | 0.05 | 1.21 | 0.05 | 1.06 | 0.09 | 1.39 | 0.10 | 1.89 | 0.13 | 1.57 | 0.37 | 0.37 | 2.76 | 0.21 |
| **Jul** | 0.04 | 0.82 | 0.05 | 0.46 | < 0.01 | 0.12 | 0.03 | 0.96 | 0.02 | 0.46 | 0.05 | 1.02 | 0.03 | 0.90 | 0.09 | 1.19 | 0.06 | 1.28 | 0.10 | 1.48 | 0.39 | 0.39 | 2.97 | 0.22 |
| **Aug** | 0.04 | 0.77 | 0.05 | 0.27 | < 0.01 | 0.11 | 0.01 | 0.80 | 0.01 | 0.31 | 0.04 | 1.00 | 0.03 | 0.66 | 0.06 | 1.16 | 0.05 | 1.07 | 0.09 | 1.26 | 0.15 | 0.15 | 1.88 | 0.14 |
| **Sep** | 0.07 | 0.98 | 0.05 | 0.38 | < 0.01 | 0.14 | < 0.01 | 0.65 | 0.01 | 0.22 | 0.04 | 0.96 | 0.04 | 0.51 | 0.05 | 1.13 | 0.08 | 1.20 | 0.09 | 1.34 | 0.16 | 0.16 | 2.02 | 0.15 |
| **Oct** | 0.08 | 0.60 | 0.03 | 0.30 | < 0.01 | 0.06 | 0.03 | 0.80 | 0.03 | 0.42 | 0.04 | 1.05 | 0.09 | 0.54 | 0.05 | 1.12 | 0.11 | 1.02 | 0.07 | 1.35 | 0.22 | 0.22 | 1.41 | 0.12 |
| **Nov** | 0.18 | 2.24 | **0.16** | **0.74** | 0.01 | 0.19 | 0.02 | 1.09 | 0.08 | 0.55 | 0.06 | 1.36 | 0.18 | 1.89 | 0.15 | 1.81 | 0.26 | 2.79 | 0.22 | 2.09 | 0.37 | 0.37 | 4.85 | 0.33 |
| **Dec** | 0.11 | 1.02 | 0.07 | 0.45 | 0.17 | 0.61 | 0.06 | 1.34 | 0.20 | 1.37 | 0.12 | 1.62 | 0.27 | 2.04 | 0.17 | 1.87 | 0.30 | 2.39 | 0.19 | 2.07 | 0.36 | 0.36 | 5.20 | 0.36 |

## 4.4 Characterization of Station 4 (off Ria Formosa)

### 4.4.1 Chlorophyll-a Concentration

Fig. 4.13(a-c) shows the annual and monthly variability of the Chl-*a* for the Station 4 in the east side of the south coast of Algarve. The time series plot is shown in Fig. 4.13(a) and exhibits seasonal behaviour that was also shown by the Fig. A.1. at Appendix A. The seasonal pattern shows a peak seasonal amplitude in year 2010 and 2011. The seasonal period of Chl-*a* can be characterised by higher values in March and low values in June, as shown in Fig. 4.13(c).

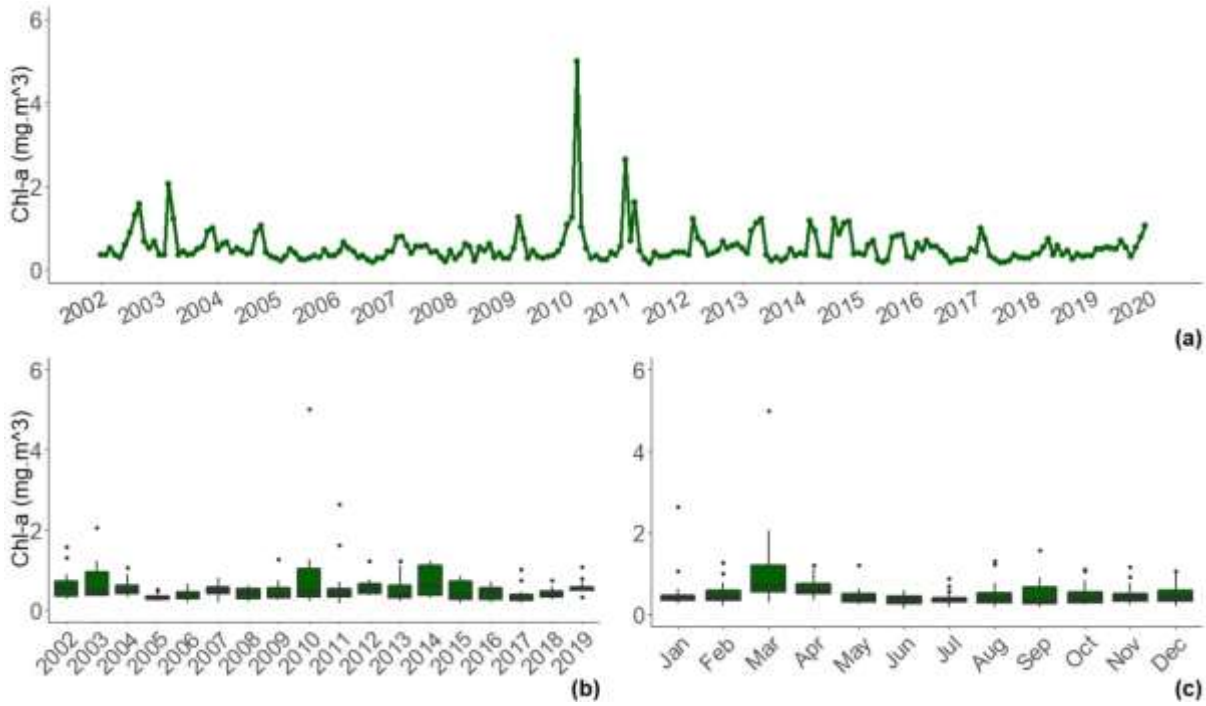


***Fig. 4.13.*** *Monthly chlorophyll-a concentration (Chl-a mg $m^{-3}$): (a) the time series plot; the boxplot (b) by year, and (c) by month for Station 4 (off Ria Formosa).*

The maximum value of Chl-*a* was identified in March 2010 (5 mg $m^{-3}$) and the minimum values in June 2011 (0.1 mg $m^{-3}$). The highest median value of 0.6 mg $m^{-3}$ was found in 2014 (Table 4.19). Regarding the dispersion of the data, the IQR was high in 2014(0.8 mg $m^{-3}$), with 50% of the data between 0.4 and 1.1 mg $m^{-3}$. The lowest IQR was in 2019 (0.1 mg $m^{-3}$), with 50% of the data values falling within [0.5, 0.6 mg $m^{-3}$].

***Table 4.19**. Statistical descriptive measures of chlorophyll-a concentration (Chl-a mg $m^{-3}$) by year for Station 4 (off Ria Formosa).*

| Year | IQR | Min | $Q_1$ | Median | $Q_3$ | Max |
|---|---|---|---|---|---|---|
| **2002** | 0.37 | 0.29 | 0.35 | 0.55 | 0.72 | 1.57 |
| **2003** | 0.58 | 0.34 | 0.36 | 0.47 | 0.94 | 2.06 |
| **2004** | 0.21 | 0.32 | 0.40 | 0.46 | 0.61 | 1.05 |
| **2005** | 0.08 | 0.22 | 0.27 | 0.29 | 0.35 | 0.50 |
| **2006** | 0.16 | 0.18 | 0.27 | 0.33 | 0.43 | 0.65 |
| **2007** | 0.16 | 0.20 | 0.40 | 0.49 | 0.56 | 0.79 |
| **2008** | 0.25 | 0.20 | 0.29 | 0.42 | 0.54 | 0.62 |
| **2009** | 0.24 | 0.27 | 0.30 | 0.39 | 0.54 | 1.26 |
| **2010** | 0.71 | 0.22 | 0.32 | 0.45 | 1.03 | 4.99 |
| **2011** | 0.20 | 0.15 | 0.32 | 0.41 | 0.52 | 2.64 |
| **2012** | 0.24 | 0.35 | 0.40 | 0.55 | 0.64 | 1.22 |
| **2013** | 0.33 | 0.22 | 0.29 | 0.38 | 0.62 | 1.21 |
| **2014** | 0.77 | 0.30 | 0.35 | 0.62 | 1.12 | 1.22 |
| **2015** | 0.46 | 0.17 | 0.26 | 0.37 | 0.72 | 0.84 |
| **2016** | 0.31 | 0.17 | 0.25 | 0.45 | 0.56 | 0.70 |
| **2017** | 0.14 | 0.18 | 0.24 | 0.28 | 0.38 | 1.00 |
| **2018** | 0.13 | 0.25 | 0.34 | 0.37 | 0.47 | 0.73 |
| **2019** | 0.09 | 0.32 | 0.49 | 0.52 | 0.57 | 1.06 |

Month variability of Chl-*a* reveals the highest median values in March (0.7 mg $m^{-3}$) (Fig. 4.13(c) and Table 4.20 and it was also in March, that show the dispersion presents the highest IQR value (0.7 mg $m^{-3}$), with 50% of Chl-*a* values falling within the interval [0.5, 1.2 mg $m^{-3}$]. In July, the smallest dispersion was noted (IQR=0.1 mg m-3). For the lowest dispersion, 25% of Chl-*a* data values were found to be above 0.4 and below 0.3 mg $m^{-3}$.

***Table 4.20.** Statistical descriptive measures of chlorophyll-a concentration (Chl-a mg $m^{-3}$) by month for Station 4 (off Ria Formosa).*

| Month | IQR | Min | $Q_1$ | Median | $Q_3$ | Max |
|---|---|---|---|---|---|---|
| **Jan** | 0.12 | 0.27 | 0.34 | 0.40 | 0.46 | 2.64 |
| **Feb** | 0.23 | 0.22 | 0.35 | 0.42 | 0.58 | 1.26 |
| **Mar** | 0.67 | 0.30 | 0.54 | 0.72 | 1.20 | 4.99 |
| **Apr** | 0.24 | 0.34 | 0.50 | 0.59 | 0.75 | 1.21 |
| **May** | 0.22 | 0.24 | 0.30 | 0.39 | 0.52 | 1.21 |
| **Jun** | 0.19 | 0.15 | 0.26 | 0.36 | 0.45 | 0.59 |
| **Jul** | 0.10 | 0.18 | 0.30 | 0.34 | 0.40 | 0.88 |
| **Aug** | 0.24 | 0.17 | 0.27 | 0.39 | 0.52 | 1.31 |
| **Sep** | 0.40 | 0.18 | 0.26 | 0.35 | 0.66 | 1.57 |
| **Oct** | 0.26 | 0.24 | 0.29 | 0.39 | 0.55 | 1.11 |
| **Nov** | 0.20 | 0.25 | 0.31 | 0.42 | 0.51 | 1.16 |
| **Dec** | 0.27 | 0.20 | 0.32 | 0.40 | 0.59 | 1.06 |

### 4.4.2 Sea Surface Temperature

The time series plot shown in Fig. 4.14(a) shows a stable annual cycle and constant seasonal amplitude and patterns over the SST time series. The seasonal pattern presented in Fig.4.14(c) shows that the SST are at a minimum in February, steadily increases until August and then begins declining until February.

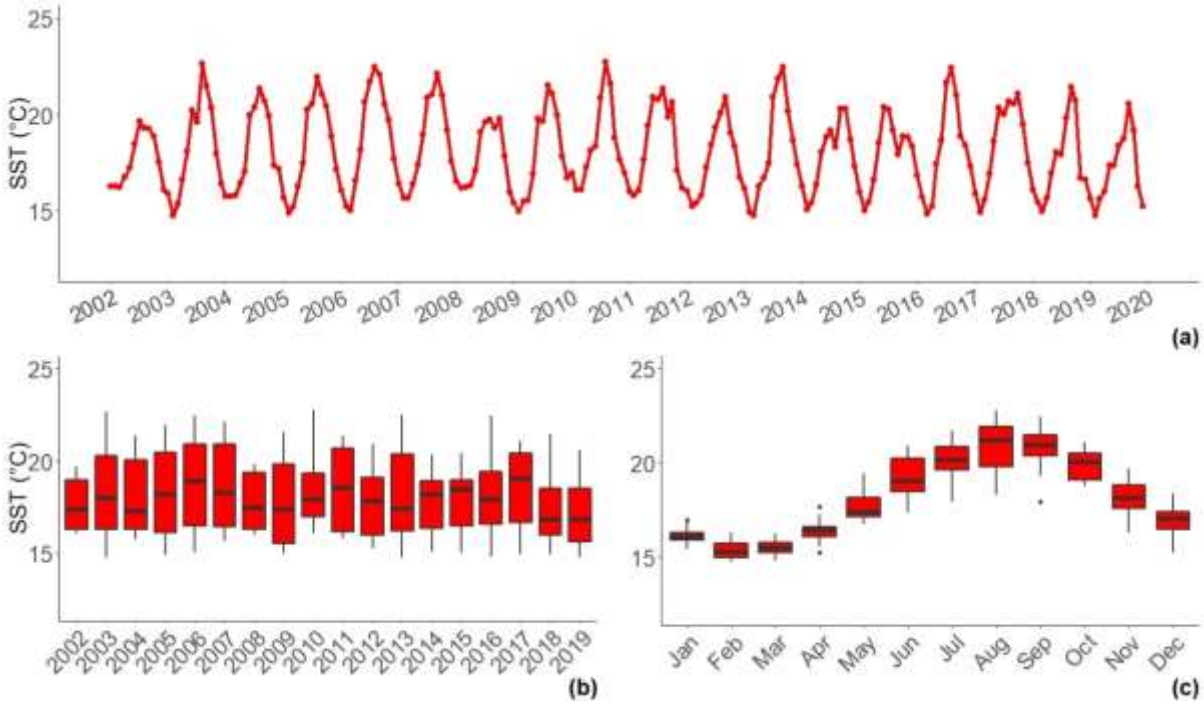


***Fig. 4.14.*** *Monthly time series of sea surface temperature (SST-ºC): (a) the time series plot; the boxplot (b) by year, and (c) by month for Station 4 (off Ria Formosa).*

Fig. 4.14 (b) and Table 4.21-4.22 depicts the minimum and maximum values of the SST in March 2003 (13.9 ºC) and in August 2010 (22.7 ºC), respectively. The highest median value of SST was found in the year 2017 (19.1 ºC). The highest IQR was found in 2011 (4.5 ºC), with 50% of the data found between 16.2 and 20.7 ºC. The smallest IQR was found in 2010 (2.4 ºC), with half of the data falling within [17.0, 19.3 ºC].

Monthly variability of SST (Fig. 4.14 (c) and Table 4.22), displays that the month of August was the one that show the highest median (21.2 ºC) and the highest dispersion (IQR = 2.2 ºC) where 50% of the SST values falling within the interval [19.8, 21.9 ºC]. Alternatively, the smallest dispersion was noted in January (IQR=0.4 ºC), with 25% of values being above 16.3 ºC and below 15.9 ºC.

***Table 4.21.*** *Statistical descriptive measures of sea surface temperature (SST-ºC) by year for Station 4(off Ria Formosa).*

| Year | IQR | Min | $Q_1$ | Median | $Q_3$ | Max |
|---|---|---|---|---|---|---|
| **2002** | 2.7 | 16.1 | 16.3 | 17.4 | 19.0 | 19.7 |
| **2003** | 4.0 | 14.8 | 16.3 | 18.0 | 20.3 | 22.7 |
| **2004** | 3.8 | 15.7 | 16.3 | 17.3 | 20.1 | 21.4 |
| **2005** | 4.3 | 14.9 | 16.1 | 18.2 | 20.5 | 22.0 |
| **2006** | 4.5 | 15.0 | 16.5 | 18.9 | 20.9 | 22.5 |
| **2007** | 4.5 | 15.7 | 16.4 | 18.3 | 20.9 | 22.1 |
| **2008** | 3.1 | 16.0 | 16.3 | 17.5 | 19.4 | 19.8 |
| **2009** | 4.3 | 15.0 | 15.5 | 17.4 | 19.8 | 21.5 |
| **2010** | 2.4 | 16.1 | 17.0 | 17.9 | 19.3 | 22.7 |
| **2011** | 4.5 | 15.8 | 16.2 | 18.6 | 20.7 | 21.3 |
| **2012** | 3.1 | 15.3 | 16.0 | 17.8 | 19.1 | 20.9 |
| **2013** | 4.1 | 14.8 | 16.2 | 17.4 | 20.4 | 22.5 |
| **2014** | 2.6 | 15.1 | 16.4 | 18.2 | 18.9 | 20.3 |
| **2015** | 2.5 | 15.0 | 16.5 | 18.5 | 19.0 | 20.4 |
| **2016** | 2.8 | 14.8 | 16.6 | 17.9 | 19.4 | 22.4 |
| **2017** | 3.7 | 14.9 | 16.7 | 19.1 | 20.4 | 21.1 |
| **2018** | 2.5 | 15.0 | 16.0 | 16.8 | 18.5 | 21.4 |
| **2019** | 2.9 | 14.8 | 15.6 | 16.8 | 18.5 | 20.6 |

***Table 4.22.*** *Statistical descriptive measures of sea surface temperature (SST-ºC) by month for Station 4 (off Ria Formosa).*

| Month | IQR | Min | $Q_1$ | Median | $Q_3$ | Max |
|---|---|---|---|---|---|---|
| **Jan** | 0.4 | 15.4 | 15.9 | 16.0 | 16.3 | 17.0 |
| **Feb** | 0.8 | 14.8 | 15.0 | 15.2 | 15.7 | 16.3 |
| **Mar** | 0.5 | 14.8 | 15.2 | 15.5 | 15.8 | 16.2 |
| **Apr** | 0.5 | 15.2 | 16.1 | 16.4 | 16.6 | 17.7 |
| **May** | 1.0 | 16.7 | 17.1 | 17.4 | 18.1 | 19.4 |
| **Jun** | 1.8 | 17.4 | 18.4 | 19.0 | 20.2 | 20.9 |
| **Jul** | 1.2 | 17.9 | 19.6 | 20.1 | 20.9 | 21.7 |
| **Aug** | 2.2 | 18.3 | 19.8 | 21.2 | 21.9 | 22.7 |
| **Sep** | 1.1 | 17.9 | 20.4 | 20.9 | 21.5 | 22.5 |
| **Oct** | 1.4 | 18.8 | 19.1 | 20.1 | 20.5 | 21.1 |
| **Nov** | 1.2 | 16.3 | 17.6 | 18.2 | 18.8 | 19.7 |
| **Dec** | 0.9 | 15.2 | 16.5 | 17.0 | 17.4 | 18.4 |

### 4.4.3 Nutrients

The monthly mean time series plot (Fig. 4.15(a)) shows that $NH_4^+$, $PO_4^{-3}$, and $SiO_4^{-4}$ nutrients showed constant seasonal amplitude and patterns over time.; however, for $NO_3^-$ the

seasonal pattern shows a seasonal amplitude peak in 2010 and increasing seasonal pattern trend between 2011-2016.

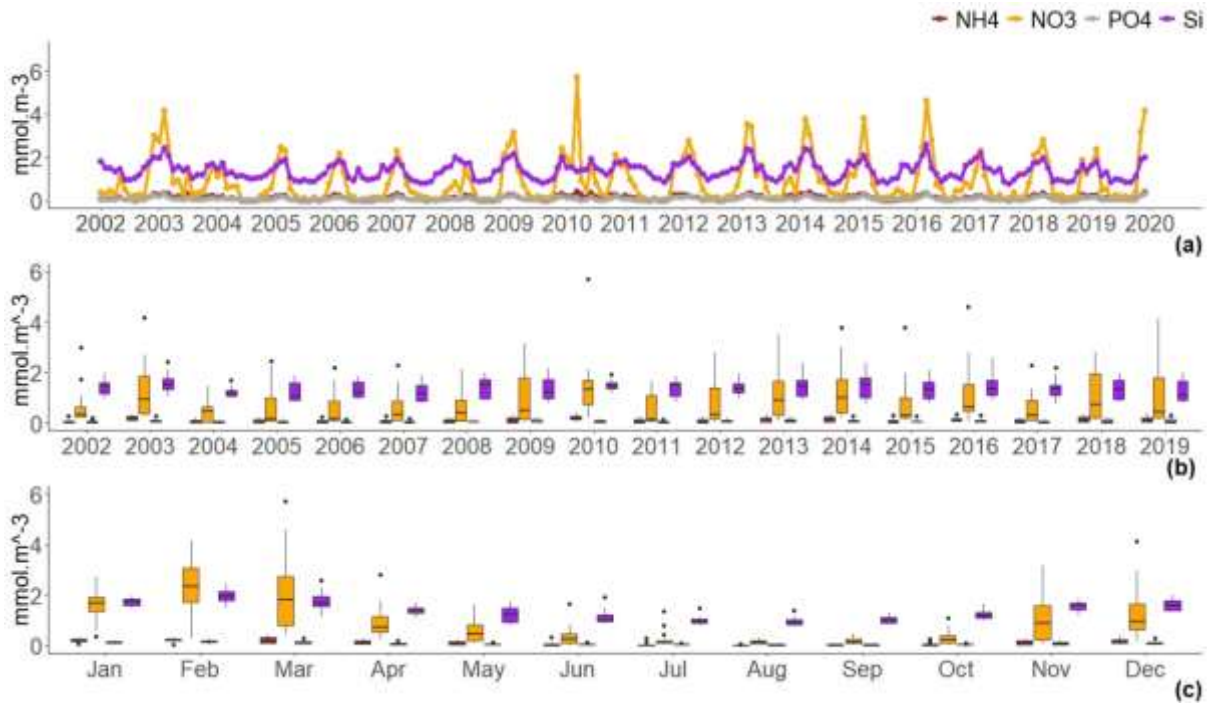


***Fig. 4.15.*** *Monthly time series of nutrients ($NH_4^+$, $NO_3^-$, $PO_4^{-3}$, and $SiO_4^{-4}$): (a) the time series plot; the boxplot (b) by year, and (c) by month for Station 4 (off Ria Formosa).*

$PO_4^{-3}$ and $SiO_4^{-4}$ revealed maximum values in March 2016 with 0.31 and 2.57 mmol.m$^{-3}$ of concentration values, respectively (Fig. 4.15(b-c); Table (4.23 and 4.24)). $NH_4^+$ and $NO_3^-$ exhibited the maximum concentration value in March 2010 with 0.42 and 5.71 mmol.m$^{-3}$, respectively. The minimum concentration values for both $NH_4^+$ and $NO_3^-$ were found in June 2006 at 0.1 mmol.m$^{-3}$, respectively. The minimum values discovered in August 2014 (0.76 mmol.m$^{-3}$) for $SiO_4^{-4}$ and August 2016 (0.1 mmol.m$^{-3}$) for $PO_4^{-3}$.

Annual variability of nutrients (Fig. 4.15(b) and Table 4.23) reveals the highest median values in 2010 for $NH4^+$ and $NO_3^-$ with greater than 0.19, and 1.32 mmol.m$^{-3}$, respectively. The highest median value for $PO_4^{-3}$ was found in 2013 (0.08 mmol.m$^{-3}$) and for $SiO_4^{-4}$ was identified in 2014 (01.54 mmol.m$^{-3}$). $NO_3^-$ and $PO_4^{-3}$ revealed the highest IQR value in 2018 with 1.73 and 0.12 mmol.m$^{-3}$, respectively. The highest IQR for $NH_4^+$ was found in 2009 (0.25 mmol.m$^{-3}$). The lowest IQR value for $NH_4^+$, $NO_3^-$ and $PO_4^{-3}$ was revealed in 2002 with 0.07,0.4 and 0.03 mmol.m$^{-3}$, respectively. The highest IQR for $SiO_4^{-4}$ was found in 2014 (0.78 mmol.m$^{-3}$) and the lowest in 2010 (0.22 mmol.m$^{-3}$).

Monthly variability (Fig. 4.15 (b) and Table 4.24) revealed the highest median values for all nutrients in February. In March, the dispersion presents the highest IQR value for $NH_4^+$ and $NO_3^-$ with 0.22 and 1.96 mmol.m$^{-3}$, respectively. For highest dispersion, 50% of $NH_4^+$ data values were found between 0.1 and 0.32 mmol.m$^{-3}$ and for $NO_3^-$ within [0.8, 1.8 mmol.m$^{-3}$]. The lowest dispersion for $NH_4^+$ was found in August (0.01) with 50% of the data found between 0.03 and 0.13 mmol.m$^{-3}$. July indicated the lowest IQR value for $NO_3^-$ (0.1 mmol.m$^{-3}$) with half the values falling within [0.1, 0.2]. In November, $PO_4^{-3}$ presents the highest IQR (0.1) with half of the data found between 0.02 and 0.13 mmol.m$^{-3}$. The lowest dispersion for $PO_4^{-3}$ was found in August (IQR=0.1), with half of the data falling between [0.01, 0.0 mmol.m$^{-3}$]. $SiO_4^{-4}$ showed the highest IQR value in May (0.6 mmol.m$^{-3}$) with 50% values falling within [0.9, 1.5 mmol.m$^{-3}$] and lowest IQR value in July (0.162 mmol.m$^{-3}$) with 25% of data values above 1.1 and below 0.9 mmol.m$^{-3}$.

***Table 4.23.*** *Statistical descriptive measures of nutrients ($NH_4^+$, $NO_3^-$, $PO_4^{-3}$, and $SiO_4^{-4}$) mmol.m$^{-3}$ by year for Station 4 (off Ria Formosa).*

| Year | $NH_4^+$ | $NO_3^-$ | $PO_4^{-3}$ | $SiO_4^{-4}$ | $NH_4^+$ | $NO_3^-$ | $PO_4^{-3}$ | $SiO_4^{-4}$ | $NH_4^+$ | $NO_3^-$ | $PO_4^{-3}$ | $SiO_4^{-4}$ | $NH_4^+$ | $NO_3^-$ | $PO_4^{-3}$ | $SiO_4^{-4}$ | $NH_4^+$ | $NO_3^-$ | $PO_4^{-3}$ | $SiO_4^{-4}$ | $NH_4^+$ | $NO_3^-$ | $PO_4^{-3}$ | $SiO_4^{-4}$ |
|---|---|---|---|---|---|---|---|---|---|---|---|---|---|---|---|---|---|---|---|---|---|---|---|---|
| | **IQR** | | | | **Min** | | | | **$Q_1$** | | | | **Median** | | | | **$Q_3$** | | | | **Max** | | | |
| **2002** | 0.07 | 0.38 | 0.03 | 0.43 | 0.01 | 0.19 | 0.02 | 0.97 | 0.02 | 0.26 | 0.02 | 1.15 | 0.04 | 0.33 | 0.04 | 1.47 | 0.09 | 0.64 | 0.05 | 1.58 | 0.29 | 2.98 | 0.21 | 2.01 |
| **2003** | 0.16 | 1.48 | 0.09 | 0.43 | 0.06 | 0.26 | 0.01 | 1.04 | 0.11 | 0.38 | 0.03 | 1.33 | 0.18 | 0.93 | 0.07 | 1.52 | 0.27 | 1.85 | 0.12 | 1.75 | 0.33 | 4.16 | 0.28 | 2.44 |
| **2004** | 0.10 | 0.60 | 0.04 | 0.22 | < 0.01 | 0.02 | 0.01 | 1.01 | 0.00 | 0.05 | 0.02 | 1.08 | 0.07 | 0.48 | 0.03 | 1.16 | 0.10 | 0.65 | 0.06 | 1.30 | 0.20 | 1.47 | 0.11 | 1.71 |
| **2005** | 0.15 | 0.93 | 0.06 | 0.69 | < 0.01 | 0.02 | 0.01 | 0.86 | 0.00 | 0.08 | 0.02 | 0.89 | 0.02 | 0.19 | 0.03 | 1.07 | 0.16 | 1.01 | 0.08 | 1.58 | 0.21 | 2.44 | 0.17 | 1.89 |
| **2006** | 0.09 | 0.76 | 0.05 | 0.56 | < 0.01 | 0.00 | 0.01 | 0.92 | 0.01 | 0.11 | 0.01 | 1.05 | 0.02 | 0.16 | 0.03 | 1.24 | 0.10 | 0.87 | 0.06 | 1.61 | 0.25 | 2.18 | 0.15 | 1.83 |
| **2007** | 0.09 | 0.74 | 0.05 | 0.63 | < 0.01 | 0.07 | 0.00 | 0.79 | 0.01 | 0.12 | 0.01 | 0.88 | 0.04 | 0.33 | 0.03 | 1.17 | 0.11 | 0.87 | 0.06 | 1.51 | 0.28 | 2.30 | 0.18 | 1.89 |
| **2008** | 0.14 | 0.84 | 0.06 | **0.78** | < 0.01 | 0.04 | 0.02 | 0.88 | 0.00 | 0.06 | 0.03 | 0.96 | 0.07 | 0.41 | 0.05 | 1.49 | 0.14 | 0.90 | 0.08 | 1.74 | 0.22 | 2.13 | 0.16 | 1.99 |
| **2009** | **0.21** | 1.63 | 0.12 | 0.75 | < 0.01 | 0.09 | 0.01 | 0.80 | 0.01 | 0.16 | 0.03 | 0.96 | 0.06 | 0.51 | 0.06 | 1.25 | 0.22 | 1.78 | 0.14 | 1.71 | 0.31 | 3.16 | 0.20 | 2.15 |
| **2010** | 0.14 | 0.99 | 0.08 | 0.22 | 0.04 | 0.20 | 0.00 | 1.17 | 0.13 | 0.72 | 0.01 | 1.37 | **0.19** | **1.32** | 0.07 | 1.45 | 0.27 | 1.71 | 0.09 | 1.59 | **0.42** | **5.71** | 0.16 | 1.93 |
| **2011** | 0.14 | 1.04 | 0.04 | 0.54 | < 0.01 | 0.02 | 0.00 | 0.85 | 0.01 | 0.08 | 0.01 | 1.06 | 0.04 | 0.16 | 0.03 | 1.53 | 0.15 | 1.12 | 0.05 | 1.60 | 0.26 | 1.67 | 0.15 | 1.86 |
| **2012** | 0.14 | 1.22 | 0.07 | 0.38 | < 0.01 | 0.04 | 0.02 | 0.96 | 0.01 | 0.17 | 0.03 | 1.19 | 0.04 | 0.34 | 0.05 | 1.37 | 0.15 | 1.39 | 0.11 | 1.56 | 0.27 | 2.78 | 0.20 | 1.97 |
| **2013** | 0.16 | 1.36 | 0.10 | 0.63 | 0.02 | 0.11 | 0.01 | 0.89 | 0.05 | 0.30 | 0.04 | 1.07 | 0.18 | 0.90 | **0.08** | 1.46 | 0.21 | 1.66 | 0.13 | 1.70 | 0.35 | 3.53 | 0.26 | 2.39 |
| **2014** | 0.19 | 1.32 | 0.09 | 0.78 | 0.02 | 0.25 | 0.02 | 0.76 | 0.05 | 0.39 | 0.04 | 1.01 | 0.18 | 1.00 | 0.07 | 1.54 | 0.24 | 1.71 | 0.12 | 1.78 | 0.37 | 3.77 | 0.27 | 2.39 |
| **2015** | 0.10 | 0.81 | 0.05 | 0.65 | < 0.01 | 0.10 | 0.02 | 0.81 | 0.01 | 0.20 | 0.03 | 0.97 | 0.04 | 0.29 | 0.04 | 1.33 | 0.12 | 1.00 | 0.08 | 1.62 | 0.30 | 3.79 | 0.27 | 2.08 |
| **2016** | 0.10 | 1.07 | 0.08 | 0.60 | 0.01 | 0.08 | 0.00 | 0.89 | 0.07 | 0.46 | 0.04 | 1.09 | 0.13 | 0.65 | 0.06 | 1.36 | 0.18 | 1.53 | 0.12 | 1.69 | 0.34 | 4.60 | **0.31** | **2.57** |
| **2017** | 0.14 | 0.80 | 0.07 | 0.38 | 0.01 | 0.07 | 0.00 | 0.77 | 0.02 | 0.10 | 0.01 | 1.12 | 0.05 | 0.31 | 0.02 | 1.36 | 0.15 | 0.89 | 0.08 | 1.49 | 0.21 | 2.29 | 0.18 | 2.18 |
| **2018** | 0.20 | **1.73** | **0.12** | 0.76 | 0.01 | 0.11 | 0.00 | 0.83 | 0.04 | 0.22 | 0.02 | 0.92 | 0.12 | 0.74 | 0.06 | 1.33 | 0.24 | 1.95 | 0.14 | 1.68 | 0.34 | 2.82 | 0.21 | 1.96 |
| **2019** | 0.18 | 1.60 | 0.11 | 0.75 | 0.01 | 0.13 | 0.00 | 0.83 | 0.03 | 0.19 | 0.03 | 0.92 | 0.07 | 0.43 | 0.03 | 1.12 | 0.22 | 1.80 | 0.13 | 1.67 | 0.39 | 4.14 | 0.30 | 2.00 |

***Table 4.24.*** *Statistical descriptive measures of Nutrients ($NH_4^+$, $NO_3^-$, $PO_4^{-3}$, and $SiO_4^{-4}$) mmol.$m^{-3}$ by month for Station 4 (off Ria Formosa).*

| Month | $NH_4^+$ | $NO_3^-$ | $PO_4^{-3}$ | $SiO_4^{-4}$ | $NH_4^+$ | $NO_3^-$ | $PO_4^{-3}$ | $SiO_4^{-4}$ | $NH_4^+$ | $NO_3^-$ | $PO_4^{-3}$ | $SiO_4^{-4}$ | $NH_4^+$ | $NO_3^-$ | $PO_4^{-3}$ | $SiO_4^{-4}$ | $NH_4^+$ | $NO_3^-$ | $PO_4^{-3}$ | $SiO_4^{-4}$ | $NH_4^+$ | $NO_3^-$ | $PO_4^{-3}$ | $SiO_4^{-4}$ |
|---|---|---|---|---|---|---|---|---|---|---|---|---|---|---|---|---|---|---|---|---|---|---|---|---|
| | IQR | | | | Min | | | | $Q_1$ | | | | Median | | | | $Q_3$ | | | | Max | | | |
| **Jan** | 0.07 | 0.57 | 0.06 | 0.25 | 0.07 | 0.36 | 0.04 | 1.47 | 0.18 | 1.36 | 0.09 | 1.59 | 0.20 | 1.68 | 0.12 | 1.76 | 0.25 | 1.92 | 0.15 | 1.85 | 0.28 | 2.73 | 0.19 | 1.98 |
| **Feb** | 0.07 | 1.35 | 0.08 | 0.37 | 0.03 | 0.30 | 0.02 | 1.49 | 0.20 | 1.71 | 0.12 | 1.77 | **0.23** | **2.34** | **0.17** | **1.93** | 0.28 | 3.06 | 0.20 | 2.13 | 0.33 | 4.16 | 0.28 | 2.44 |
| **Mar** | **0.22** | **1.96** | 0.10 | 0.39 | 0.06 | 0.46 | 0.03 | 1.14 | 0.10 | 0.78 | 0.06 | 1.56 | 0.17 | 1.80 | 0.13 | 1.67 | 0.32 | 2.74 | 0.16 | 1.94 | **0.42** | **5.71** | **0.31** | **2.57** |
| **Apr** | 0.12 | 0.64 | 0.06 | 0.20 | 0.02 | 0.22 | < 0.01 | 1.08 | 0.06 | 0.53 | 0.04 | 1.30 | 0.10 | 0.71 | 0.06 | 1.40 | 0.18 | 1.17 | 0.09 | 1.50 | 0.27 | 2.80 | 0.18 | 1.70 |
| **May** | 0.13 | 0.62 | 0.04 | **0.55** | 0.01 | 0.09 | < 0.01 | 0.83 | 0.02 | 0.20 | 0.02 | 0.93 | 0.04 | 0.45 | 0.04 | 1.22 | 0.15 | 0.82 | 0.06 | 1.47 | 0.22 | 1.65 | 0.13 | 1.71 |
| **Jun** | 0.06 | 0.36 | 0.03 | 0.28 | < 0.01 | < 0.01 | 0.01 | 0.86 | 0.01 | 0.09 | 0.02 | 0.95 | 0.03 | 0.27 | 0.03 | 0.99 | 0.06 | 0.45 | 0.04 | 1.23 | 0.32 | 1.63 | 0.13 | 1.93 |
| **Jul** | 0.02 | 0.11 | 0.02 | 0.16 | < 0.01 | 0.04 | < 0.01 | 0.78 | 0.00 | 0.09 | 0.02 | 0.89 | 0.01 | 0.15 | 0.02 | 0.95 | 0.02 | 0.19 | 0.03 | 1.05 | 0.31 | 1.34 | 0.11 | 1.48 |
| **Aug** | 0.01 | 0.14 | 0.01 | 0.19 | < 0.01 | 0.02 | < 0.01 | 0.76 | 0.00 | 0.07 | 0.01 | 0.83 | 0.01 | 0.13 | 0.01 | 0.93 | 0.02 | 0.21 | 0.02 | 1.02 | 0.07 | 0.30 | 0.04 | 1.38 |
| **Sep** | 0.04 | 0.18 | 0.02 | 0.23 | < 0.01 | 0.04 | < 0.01 | 0.85 | 0.00 | 0.08 | 0.01 | 0.88 | 0.02 | 0.15 | 0.02 | 0.98 | 0.04 | 0.26 | 0.03 | 1.11 | 0.08 | 0.51 | 0.06 | 1.27 |
| **Oct** | 0.04 | 0.29 | 0.02 | 0.25 | < 0.01 | 0.02 | < 0.01 | 0.98 | 0.01 | 0.10 | 0.02 | 1.08 | 0.04 | 0.24 | 0.02 | 1.17 | 0.05 | 0.39 | 0.03 | 1.33 | 0.26 | 1.09 | 0.09 | 1.66 |
| **Nov** | 0.17 | 1.37 | **0.11** | 0.26 | 0.01 | 0.07 | 0.01 | 1.19 | 0.04 | 0.21 | 0.02 | 1.41 | 0.14 | 0.88 | 0.07 | 1.60 | 0.21 | 1.58 | 0.13 | 1.68 | 0.27 | 3.18 | 0.23 | 1.88 |
| **Dec** | 0.12 | 1.05 | 0.09 | 0.37 | 0.03 | 0.19 | 0.02 | 1.36 | 0.10 | 0.61 | 0.05 | 1.40 | 0.16 | 0.97 | 0.08 | 1.59 | 0.22 | 1.66 | 0.14 | 1.77 | 0.39 | 4.14 | 0.30 | 2.01 |

## 4.5 Characterization of Station 5 (off Guadiana Estuary)

### 4.5.1 Chlorophyll-a Concentration

The extreme east station off Guadiana Estuary also shows a seasonal behaviour and the other stations (Fig. 4.16(a) and Fig. A.1 at Appendix A). The time series shows higher values in 2010 and 2011. The seasonally in this case have higher values in February and March, as seen in Fig. 4.16.(c).

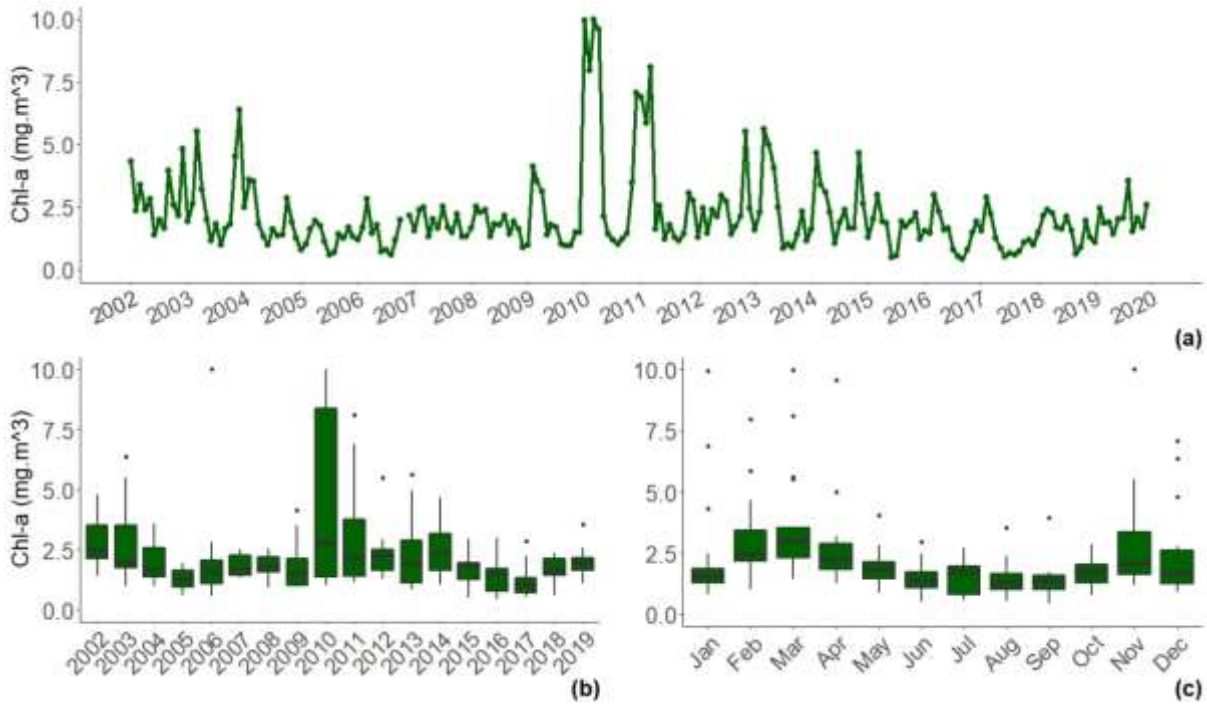


***Fig. 4.16.*** *Monthly chlorophyll-a concentration (Chl-a mg $m^{-3}$): (a) the time series plot; the boxplot (b) by year, and (c) by month for Station 5 (off Guadiana Estuary).*

Fig.4.16(b-c) and Table 4.25-26 indicated the maximum values of Chl-*a* in March 2010 (10 mg $m^{-3}$) and the minimum values in September 2016 (0.4 mg $m^{-3}$). The highest median and dispersion of Chl-*a* were found in 2010, with 50% of this year data falling between 1.4 and 8.4 mg $m^{-3}$. The year with the smallest dispersion is 2019 (IQR=0.5 mg $m^{-3}$), with 50% of the data values falling within [1.7, 2.2 mg $m^{-3}$].

Fig. 4.16(c) and Table 4.26 indicates the monthly variability of Chl-*a*. The higher median value was found in March (3.0 mg $m^{-3}$). In November, the dispersion presents the highest IQR value (1.7 mg $m^{-3}$), with 50% of Chl-*a* values falling within the interval [1.6, 3.4 mg $m^{-3}$]. January and September recorded the smallest dispersion (IQR=0.6 mg m-3), with half the Chl-*a* values falling within [1.3, 1.8 mg $m^{-3}$] and [1.0, 1.6 mg $m^{-3}$], respectively.

***Table 4.25.*** *Statistical descriptive measures of chlorophyll-a concentration (Chl-a mg $m^{-3}$) by year for Station 5(off Guadiana Estuary).*

| Year | IQR | Min | $Q_1$ | Median | $Q_3$ | Max |
|---|---|---|---|---|---|---|
| **2002** | 1.42 | 1.39 | 2.11 | 2.48 | 3.53 | 4.81 |
| **2003** | 1.76 | 1.00 | 1.76 | 1.96 | 3.52 | 6.38 |
| **2004** | 1.23 | 0.98 | 1.35 | 1.72 | 2.57 | 3.60 |
| **2005** | 0.69 | 0.60 | 0.95 | 1.28 | 1.65 | 1.94 |
| **2006** | 0.94 | 0.58 | 1.10 | 1.57 | 2.04 | 10.02 |
| **2007** | 0.82 | 1.32 | 1.44 | 1.67 | 2.26 | 2.51 |
| **2008** | 0.62 | 0.90 | 1.57 | 1.80 | 2.19 | 2.53 |
| **2009** | 1.09 | 0.94 | 1.02 | 1.49 | 2.11 | 4.13 |
| **2010** | 7.00 | 1.00 | 1.36 | 2.79 | 8.36 | 9.99 |
| **2011** | 2.35 | 1.17 | 1.40 | 2.17 | 3.75 | 8.09 |
| **2012** | 0.86 | 1.30 | 1.66 | 2.26 | 2.52 | 5.51 |
| **2013** | 1.76 | 0.84 | 1.12 | 1.93 | 2.88 | 5.63 |
| **2014** | 1.52 | 1.05 | 1.64 | 2.35 | 3.16 | 4.66 |
| **2015** | 0.70 | 0.49 | 1.26 | 1.88 | 1.96 | 2.98 |
| **2016** | 0.94 | 0.42 | 0.78 | 1.52 | 1.72 | 2.99 |
| **2017** | 0.62 | 0.52 | 0.71 | 1.05 | 1.32 | 2.87 |
| **2018** | 0.67 | 0.61 | 1.44 | 1.65 | 2.12 | 2.38 |
| **2019** | 0.51 | 1.09 | 1.65 | 1.97 | 2.16 | 3.55 |

***Table 4.26.*** *Statistical descriptive measures of chlorophyll-a concentration (Chl-a mg $m^{-3}$) by month for Station 5(off Guadiana Estuary).*

| Month | IQR | Min | $Q_1$ | Median | $Q_3$ | Max |
|---|---|---|---|---|---|---|
| **Jan** | 0.57 | 0.79 | 1.28 | 1.57 | 1.85 | 9.95 |
| **Feb** | 1.24 | 1.01 | 2.18 | 2.45 | 3.42 | 7.95 |
| **Mar** | 1.21 | 1.46 | 2.32 | 2.98 | 3.53 | 9.99 |
| **Apr** | 1.06 | 1.24 | 1.85 | 2.28 | 2.90 | 9.58 |
| **May** | 0.66 | 0.86 | 1.47 | 1.83 | 2.13 | 4.05 |
| **Jun** | 0.68 | 0.49 | 1.07 | 1.40 | 1.75 | 2.94 |
| **Jul** | 1.15 | 0.57 | 0.81 | 1.73 | 1.95 | 2.72 |
| **Aug** | 0.67 | 0.53 | 1.00 | 1.32 | 1.67 | 3.55 |
| **Sep** | 0.58 | 0.42 | 1.01 | 1.40 | 1.59 | 3.96 |
| **Oct** | 0.76 | 0.78 | 1.29 | 1.72 | 2.05 | 2.85 |
| **Nov** | 1.73 | 1.19 | 1.63 | 2.06 | 3.37 | 10.02 |
| **Dec** | 1.35 | 0.90 | 1.25 | 1.70 | 2.61 | 7.07 |

### 4.5.2 Sea Surface Temperature

A stable seasonality patterns are revealed over the time series in Fig. 4.17(a). The seasonal pattern presented in Fig.4.23(c) shows that the SST are at a minimum in February, steadily increases until August and then begins declining until February.

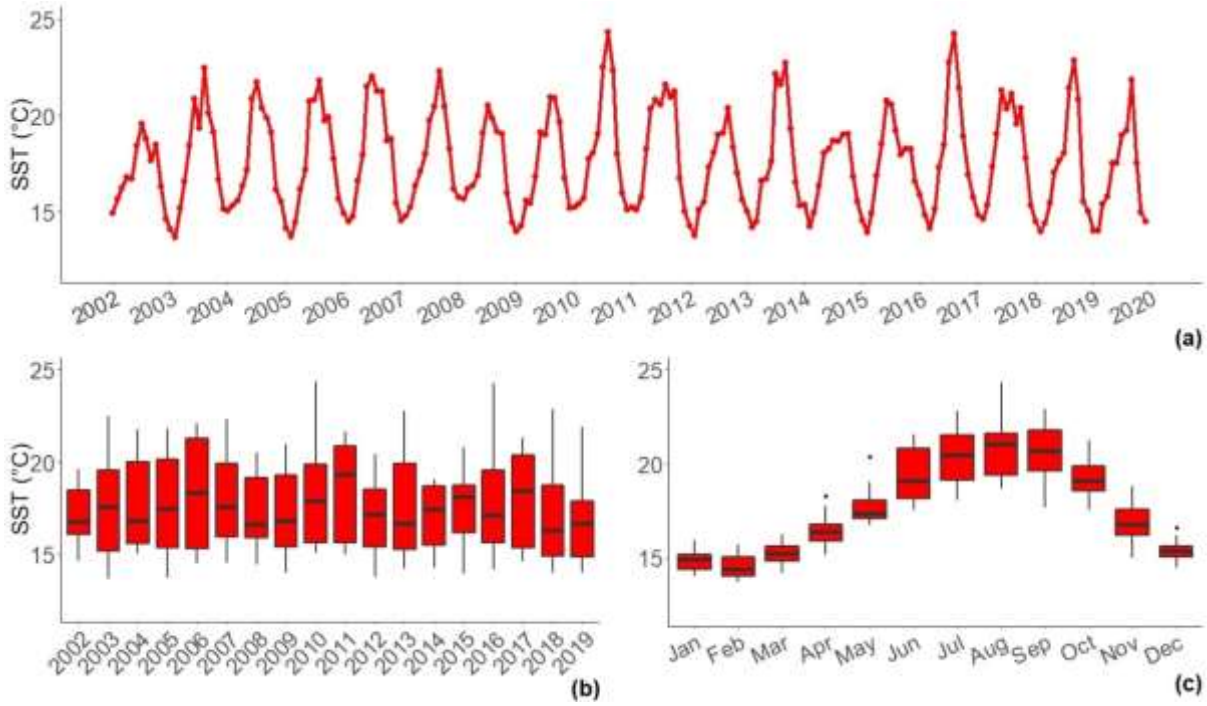


***Fig. 4.17.*** *Monthly time series of sea surface temperature (SST-°C): (a) the time series plot; the boxplot (b) by year, and (c) by month for Station 5(off Guadiana Estuary).*

The minimum and the maximum values of the SST were found in February 2005 (13.7 ºC) and in August 2016 (24.3 ºC), respectively (Fig. 4.17(b–c); Table (4.27 and 4.28)). The highest median value of the dataset was found in the year 2011 (19.3 ºC). The dispersion of the data (IQR) was high in 2006 (5.9 ºC), with 50% of the data found between 15.3-21.3 ºC, while the smallest dispersion was found in 2002 (IQR=2.4 ºC), falling within [16.1, 18.4 ºC] interval.

***Table 4.27.*** *Statistical descriptive measures of sea surface temperature (SST-ºC) by year for Station 5(off Guadiana Estuary).*

| Year | IQR | Min | $Q_1$ | Median | $Q_3$ | Max |
|---|---|---|---|---|---|---|
| **2002** | 2.4 | 14.6 | 16.1 | 16.8 | 18.4 | 19.6 |
| **2003** | 4.4 | 13.7 | 15.2 | 17.6 | 19.6 | 22.5 |
| **2004** | 4.4 | 15.1 | 15.6 | 16.8 | 20.0 | 21.7 |
| **2005** | 4.8 | 13.7 | 15.4 | 17.5 | 20.1 | 21.8 |
| **2006** | 5.9 | 14.5 | 15.3 | 18.3 | 21.3 | 22.1 |
| **2007** | 4.0 | 14.6 | 15.9 | 17.6 | 19.9 | 22.3 |
| **2008** | 3.2 | 14.5 | 15.9 | 16.6 | 19.1 | 20.5 |
| **2009** | 3.9 | 14.0 | 15.4 | 16.8 | 19.3 | 20.9 |
| **2010** | 4.2 | 15.1 | 15.6 | 17.9 | 19.9 | 24.3 |
| **2011** | 5.2 | 15.0 | 15.6 | 19.3 | 20.8 | 21.6 |
| **2012** | 3.1 | 13.8 | 15.4 | 17.2 | 18.5 | 20.4 |
| **2013** | 4.7 | 14.2 | 15.2 | 16.7 | 19.9 | 22.8 |
| **2014** | 3.2 | 14.2 | 15.5 | 17.4 | 18.7 | 19.0 |
| **2015** | 2.6 | 13.9 | 16.2 | 18.1 | 18.7 | 20.8 |
| **2016** | 3.9 | 14.2 | 15.6 | 17.1 | 19.5 | 24.3 |
| **2017** | 5.0 | 14.6 | 15.4 | 18.4 | 20.4 | 21.3 |
| **2018** | 3.8 | 14.0 | 14.9 | 16.3 | 18.8 | 22.9 |
| **2019** | 3.0 | 14.0 | 14.9 | 16.6 | 17.9 | 21.9 |

The highest median value was found in August (21.0 ºC) (Fig. 4.17 (c) and Table 4.28). The highest dispersion was observed in June (IQR = 2.6 ºC), with 50% of the SST values falling within the interval [18.2, 20.8 ºC]. Alternatively, the smallest dispersion was noted in December (IQR=0.5 ºC), with 25% of values being above 15.6 ºC and below 15ºC.

***Table 4.28.*** *Statistical descriptive measures of sea surface temperature (SST-ºC) by month for Station 5(off Guadiana Estuary).*

| Month | IQR | Min | $Q_1$ | Median | $Q_3$ | Max |
|---|---|---|---|---|---|---|
| **Jan** | 0.8 | 14.0 | 14.3 | 14.9 | 15.2 | 15.9 |
| **Feb** | 1.0 | 13.7 | 14.0 | 14.4 | 15.0 | 15.7 |
| **Mar** | 0.8 | 14.2 | 14.8 | 15.2 | 15.6 | 16.2 |
| **Apr** | 0.9 | 15.1 | 15.9 | 16.4 | 16.8 | 18.3 |
| **May** | 1.0 | 16.7 | 17.1 | 17.3 | 18.1 | 20.4 |
| **Jun** | 2.6 | 17.5 | 18.2 | 19.1 | 20.8 | 21.5 |
| **Jul** | 2.4 | 18.1 | 19.1 | 20.4 | 21.5 | 22.8 |
| **Aug** | 2.2 | 18.7 | 19.4 | 21.0 | 21.6 | 24.3 |
| **Sep** | 2.2 | 17.7 | 19.6 | 20.7 | 21.8 | 22.9 |
| **Oct** | 1.3 | 17.5 | 18.5 | 19.1 | 19.9 | 21.2 |
| **Nov** | 1.4 | 15.0 | 16.2 | 16.8 | 17.6 | 18.8 |
| **Dec** | 0.5 | 14.5 | 15.0 | 15.3 | 15.6 | 16.6 |

### 4.5.3 Nutrients

The time series plot (Fig. 4.18(a)) for Station 5 shows that for nutrients $NH_4^+$, $PO_4^{-3}$, and $SiO_4^{-4}$ the seasonal amplitude and patterns are constant over the time. For $NO_3^-$ the seasonal pattern shows a peak in 2010 and shows a different seasonal amplitude for the remaining period.

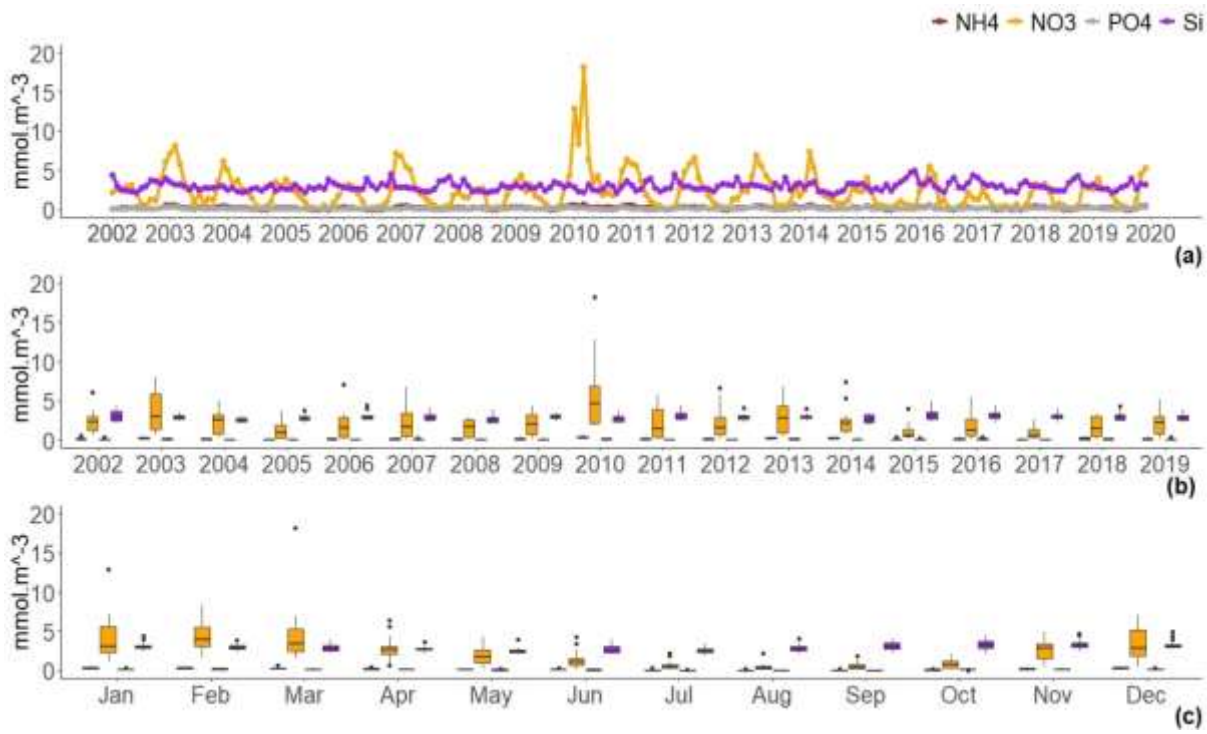


***Fig. 4.18.*** *Monthly time series of nutrient ($NH_4^+$, $NO_3^-$, $PO_4^{-3}$, and $SiO_4^{-4}$): (a) the time series plot; the boxplot (b) by year, and (c) by month for Station 5 (off Guadiana Estuary).*

$NH_4^+$ and $NO_3^-$ (Fig. 4.18(b) and Table (4.29)) revealed maximum values in March 2010, with 0.7 and 18.2 mmol.m$^{-3}$ of concentration values, respectively. The maximum concentration value for $PO_4^{-3}$ found in March 2016 (0.4 mmol.m$^{-3}$) and for $SiO_4^{-4}$ found in December 2015 (4.97 mmol.m$^{-3}$). The minimum concentration values for $NH_4^+$ found in August 2005 (0.01 mmol.m$^{-3}$), for $NO_3^-$ found in August 2016 (0.08 mmol.m$^{-3}$), $SiO_4^{-4}$ found in August 2010 (0.01 mmol.m$^{-3}$) and for $PO_4^{-3}$ discovered in July 2014 with 1.9 mmol.m$^{-3}$.

The highest median was found in 2010 for two nutrients $NO_3^-$ and $NH4^+$with greater than 0.3 and 4.6 mmol.m$^{-3}$, respectively. The highest median value for $PO_4^{-3}$ discovered in 2013 (0.13 mmol.m$^{-3}$) and for $SiO_4^{-4}$ found in 2016 (3.2 mmol.m$^{-3}$).

Table 4.29 displays the lowest IQR value for $NO_3^-$ and $NH4^+$ in 2015 with 0.9 and 0.07 mmol.m$^{-3}$, respectively. The lowest IQR value for $PO_4^{-3}$ revealed in 2005(0.03 mmol.m$^{-3}$) and

for $SiO_4^{-4}$ in 2004 with 0.4 mmol.m$^{-3}$. The higher IQR value for $NO_3^-$ and $PO_4^{-3}$ discovered in 2010 with values of 4.7 and 0.18 mmol.m$^{-3}$, respectively. The higher IQR value for $NH4^+$ discovered in 2018 (0.3 mmol.m$^{-3}$) and for $SiO_4^{-4}$ found in 2002 (1.2 mmol.m$^{-3}$).

The higher dispersion for $PO_4^{-3}$ showed half of the data between 0.03 and 0.21 mmol.m$^{-3}$, while the smallest dispersion falls within [0.05 mmol.m$^{-3}$, 0.09 mmol.m$^{-3}$]. $SiO_4^{-4}$ showed 50% of the data value for higher dispersion between 2.93 and 3.6 mmol.m$^{-3}$ and for smallest dispersion between 2.6 and 2.8 mmol.m$^{-3}$. Half of the $NH_4^+$data for higher dispersion found between 0.04 and 0.33 mmol.m$^{-3}$ and for smallest dispersion falls within [0.03, 0.1 mmol.m$^{-3}$]. 50% of $NO_3^-$ data for higher dispersion found between 2.2 and 6.83 mmol.m$^{-3}$ and for smallest dispersion falls within [0.5, 1.4 mmol.m$^{-3}$].

Fig. 4.18 (c) and Table 4.30 illustrates the monthly variability of nutrients. The highest median value for $NH_4^+$, $NO_3^-$ and $PO_4^{-3}$ recorded in February with 0.3, 4.0 and 0.2 mmol.m$^{-3}$, respectively. The highest median value for $SiO_4^{-4}$ found in November with value of 3.3 mmol.m$^{-3}$. In November, the dispersion presents the highest IQR value for $NH_4^+$ and $NO_3^-$ with 0.2 and 0.74 mmol.m$^{-3}$, respectively. For highest dispersion, 50% of $NH_4^+$ data values were found between 0.21 and 0.41 mmol.m$^{-3}$ and for $NO_3^-$ within [1.9, 5.14 mmol.m$^{-3}$]. March present the higher dispersion (IQR=0.14) for $PO_4^{-3}$ with half of the data falling within [0.07, 0.21 mmol.m$^{-3}$]. In October, the dispersion presents the highest IQR value for $SiO_4^{-4}$ (0.88 mmol.m$^{-3}$) and the lowest IQR value for $PO_4^{-3}$(0.01). For highest dispersion, half of $SiO_4^{-4}$ data for found between 0.42 and 1.02 mmol.m$^{-3}$. For lowest dispersion, 50% of $PO_4^{-3}$ data values falling within [0.06, 0.07 mmol.m$^{-3}$]. $NO_3^-$showed the lowest IQR value in August (0.4 mmol.m$^{-3}$) with 50% values falling within [0.16, 0.52 mmol.m$^{-3}$]. $NH_4^+$ showed the lowest IQR value in July (0.03 mmol.m$^{-3}$) with 50% values falling within [0.02, 0.05 mmol.m$^{-3}$]. May indicated the lowest IQR value for $SiO_4^{-4}$ (0.32 mmol.m$^{-3}$) with half the values falling within [2.3, 2.62 mmol.m$^{-3}$].

***Table 4.29.*** *Statistical descriptive measures of Nutrients ($NH_4^+$, $NO_3^-$, $PO_4^{-3}$, and $SiO_4^{-4}$) mmol.$m^{-3}$ by year for Station 5 (off Guadiana Estuary).*

| Year | $NH_4^+$ | $NO_3^-$ | $PO_4^{-3}$ | $SiO_4^{-4}$ | $NH_4^+$ | $NO_3^-$ | $PO_4^{-3}$ | $SiO_4^{-4}$ | $NH_4^+$ | $NO_3^-$ | $PO_4^{-3}$ | $SiO_4^{-4}$ | $NH_4^+$ | $NO_3^-$ | $PO_4^{-3}$ | $SiO_4^{-4}$ | $NH_4^+$ | $NO_3^-$ | $PO_4^{-3}$ | $SiO_4^{-4}$ | $NH_4^+$ | $NO_3^-$ | $PO_4^{-3}$ | $SiO_4^{-4}$ |
|---|---|---|---|---|---|---|---|---|---|---|---|---|---|---|---|---|---|---|---|---|---|---|---|---|
| | IQR | | | | Min | | | | $Q_1$ | | | | Median | | | | $Q_3$ | | | | Max | | | |
| **2002** | 0.11 | 1.69 | 0.06 | 1.15 | 0.02 | 0.56 | 0.03 | 2.18 | 0.09 | 1.27 | 0.06 | 2.48 | 0.13 | 2.32 | 0.07 | 2.93 | 0.19 | 2.96 | 0.12 | 3.63 | 0.54 | 6.09 | 0.31 | 4.34 |
| **2003** | 0.17 | 4.49 | 0.11 | 0.38 | 0.11 | 0.67 | 0.01 | 2.48 | 0.19 | 1.34 | 0.05 | 2.72 | 0.27 | 3.04 | 0.10 | 2.93 | 0.36 | 5.84 | 0.16 | 3.10 | 0.51 | 8.12 | 0.31 | 3.54 |
| **2004** | 0.12 | 2.38 | 0.05 | 0.36 | 0.01 | 0.22 | 0.01 | 2.12 | 0.08 | 0.84 | 0.03 | 2.39 | 0.17 | 2.52 | 0.06 | 2.56 | 0.20 | 3.22 | 0.08 | 2.75 | 0.24 | 4.99 | 0.11 | 3.16 |
| **2005** | 0.17 | 1.63 | 0.03 | 0.45 | < 0.01 | 0.09 | 0.01 | 2.13 | 0.02 | 0.27 | 0.05 | 2.60 | 0.08 | 0.95 | 0.06 | 2.77 | 0.19 | 1.90 | 0.09 | 3.06 | 0.22 | 3.81 | 0.10 | 3.81 |
| **2006** | 0.18 | 2.55 | 0.08 | 0.48 | < 0.01 | 0.08 | 0.03 | 2.56 | 0.02 | 0.35 | 0.03 | 2.64 | 0.11 | 1.60 | 0.06 | 2.86 | 0.20 | 2.90 | 0.11 | 3.12 | 0.35 | 7.08 | 0.13 | 4.46 |
| **2007** | 0.16 | 2.88 | 0.07 | 0.77 | 0.02 | 0.19 | 0.01 | 2.24 | 0.05 | 0.52 | 0.03 | 2.51 | 0.15 | 1.71 | 0.07 | 2.75 | 0.21 | 3.40 | 0.10 | 3.28 | 0.39 | 6.76 | 0.22 | 4.12 |
| **2008** | 0.16 | 2.18 | 0.07 | 0.65 | < 0.01 | 0.19 | 0.02 | 2.20 | 0.03 | 0.34 | 0.05 | 2.26 | 0.15 | 1.71 | 0.08 | 2.61 | 0.19 | 2.53 | 0.12 | 2.92 | 0.26 | 2.99 | 0.20 | 3.86 |
| **2009** | 0.22 | 2.57 | 0.10 | 0.43 | < 0.01 | 0.15 | 0.03 | 2.39 | 0.04 | 0.67 | 0.06 | 2.76 | 0.15 | 2.01 | 0.08 | 3.01 | 0.26 | 3.24 | 0.15 | 3.19 | 0.52 | 4.34 | 0.28 | 3.49 |
| **2010** | 0.24 | 4.68 | 0.18 | 0.61 | 0.17 | 1.84 | < 0.01 | 2.13 | 0.22 | 2.15 | 0.03 | 2.39 | 0.31 | 4.62 | 0.10 | 2.69 | 0.46 | 6.83 | 0.21 | 3.00 | 0.68 | 18.16 | 0.26 | 3.63 |
| **2011** | 0.22 | 3.55 | 0.06 | 0.84 | < 0.01 | 0.10 | < 0.01 | 2.29 | 0.03 | 0.35 | 0.02 | 2.63 | 0.14 | 1.49 | 0.03 | 2.84 | 0.25 | 3.90 | 0.08 | 3.47 | 0.47 | 5.76 | 0.16 | 4.48 |
| **2012** | 0.18 | 2.21 | 0.05 | 0.43 | 0.01 | 0.15 | 0.05 | 2.23 | 0.04 | 0.73 | 0.07 | 2.65 | 0.15 | 1.59 | 0.08 | 2.92 | 0.21 | 2.94 | 0.12 | 3.07 | 0.34 | 6.60 | 0.16 | 4.06 |
| **2013** | 0.25 | 3.40 | 0.14 | 0.40 | 0.06 | 0.42 | 0.01 | 2.45 | 0.09 | 0.88 | 0.05 | 2.76 | 0.20 | 2.80 | 0.13 | 3.04 | 0.34 | 4.28 | 0.19 | 3.17 | 0.40 | 6.87 | 0.26 | 4.04 |
| **2014** | 0.21 | 1.52 | 0.12 | 1.00 | 0.04 | 0.72 | 0.04 | 1.89 | 0.09 | 1.13 | 0.06 | 2.25 | 0.17 | 2.10 | 0.08 | 2.60 | 0.31 | 2.65 | 0.18 | 3.24 | 0.49 | 7.39 | 0.31 | 3.44 |
| **2015** | 0.07 | 0.90 | 0.06 | 0.94 | < 0.01 | 0.19 | 0.03 | 2.34 | 0.03 | 0.46 | 0.04 | 2.68 | 0.06 | 0.56 | 0.07 | 3.07 | 0.10 | 1.37 | 0.10 | 3.61 | 0.40 | 3.99 | 0.26 | 4.97 |
| **2016** | 0.20 | 2.09 | 0.12 | 0.69 | 0.01 | 0.08 | 0.02 | 2.20 | 0.07 | 0.58 | 0.05 | 2.79 | 0.16 | 1.25 | 0.11 | 3.17 | 0.27 | 2.68 | 0.17 | 3.48 | 0.50 | 5.49 | 0.37 | 4.40 |
| **2017** | 0.11 | 1.01 | 0.09 | 0.50 | < 0.01 | 0.13 | 0.01 | 2.21 | 0.03 | 0.33 | 0.03 | 2.75 | 0.06 | 0.54 | 0.05 | 3.10 | 0.14 | 1.34 | 0.12 | 3.25 | 0.27 | 2.73 | 0.19 | 4.01 |
| **2018** | 0.29 | 2.48 | 0.16 | 0.65 | 0.01 | 0.15 | 0.01 | 2.35 | 0.04 | 0.50 | 0.05 | 2.54 | 0.14 | 1.45 | 0.10 | 2.91 | 0.33 | 2.98 | 0.21 | 3.18 | 0.44 | 3.31 | 0.24 | 4.28 |
| **2019** | 0.16 | 2.10 | 0.10 | 0.56 | 0.02 | 0.12 | 0.04 | 2.20 | 0.06 | 0.85 | 0.05 | 2.58 | 0.15 | 2.18 | 0.08 | 2.76 | 0.22 | 2.95 | 0.15 | 3.14 | 0.45 | 5.24 | 0.33 | 3.93 |

**Table 4.30.** Statistical descriptive measures of Nutrients ($NH_4^+$, $NO_3^-$, $PO_4^{-3}$, and $SiO_4^{-4}$) $mmol.m^{-3}$ by month for Station 5 (off Guadiana Estuary).

| Month | $NH_4^+$ | $NO_3^-$ | $PO_4^{-3}$ | $SiO_4^{-4}$ | $NH_4^+$ | $NO_3^-$ | $PO_4^{-3}$ | $SiO_4^{-4}$ | $NH_4^+$ | $NO_3^-$ | $PO_4^{-3}$ | $SiO_4^{-4}$ | $NH_4^+$ | $NO_3^-$ | $PO_4^{-3}$ | $SiO_4^{-4}$ | $NH_4^+$ | $NO_3^-$ | $PO_4^{-3}$ | $SiO_4^{-4}$ | $NH_4^+$ | $NO_3^-$ | $PO_4^{-3}$ | $SiO_4^{-4}$ |
|---|---|---|---|---|---|---|---|---|---|---|---|---|---|---|---|---|---|---|---|---|---|---|---|---|
| | IQR | | | | Min | | | | $Q_1$ | | | | Median | | | | $Q_3$ | | | | Max | | | |
| **Jan** | 0.16 | 3.22 | 0.06 | 0.39 | 0.12 | 1.24 | 0.07 | 2.46 | 0.22 | 2.34 | 0.11 | 2.83 | 0.26 | 3.10 | 0.14 | 3.01 | 0.38 | 5.57 | 0.17 | 3.22 | 0.51 | 12.86 | 0.31 | 4.34 |
| **Feb** | 0.17 | 2.49 | 0.13 | 0.41 | 0.12 | 1.64 | 0.03 | 2.33 | 0.21 | 3.04 | 0.10 | 2.72 | 0.29 | 3.97 | 0.17 | 2.81 | 0.38 | 5.53 | 0.23 | 3.13 | 0.51 | 8.31 | 0.31 | 3.86 |
| **Mar** | 0.17 | 2.88 | 0.14 | 0.59 | 0.10 | 1.52 | 0.04 | 2.21 | 0.17 | 2.36 | 0.07 | 2.56 | 0.19 | 3.44 | 0.12 | 2.76 | 0.34 | 5.24 | 0.21 | 3.15 | 0.68 | 18.16 | 0.37 | 3.80 |
| **Apr** | 0.08 | 0.96 | 0.09 | 0.32 | 0.04 | 0.62 | 0.00 | 2.12 | 0.15 | 2.10 | 0.05 | 2.58 | 0.19 | 2.61 | 0.08 | 2.67 | 0.23 | 3.07 | 0.14 | 2.90 | 0.38 | 6.34 | 0.27 | 3.59 |
| **May** | 0.11 | 1.55 | 0.05 | 0.32 | 0.02 | 0.22 | 0.00 | 2.13 | 0.07 | 1.03 | 0.04 | 2.30 | 0.14 | 1.78 | 0.06 | 2.42 | 0.19 | 2.58 | 0.09 | 2.62 | 0.29 | 4.28 | 0.16 | 3.98 |
| **Jun** | 0.08 | 0.92 | 0.06 | 0.76 | 0.00 | 0.08 | 0.01 | 2.09 | 0.06 | 0.63 | 0.02 | 2.28 | 0.09 | 1.04 | 0.06 | 2.47 | 0.13 | 1.54 | 0.08 | 3.03 | 0.29 | 4.30 | 0.11 | 3.95 |
| **Jul** | 0.03 | 0.40 | 0.03 | 0.48 | 0.00 | 0.15 | 0.00 | 1.89 | 0.02 | 0.35 | 0.02 | 2.31 | 0.04 | 0.46 | 0.03 | 2.53 | 0.05 | 0.74 | 0.05 | 2.78 | 0.34 | 2.22 | 0.14 | 3.36 |
| **Aug** | 0.03 | 0.36 | 0.02 | 0.45 | 0.00 | 0.08 | 0.00 | 2.12 | 0.00 | 0.16 | 0.02 | 2.57 | 0.02 | 0.33 | 0.03 | 2.78 | 0.04 | 0.52 | 0.04 | 3.02 | 0.24 | 2.17 | 0.06 | 4.05 |
| **Sep** | 0.05 | 0.55 | 0.03 | 0.83 | 0.01 | 0.12 | 0.01 | 2.21 | 0.02 | 0.19 | 0.02 | 2.71 | 0.03 | 0.38 | 0.04 | 3.06 | 0.07 | 0.74 | 0.05 | 3.54 | 0.21 | 1.88 | 0.10 | 4.04 |
| **Oct** | 0.07 | 0.81 | 0.01 | 0.88 | 0.01 | 0.11 | 0.02 | 2.13 | 0.03 | 0.35 | 0.06 | 2.84 | 0.08 | 0.81 | 0.06 | 3.21 | 0.10 | 1.16 | 0.07 | 3.72 | 0.23 | 2.09 | 0.10 | 4.48 |
| **Nov** | 0.17 | 1.93 | 0.12 | 0.54 | 0.04 | 0.47 | 0.03 | 2.42 | 0.13 | 1.51 | 0.07 | 3.00 | 0.24 | 2.82 | 0.13 | 3.31 | 0.30 | 3.44 | 0.19 | 3.54 | 0.44 | 4.95 | 0.33 | 4.73 |
| **Dec** | 0.20 | 3.25 | 0.09 | 0.38 | 0.06 | 0.45 | 0.06 | 2.75 | 0.21 | 1.89 | 0.10 | 2.94 | 0.27 | 2.81 | 0.14 | 3.07 | 0.41 | 5.14 | 0.19 | 3.32 | 0.54 | 7.08 | 0.33 | 4.97 |

## 4.6 Comparison between Stations for Chl-*a* and SST

Fig. 4.19 shows the inter-annual variability of Chl-*a* and SST where the seasonal component is compared for different years of the time series. In this figure, it is possible to see a clear inverse relationship between SST and Chl-*a* for all stations. For the time interval 2002-2019, a similar Chl-*a* seasonal amplitude and variations over the years is observed with a relatively good level of correspondence in the southern-western transition stations (Station 1, 2 and 3). In common with Stations 4 and 5, peak Chl-*a* were observed in the year 2010 and 2011 in contrast to the other three stations.

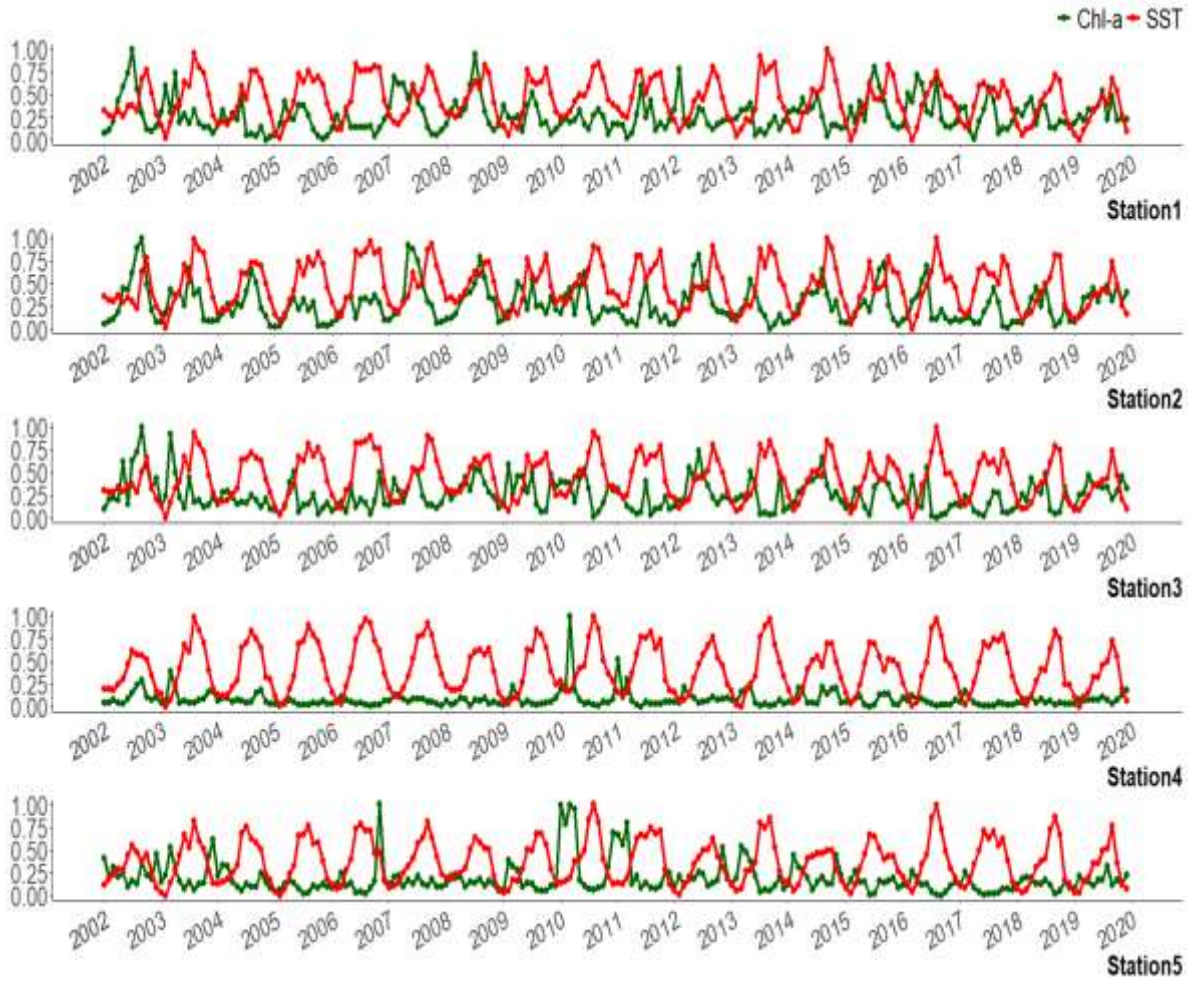


***Fig. 4.19.*** *Time series plot between chlorophyll-a concentration (Chl-a mg $m^{-3}$) and sea surface temperature (SST-ºC) for all Stations in the south coast of Portugal (Algarve coast).*

Monthly Chl-*a* concentrations, at a seasonal time scale, show an evident general tendency to behave an opposite relation to SST, where when Chl-*a* values increases/decreases SST values decreases/increases (Fig. 4.20). Seasonal SST patterns are evident in all stations, with high

median values of SST during Summer and Autumn and falling during winter. It also observed that the median SST value generally decreased towards from Station 5 to Station 1. For all South-western transition stations (Station1, 2 and 3), the Chl-*a* concentration values were found to increase during early spring until summer and decrease during Autumn. For Station 4 and 5, high Chl-*a* values were found only in winter and spring. Generally, a high range of Chl-*a* was observed in south-western study stations (1, 2 and 3), during the summer (Jun-Sept) than in the south-eastern study stations.

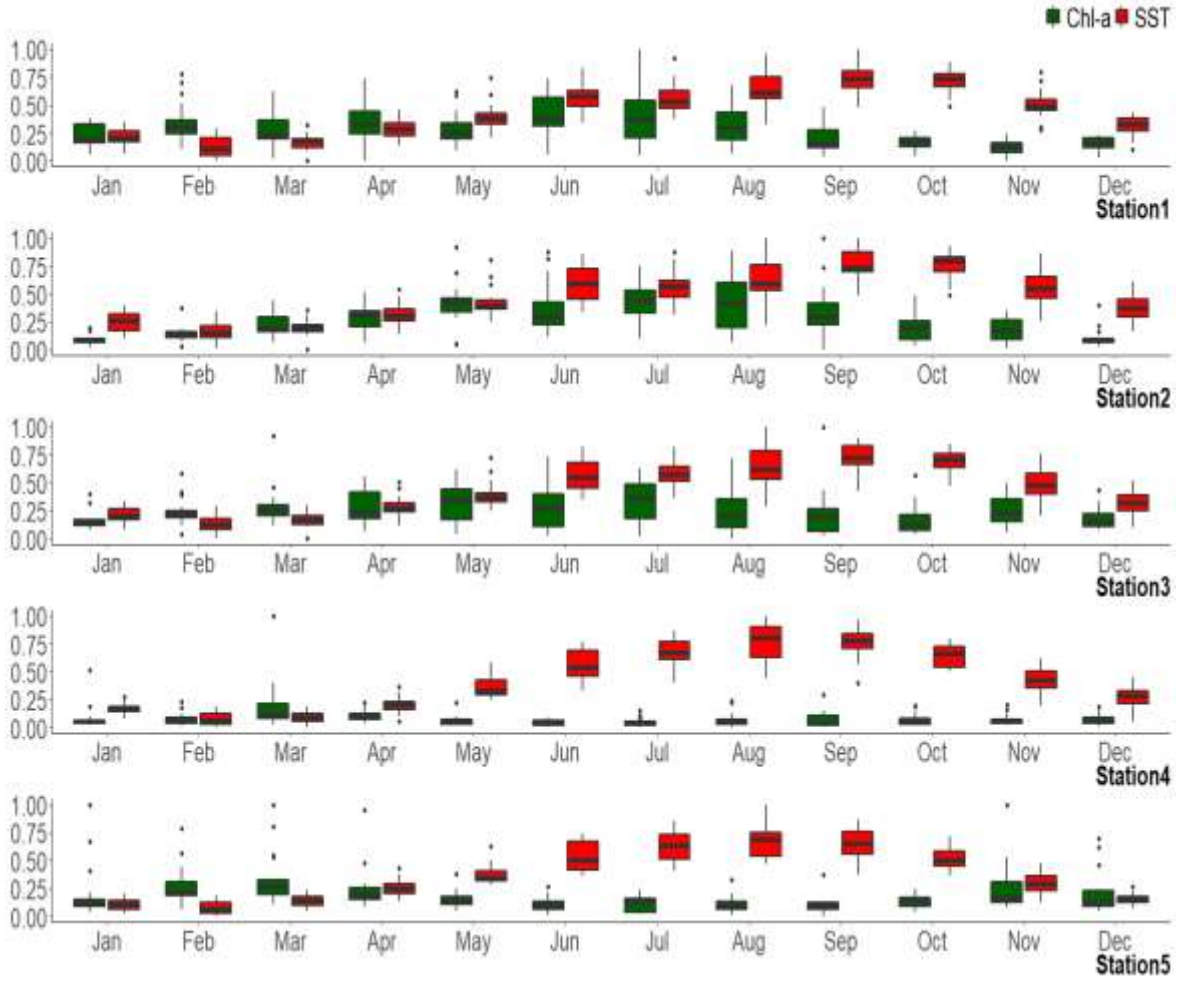


***Fig. 4.20.*** *Boxplot by month between chlorophyll-a concentration (Chl-a mg $m^{-3}$) and sea surface temperature (SST-ºC) for all Stations in the south coast of Portugal (Algarve coast).*

The highest median (1.77 mg $m^{-3}$), the maximum (10 mg $m^{-3}$) and the higher dispersion (IQR=1.7 mg $m^{-3}$) of Chl-*a* values are observed at Station 5 , The lowest median (0.1 mg $m^{-3}$) and the smallest dispersion (IQR=0.1 mg $m^{-3}$) of Chl-*a* values are observed at Sation-4. The minimum values were observed in winter for the Stations 3, 4 and 5 and late autumn for stations 1 and 2. Generally, the higher dispersion for SST were identify between the months of June to

August in all the stations. For Stations 1, 2 and 3 the higher dispersion for Chl-*a* was also record during the months of summer in opposite to Station 4 and 5 where the higher dispersion was recorded in the months of March and November, respectively.

## 4.7 Comparison between Stations for Chl-*a* and Nutrients

Fig. 4.21 shows the inter-annual variability between Chl-*a* and nutrients ($NH_4^+$, $NO_3^-$, $PO_4^{-3}$, and $SiO_4^{-4}$) where the seasonal component is compared for different years of the time series. Generally, between all the stations is the Station 5 that shown the high median values for Chl-a and for $NH_4^+$, $NO_3^-$ and $SiO_4^{-4}$ and is Station 4 with the lower median values for Chl-a and for the nutrients for the study period. The Stations 1, 2 and 3 are similar, however, is the Station 3 that show higher median for Chl-a and $SiO_4^{-4}$ is the Station 2 with higher $NH_4^+$ and $NO_3^-$ .

***Table 4. 31**: The median values of chlorophyll-a concentration (Chl-a mg $m^{-3}$) and nutrients (NH4+, NO3-, PO4-3, and SiO4-4) for each station during the study period.*

| | **Station 1** | **Station 2** | **Station 3** | **Station 4** | **Station 5** |
|---|---|---|---|---|---|
| **Chl-*a*** | 0.65 | 0.82 | 1.02 | 0.41 | 1.77 |
| **$NH_4^+$** | 0.13 | 0.14 | 0.11 | 0.07 | 0.16 |
| **$NO_3^-$** | 1.22 | 1.26 | 1.23 | 0.47 | 1.80 |
| **$PO_4^{-3}$** | 0.10 | 0.10 | 0.10 | 0.04 | 0.07 |
| **$SiO_4^{-4}$** | 1.49 | 1.45 | 1.54 | 1.37 | 2.85 |

For **Station 1**, the Chl-*a* concentration showed low seasonal amplitude in 2006, 2010 and 2013 compared to nutrients, while the rest of the year both showed the same annual seasonal pattern (Fig. 4.21). When the Chl-*a* concentration was low between November and March the four-target nutrient concentration value was high (Fig. 4.22). Between June and October, Chl-*a* and $SiO_4^{-4}$ showed higher value when $NH_4^+$, $NO_3^-$ and $PO_4^{-3}$ showed low concentration value. The $NH_4^+$, $NO_3^-$ and $PO_4^{-3}$ showed a strong seasonal cycle with maxima in winter/spring and minima in summer/autumn compared to Chl-*a*. In contrast to nutrients, the Chl-*a* showed a strong seasonality with maxima in summer and minima in winter. Considering the median concentration value, $NO_3^-$ and $SiO_4^{-4}$ observed highest value during winter (February) (Fig. 4.5 (c)) and during summer Chl-*a* observed the highest median value (June) (Fig. 4.1 (c)).

Regarding Station 2 , seasonal amplitude is variable between Chl-*a* and nutrients (Fig. 4.21). The Chl-*a* presents higher concentration value during summer (June-August), while nutrients present higher concentration value between winter and spring (November-May) (Fig. 4.22). In

contrast to nutrients, with months of December-February Chl-*a* presents very low values in the study area.

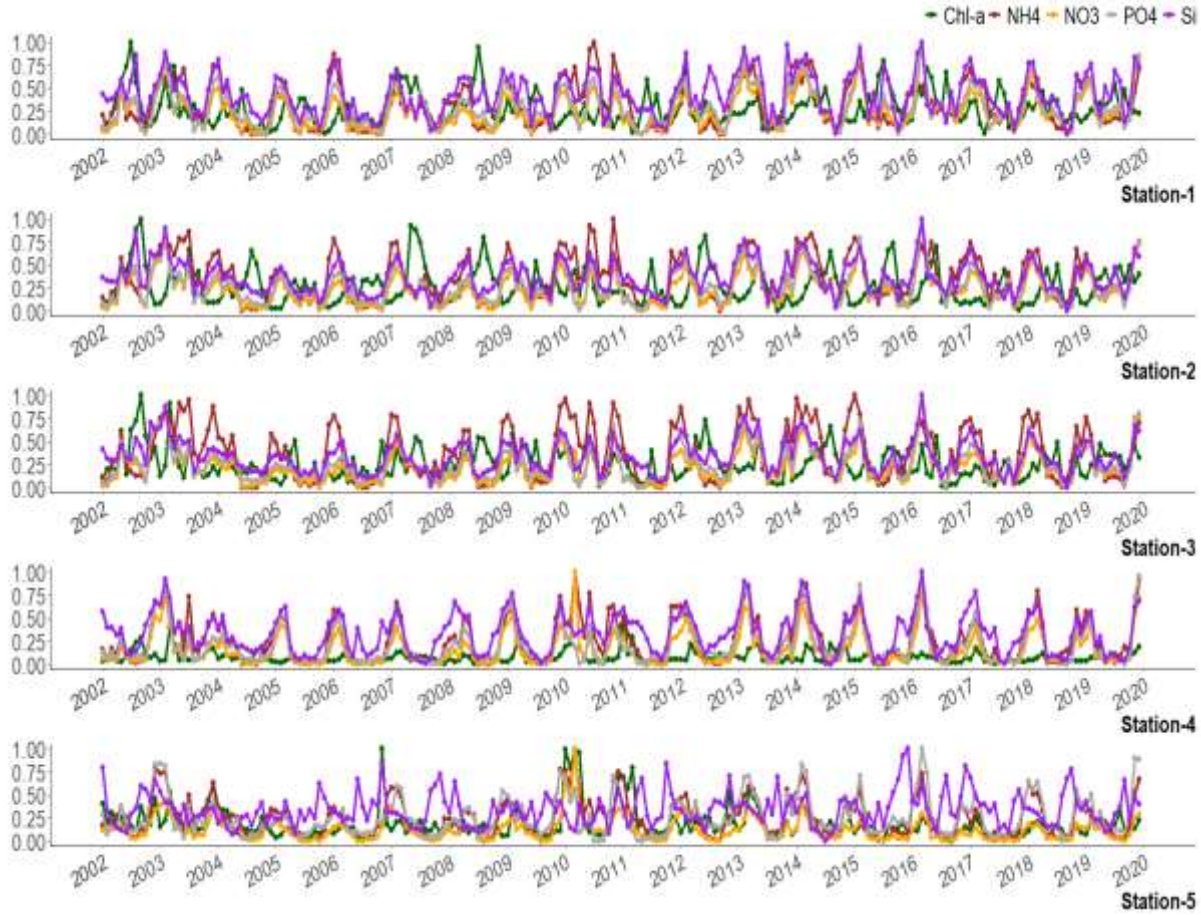


***Fig. 4.21.*** *Timeseries plot between Chl-a and Nutrients for all Stations.*

Concerning Station 3, a seasonal amplitude of Chl-*a* showed a little delayed with respect to nutrients (Fig. 4.21). The targeted nutrients showed a clear inverse seasonal cycle with a maximum in winter and spring and minima in summer compared to Chl-*a* for this station (Fig. 4.22). When the Chl-*a* present some low values during winter (December to March) the four-target nutrient concentration values was high. The Chl-*a* present higher concentration value during summer (June to September) while all nutrients present a low concentration value. Station 4 has a general tendency to present low Chl-*a* and nutrient values during summer periods and highest concentration values mainly during winter and spring. In 2010 a high $NO_3^-$ seasonal peak observed. Station 5 clearly showed the direct seasonal cycle relation between Chl-*a* and nutrients. In 2010 and 2011 higher $NH_4^+$, $NO_3^-$ and $PO_4^{-3}$ and Chl-*a* seasonal peaks observed (Fig. 4.22). The Chl-*a* and $NH_4^+$, $NO_3^-$ and $PO_4^{-3}$ have a general tendency to present some low concentration values during June to November, while $SiO_4^{-4}$ showed higher values.

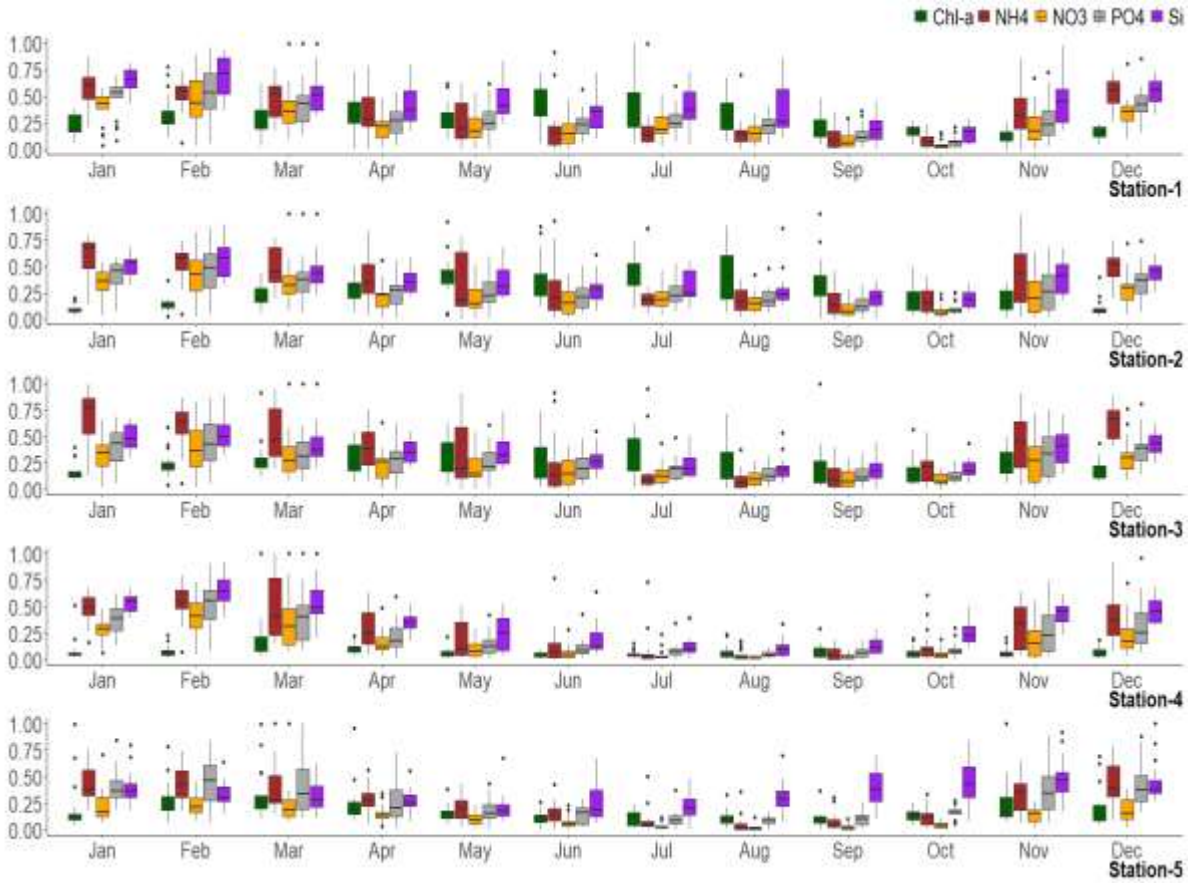


***Fig. 4.22.*** *Boxplot by month between Chl-a and Nutrients for all Stations.*

## 4.8 Relationship between Chl-*a* and SST

The Spearman's rank correlation coefficients between of SST and Chl-*a* were calculated for the selected stations, and the results are shown in Table 4.31 (see Appendix A for scatter plot, Fig.A.13.). A statistically significant association (at 5% level of significance) were found for the study stations, with exception of Station 2 . The association between the Chl-*a* and SST is negative for Station 1 , 3, 4 and 5. There was a weak correlation for Station 1 and 3, and a moderate negative correlation for Station 4 and 5 (Table 4.31).

***Table 4.32.*** *Spearman's Correlation coefficients (rs) between sea surface temperature (SST-ºC) and chlorophyll-a concentration (Chl-a mg $m^{-3}$) from 2002 to 2019 for the study Stations off the south coast of Portugal.*

| | $r_s$ | p-value |
|---|---|---|
| **Station 1** | -0.19 | 0.01 |
| **Station 2** | 0.1 | 0.16 |
| **Station 3** | -0.24 | 0.0004 |
| **Station 4** | -0.4 | $1.1e^{-9}$ |
| **Station 5** | -0.48 | $2.2e^{-16}$ |

## 4.9 Relationship between Chl-*a* and Nutrients

The $r_s$ computed between Chl-*a* and selected nutrients ($NO_3^-$, $NH_4^+$, $PO_4^{-3}$, and $SiO_4^{-4}$) for all stations are shown in Table 4.32 (scatter plot are in Appendix A in Fig A. (14-17)). Significant correlation coefficients were found between Chl-*a* with $NO_3^-$ and $PO_4^{-3}$ in all four Stations with exception for Station 2, with $NH_4^+$ observed in Station (2, 4 and 5) and with $SiO_4^{-4}$ found in Station (1, 3 and 4). There was a moderate positive association between Chl-*a* and $NO_3^-$, $NH_4^+$, and $PO_4^{-3}$ for Station 5. Chl-*a* presents a weak relationship with $NH_4^+$ and $SiO_4^{-4}$ for Station 2, as seen in Table 4.33.

***Table 4.33.*** *Spearman's Correlation coefficients ($r_s$) between Nutrients and chlorophyll-a concentration (Chl-a mg $m^{-3}$) from 2002 to 2019 for the study Stations.*

| | $NH_4^+$ | | $NO_3^-$ | | $PO_4^{-3}$ | | $SiO_4^{-4}$ | |
|---|---|---|---|---|---|---|---|---|
| | $r_s$ | p-value | $r_s$ | p-value | $r_s$ | p-value | $r_s$ | p-value |
| **Station 1** | 0.11 | 0.12 | 0.27 | 0.0001 | 0.26 | 0.0002 | 0.16 | 0.02 |
| **Station 2** | -0.18 | 0.01 | 0.02 | 0.78 | 0.02 | 0.77 | -0.11 | 0.10 |
| **Station 3** | 0.07 | 0.27 | 0.33 | $1.0e^{-06}$ | 0.30 | $7.1e^{-06}$ | 0.26 | 0.0001 |
| **Station 4** | 0.28 | $2.2e^{-05}$ | 0.36 | $7.3e^{-08}$ | 0.34 | $4.7e^{-07}$ | 0.23 | 0.001 |
| **Station 5** | 0.48 | $1.2e^{-13}$ | 0.57 | $2.2e^{-16}$ | 0.47 | $2.2e^{-16}$ | -0.02 | 0.74 |

# Chapter 5: Discussion

The Chl-*a* distribution and variability in the coastal region are highly correlated with environmental factors, e.g., SST, river discharge, coastal upwelling, and frontal zones. Also, these factors are intercorrelated. For example, a wind-driven upwelling event can impact the nutrient distribution and subsequently determine the Chl-*a* levels (Yu *et al.* 2019). In addition to the impact on Chl-*a*, the upwelling event also brought deep and cold ocean water to surface water, which induced a decrease in SST and increase nutrient concentration (Kämpf & Chapman 2016). Wind-driven upwelling and riverine input are the major factors influencing phytoplankton communities in the Portuguese coast (Krug *et al.* 2017b, Afonso Ferreira *et al.* 2021). This probably why our findings show low Chl-*a* concentration in Station 4 and 5 which they are far away from the upwelling region. Our result observed lower Chl-*a* values during summer in these stations compared to southwest transitional zone (Station 1, 2 and 3).

The southwestern transition zone of coastal stations (Station 1, 2 and 3) has a showed a similar seasonal pattern, with Chl-*a* concentration increasing during early spring and reaching the maximum during summer. The same findings were also previously reported by Navarro & Ruiz (2006) and Ferreira *et al.* (2021). In contrast to the west side the coastal stations in the east side of Algarve coast (Station 4 and 5), have typical Chl-*a* maximum in spring and decline toward summer, that was also consistent with previous results by Ferreira *et al.* (2021) showing a decreasing in Chl-*a* from spring to summer near Gulf of Cádiz. As a result, the high Chl-*a* values are associated with low SST values.

The nutrients ($NH_4^+$, $NO_3^-$ , $PO_4^{-3}$, and $SiO_4^{-4}$) higher values were observed during March much early when compared to Chl-*a* for all stations. This is probably the reason high Chl-*a* recorded later on during summer after the phytoplankton thrive.

In particular for **Station 1** (off Aljezur), the correlation among Chl-*a* time series and the corresponding SST were found statistically significance at $\alpha$=5%. In addition, there was a weak negative relationship between Chl-*a* and SST, and a weak positive relationship between Chl-*a* and nutrients ($NH_4^+$, $NO_3^-$ , $PO_4^{-3}$, and $SiO_4^{-4}$). This finding revealed that the coupling between Chl-*a* and SST and nutrients could independently impact on the Chl-*a* variability. The seasonality exhibited by Chl-*a* and SST was consistent with the earlier observations (Danchenko *et al.* 2019). Danchenko *et al.* (2019) result suggested that the high magnitude of upwelling caused SST to be decrease in response to wind forcing in the second half of January

2015. Our result also showed a minimum recorded SST value during February 2015. It is to be noted that low SST observation values are associated with strong upwelling events (Loureiro *et al.* 2005, Danchenko *et al.* 2019). The upwelling season in this region appears during summer (March to September) and is characterised by a well-defined upwelling season in response to northerly wind and during winter, characterised by generalised northward flow (Relvas *et al.* 2009). Danchenko *et al.* (2019) found a higher nutrient concentration from March to early April 2016 due to an upwelling event in the study area. Our result also found the maximum value of $NO_3^-$, $PO_4^{-3}$, and $SiO_4^{-4}$ recorded in March 2016. As the results of Danchenko *et al.* (2019), our results show that the concentration of $NO_3^-$ and $SiO_4^{-4}$ were the main nutrients that showed higher variability in February and August.

Chl-*a* in **Station 2** (off Sagres) followed a seasonal cycle like that of Station 1 . The results generally showed high SST values during summer and higher nutrient concentration values during winter (March). According to Loureiro *et al.* (2005), this region's seasonal upwelling occurs mainly during early spring to late summer. Our findings showed high nutrient concentration values and low SST values in early spring, this result probably related to the upwelling event in the region. Similar to the results of Goela *et al.* (2014), our results show a negative correlation between Chl-*a* and the concentration of $SiO_4^{-4}$ ($r_s$=-0.11, p-value< 0.05). This suggests that silicates act as a limiting nutrient since silicate is essential for phytoplankton bloom development (Danchenko *et al.* 2019). Previous studies by Loureiro *et al.* (2005) and Danchenko *et al.* (2019) revealed that spring and summer phytoplankton blooms are caused by the nutrient enrichment caused by upwelling events and occur from March to August in the Sagres region.

Cardeira *et al.* (2013) showed that Chl-*a* is negatively correlated with SST and positively correlated to nutrients ($NH_4^+$, $NO_3^-$ , $PO_4^{-3}$, and $SiO_4^{-4}$) in the **Station 3 (**off Portimão), which is consistent with our results. The correlation among Chl-*a* with SST and nutrients ($NO_3^-$ , $PO_4^{-3}$, and $SiO_4^{-4}$) were statistically significant (p-value < 0.05). Additionally, the Chl-*a* concentration values varies between 0.43 and 2.25 mg $m^3$ in October (2002-2019). Likewise, based on satellite data Cardeira *et al.* (2013) found very similar nearshore Chl-*a* values for the same month but for the year of 2006 (0.3 and 3 mg $m^3$) and have suggested that this results were due to an upwelling event occurred in October near this study station.

At **Station 4** (off Ria Formosa), the Chl-*a* concentration attains its maximum in in early spring. This summer (march-sept) upwelling event was previously reported by Cardeira *et al.*

(2013), and Krug *et al.* (2017). This event can be seen also in our results, although Chl-*a* values during winter (March) are slightly higher. Our findings showed that during 2010 the maximum Chl-*a* (5 mg $m^{-3}$) was associated with higher nitrate and ammonium values, for early spring that can be related with occurance of a phytoplanton bloom in the coastal station.

In general, Chl-*a* in **Station 5** (off Guadiana Estuary) have a seasonal pattern, with high values during winter and low values during summer. The maximum Chl-*a* (10 mg $m^{-3}$) were found in early spring (March) 2010 and 2011 and associated with higher nitrate, phosphate, and ammonium values. This results can be associated to the significant water release from the Alqueva dam to the Guadiana River, during the first months of 2010 and 2011, with discharge roughly between 1,000 and 2,500 $m^3$/s according to Garel (2017). Furthermore, in this station a moderate negative relation between Chl-*a* and SST, and a positive relationship between Chl-*a* and nutrients were observed, except silicate.

To summarise, the oceanography of the south coast of Portugal (Algarve) is characterised by a marked seasonal upwelling related to the large-scale wind climatology (Relvas & Barton 2002). Because of the strong seasonality of the upwelling in the region, the high nutrient availability and low SST have might an impact on the Chl-*a* concentration along the south coast of Portugal. Chl-*a* has been used as the leading indicator of the productivity trophic condition and proxy of phytoplankton biomass in estuaries and coastal and oceanic systems for a long period of time (Boyer *et al.* 2009, Goela *et al.* 2014, Agirbas & Karadeniz 2020). Chl-*a* reflects the overall phytoplankton growth and loss process in coastal waters. As a result, the factors impact on the distribution of phytoplankton should be accounted for in marine management processes to maintain the provision of utilised ecosystem service. The study area is well known for aquaculture's economic activity, which depends on phytoplankton production. Therefore, it is important to consider phytoplankton growth development in the southern Portugal coast as an indicator of restoration success because blooms could significantly harm the coastal systems. Phytoplankton management must be accounted in marine management processes, to maintain provision of utilised ecosystem service (Tweddle *et al.* 2018). Its importance to the climate cycle, ecosystem functions, and benefits to people, should be considered within marine management decision-making.

# Conclusions and Recommendation

This thesis aimed to characterise the inter-annual variability of the Chl-*a* concentration retrieved by multi ocean colour sensors data and relate these variabilities to the coastal environmental changes in the south Portuguese coast. For seventeen years, Chl-*a*, SST, and nutrients ($NH_4^+$, $NO_3^-$, $PO_4^{-3}$, and $SiO_4^{-4}$) monthly data obtained from Copernicus Marine Service as Level-4 product was used. Statistical analyses have been performed for five stations distributed over the whole study area.

To conclude, the following answer are made regarding to the research questions:

**What is the seasonal behaviour of the Chl-*a* concentration along the southern Portugal coast?**

In general, Station 1, 2 and 3 have a similar seasonal pattern for Chl-*a*, with high values in summer and lower values in winter. Considering Stations 4 and 5, although they share a similar seasonality between them, Station 5 register higher values during winter and spring and Station 4 during the early spring.

**What is the impact of the physical and chemical variables on Chl-*a* at the coastal waters?**

Our study reveals that Chl-*a* and SST present a statistically significant association for Stations 1, 3, 4 and 5. Although they present a negative relationship in these stations, indicating that when SST decreases the Chl-*a* increases, only Station 5 present a moderate correlation coefficient.

In respect to the impact of the nutrients on Chl-*a,* Station 1 and 3 have a positive association between Chl-*a* and $NO_3^-$, $PO_4^{-3}$ and $SiO_4^{-4}$; Station 2 only show a negative significant association with $NH_4^+$; the Chl-*a* in Station 4 is statistically significant with all the nutrients; and Chl-*a* of Station 5 present the highest correlation coefficient (among all the stations) for $NH_4^+$, $NO_3^-$, and $PO_4^{-3}$.

**Which stations in southern Portugal are more susceptible to the impacts of environmental variables on the variation of the Chl-*a*?**

Stations 1, 2 and 3 are more susceptible to the impacts of the environmental variables. Especially in the summer months when higher median values of Chl-*a* and the higher IQR

ranges for SST were registered, coinciding with the season of upwelling events in the study area.

Station 5 also show that the high values of Chl-*a* and nitrate, phosphate, and ammonium values in particular years (2010, 2011) were associated with a significant water release from the Alqueva dam to the Guadiana River, during years. This indicate that the Chl-*a* variability is susceptible to the river discharges.

The Station 4 located off Ria Formosa is the one where the environmental variables have a smaller impact on the Chl-*a* variability.

**How helpful is the measurement of Chl-*a* for coastal managers and the characterisation of coastal waters using open-source satellite data?**

The satellite data showed a promising approach to characterise the Chl-*a* and confirms their efficacy as an alternative tool and valuable approach to study environmental conditions of the coastal waters. Consequently, the acquired satellite products are provided relevant information to study the coastal environmental changes on the south coast of Portugal.

## Future Scope

The present master thesis reveals the possibility of using satellite ocean colour data to study the environmental conditions of the south Portuguese coastal waters. There is a scope to improve the characterise of the coastal water dynamics by utilizing daily composite multi-sensor data. It will be worthwhile to know whether any such relation exists in daily average data. Forthcoming, this study may find utility in fishery management and water quality monitoring as Chl-*a* is a crucial information in the above field.

In this study higher nutrient availability and low SST have an impact on the Chl-*a* concentration along the southern Portugal coastal zone. It is also noted that other features such as upwelling event and river flow have great impact on the Chl-*a* availability in the area and they must be included in further investigation

More importantly, changes in phytoplankton bloom should considered in marine management and monitored to function the coastal ecosystem. Marine management such as potential marine protected area creation, regulating and licensing commercial fisheries, identifying the environmental status of the ocean, stakeholder engagement are amongst the

management initiatives. The author recommends, further studies on adaptation management using the result of this study.

# References


Agirbas, E. & Karadeniz, M.N. (2020) Phytoplankton pigment indices and pigment-based phytoplankton size classes along the south-eastern Black Sea. *Reg. Stud. Mar. Sci.*, 39, 101393, Elsevier B.V. doi:10.1016/j.rsma.2020.101393

Ángel, E.S. del, Núñez, R.M., Silvera, A.G. & Medrano, R.C. (2006) Comparison of In Situ and Remotely-Sensed Chl- a Concentrations : A Statistical Examination of the Match-up Approach, 241–259.

Arabi, B., Salama, M.S., Pitarch, J. & Verhoef, W. (2020) Integration of in-situ and multi-sensor satellite observations for long-term water quality monitoring in coastal areas. *Remote Sens. Environ.*, 239, Elsevier Inc. doi:10.1016/j.rse.2020.111632

Baban, S.M.J. (1996) Télédétection appliquée à la classification trophique et au contrôle des écosystèmes lacustres. *Hydrol. Sci. J.*, 41, 939–957. doi:10.1080/02626669609491560

Baladrón, A.A., Levier, B. & Sotillo, M.G. (2020) PRODUCT USER MANUAL: For Atlantic -Iberian Biscay Irish- Ocean Physics Reanalysis Monthly Product. *E.U. Copernicus Mar. Serv. Inf.*, 4.0.

Barbosa, A.B., Domingues, R.B. & Galvão, H.M. (2010) Environmental forcing of phytoplankton in a mediterranean estuary (guadiana estuary, south-western iberia): A decadal study of anthropogenic and climatic influences. *Estuaries and Coasts*, 33, 324–341. doi:10.1007/s12237-009-9200-x

Barlow, R., Stuart, V., Lutz, V., Sessions, H., Sathyendranath, S. & Platt, T. (2007) Seasonal pigment patterns of surface phytoplankton in the subtropical southern hemisphere, 54, 1687–1703. doi:10.1016/j.dsr.2007.06.010

Bishara, A.J. & Hittner, J.B. (2012) Testing the significance of a correlation with nonnormal data: Comparison of Pearson, Spearman, transformation, and resampling approaches. *Psychol. Methods*, 17, 399–417. doi:10.1037/a0028087

Blondeau-Patissier, D., Tilstone, G.H., Martinez-Vicente, V. & Moore, G.F. (2004) Comparison of bio-physical marine products from SeaWiFS, MODIS and a bio-optical model with in situ measurements from Northern European waters. *J. Opt. A Pure Appl. Opt.*, 6, 875–889. doi:10.1088/1464-4258/6/9/010

Blondeau, P.D., Gower, J.F.R., Dekker, A.G., Phinn, S.R. & Brando, V.E. (2014) A review of ocean color remote sensing methods and statistical techniques for the detection, mapping and analysis of phytoplankton blooms in coastal and open oceans. *Prog. Oceanogr.*, 123, 123–144, Elsevier Ltd. doi:10.1016/j.pocean.2013.12.008

Boss, E. & Behrenfeld, M. (2010) In situ evaluation of the initiation of the North Atlantic phytoplankton bloom. *Geophys. Res. Lett.*, 37, 1–5. doi:10.1029/2010GL044174

Boyer, J.N., Kelble, C.R., Ortner, P.B. & Rudnick, D.T. (2009) Phytoplankton bloom status: Chlorophyll a biomass as an indicator of water quality condition in the southern estuaries of Florida, USA. *Ecol. Indic.*, 9, 56–67. doi:10.1016/j.ecolind.2008.11.013

Brito, A.C., Garrido-Amador, P., Gameiro, C., Nogueira, M., Moita, M.T. & Cabrita, M.T. (2020) Integrating in situ and ocean color data to evaluate ecological quality under the water framework directive. *Water (Switzerland)*, 12, 1–24. doi:10.3390/w12123443

Caballero, I., Fernández, R., Escalante, O.M., Mamán, L. & Navarro, G. (2020) New capabilities of Sentinel-2A/B satellites combined with in situ data for monitoring small harmful algal blooms in complex coastal waters. *Sci. Rep.*, 10, 1–14. doi:10.1038/s41598-020-65600-1

Cabrita, M.T., Silva, A., Oliveira, P.B., Angélico, M.M. & Nogueira, M. (2015) Assessing eutrophication in the Portuguese continental Exclusive Economic Zone within the European Marine Strategy Framework Directive. *Ecol. Indic.*, 58, 286–299, Elsevier Ltd. doi:10.1016/j.ecolind.2015.05.044

Cardeira, S., Rita, F., Relvas, P. & Cravo, A. (2013) Chlorophyll a and chemical signatures during an upwelling event off the South Portuguese coast (SW Iberia). *Cont. Shelf Res.*, 52, 133–149, Elsevier. doi:10.1016/j.csr.2012.11.011

Carretero, P.P.B., Otero, J., Land, P.E., Groom, S. & Álvarez-Salgado, X.A. (2019) Seasonal and inter-annual variability of net primary production in the NW Iberian margin (1998–2016) in relation to wind stress and sea surface temperature. *Prog. Oceanogr.*, 178, Elsevier Ltd. doi:10.1016/j.pocean.2019.102135

Chatfield, C. (2004) *The Analysis of Time Series*. *J. Am. Stat. Assoc.*, Boca Raton: Chapman and Hall/CRC Press. doi:10.1080/01621459.1928.10503036

Colella, S., Böhm, E., Cesarini, C., Garnesson, P., J.Netting & Calton, B. (2021) PRODUCT

USER MANUAL: For All Ocean Colour Products. *Copernicus Mar. Serv.*

Corredor-Acosta, A., Cortés-Chong, N., Acosta, A., Pizarro-Koch, M., Vargas, A., Medellín-Mora, J., Saldías, G.S., *et al.* (2020) Spatio-temporal variability of chlorophyll-a and environmental variables in the Panama bight. *Remote Sens.*, 12. doi:10.3390/rs12132150

Cravo, A., Relvas, P., Cardeira, S., Rita, F., Madureira, M. & Sánchez, R. (2010) An upwelling filament off southwest Iberia: Effect on the chlorophyll a and nutrient export. *Cont. Shelf Res.*, 30, 1601–1613. doi:10.1016/j.csr.2010.06.007

Cristina, S., Cordeiro, C., Lavender, S., Goela, P.C., Icely, J. & Newton, A. (2016) MERIS phytoplankton time series products from the SW Iberian Peninsula (Sagres) using seasonal-trend decomposition based on loess. *Remote Sens.*, 8, MDPI AG. doi:10.3390/rs8060449

Cristina, S., Icely, J., Costa Goela, P., Angel DelValls, T. & Newton, A. (2015) Using remote sensing as a support to the implementation of the European Marine Strategy Framework Directive in SW Portugal. *Cont. Shelf Res.*, 108, 169–177, Elsevier Ltd. doi:10.1016/j.csr.2015.03.011

Cristina, S., Icely, J.D. & Newton, A. (2019) The application of remote sensing for monitoring the Ria Formosa: the sentinel missions. in *Ria Formosa: challenges of a coastal lagoonin a changing environment.* eds. Aníbal, J., Gomes, A., Mendes, I. & Moura, D., pp. 139–151, Faro: University of Algarve. https://sapientia.ualg.pt/handle/10400.1/12475

Dalwinder, S. & Birmohan, S. (2022) Feature wise normalization: An effective way of normalizing data. *Pattern Recognit.*, 122, 108307, Elsevier Ltd. doi:10.1016/j.patcog.2021.108307

Danchenko, S., Fragoso, B., Guillebault, D., Icely, J., Berzano, M. & Newton, A. (2019) Harmful phytoplankton diversity and dynamics in an upwelling region (Sagres, SW Portugal) revealed by ribosomal RNA microarray combined with microscopy. *Harmful Algae*, 82, 52–71, Elsevier. doi:10.1016/j.hal.2018.12.002

European Commission. (2000) Directive 2000/60/EC of the European Parliament and of the Council of 23 October 2000 establishing a framework for Community actions in the field of water policy. *Off. J. Eur. Communities L327/1*, 1–72.

European Commission. (2008) Directive 2008/56/EC of the European Parliament and of the

Council of 17 June 2008 establishing a framework for Community actions in the field of marine environmental policy (Marine Strategy Framework Directive). *Off. J. Eur. Communities L164/19*, 19–39.

Falkowski, P.G. (1997) Photosynthesis: The paradox of carbon dioxide efflux. *Curr. Biol.*, 7, 637–639. doi:10.1016/s0960-9822(06)00322-8

Falkowski, P.G., Katz, M.E., Knoll, A.H., Quigg, A., Raven, J.A., Schofield, O. & Taylor, F.J.R. (2004) The evolution of modern eukaryotic phytoplankton. *Science (80-. ).*, 305, 354–360. doi:10.1126/science.1095964

Farmer, A., Mee, L., Langmead, O., Cooper, P., Kannen, A., Kershaw, P. & Cherrier, V. (2012) The Ecosystem Approach in Marine Management. *EU FP7 KNOWSEAS Proj.* doi:10.4324/9781849775533

Ferreira, A., Garrido-Amador, P. & Brito, A.C. (2019) Disentangling environmental drivers of phytoplankton biomass off Western Iberia. *Front. Mar. Sci.*, 6, 1–17. doi:10.3389/fmars.2019.00044

Ferreira, Afonso, Brotas, V., Palma, C., Borges, C. & Brito, A.C. (2021) Assessing phytoplankton bloom phenology in upwelling-influenced regions using ocean color remote sensing. *Remote Sens.*, 13, 1–27. doi:10.3390/rs13040675

Ferreira, J.G., Andersen, J.H., Borja, A., Bricker, S.B., Camp, J., Cardoso da Silva, M., Garcés, E., *et al.* (2011) Overview of eutrophication indicators to assess environmental status within the European Marine Strategy Framework Directive. *Estuar. Coast. Shelf Sci.*, 93, 117–131, Elsevier Ltd. doi:10.1016/j.ecss.2011.03.014

Garel, E. (2017) Present dynamics of the Guadiana estuary. *UALG CIMA*. doi:http://hdl.handle.net/10400.1/9887

Garel, Pinto, L., Santos, A. & Ferreira, O. (2009) Estuarine , Coastal and Shelf Science Tidal and river discharge forcing upon water and sediment circulation at a rock-bound estuary ( Guadiana estuary , Portugal ). *Estuar. Coast. Shelf Sci.*, 84, 269–281, Elsevier Ltd. doi:10.1016/j.ecss.2009.07.002

Garnesson, P., Mangin, A., D'Andon, O.F., Demaria, J. & Bretagnon, M. (2019) The CMEMS GlobColour chlorophyll a product based on satellite observation: Multi-sensor merging and flagging strategies. *Ocean Sci.*, 15, 819–830. doi:10.5194/os-15-819-2019

Gibb, S.W. (2000) Surface phytoplankton pigment distributions in the Atlantic Ocean : an assessment of basin scale variability between 50 ° N and 50 ° S, 45, 339–368.

Goela, Cordeiro, C., Danchenko, S., Icely, J., Cristina, S. & Newton, A. (2016) Time series analysis of data for sea surface temperature and upwelling components from the southwest coast of Portugal. *J. Mar. Syst.*, 163, 12–22, Elsevier B.V. doi:10.1016/j.jmarsys.2016.06.002

Goela, P.C., Danchenko, S., Icely, J.D., Lubian, L.M., Cristina, S. & Newton, A. (2014) Using CHEMTAX to evaluate seasonal and interannual dynamics of the phytoplankton community off the South-west coast of Portugal. *Estuar. Coast. Shelf Sci.*, 151, 112–123, Elsevier Ltd. doi:10.1016/j.ecss.2014.10.001

Gohin, F., Druon, J.N. & Lampert, L. (2002) A five channel chlorophyll concentration algorithm applied to Sea WiFS data processed by SeaDAS in coastal waters. *Int. J. Remote Sens.*, 23, 1639–1661. doi:10.1080/01431160110071879

Gohin, F., Zande, D. Van der, Tilstone, G., Eleveld, M.A., Lefebvre, A., Andrieux-Loyer, F., Blauw, A.N., *et al.* (2019) Twenty years of satellite and in situ observations of surface chlorophyll-a from the northern Bay of Biscay to the eastern English Channel. Is the water quality improving? *Remote Sens. Environ.*, 233, Elsevier Inc. doi:10.1016/j.rse.2019.111343

Greenhalgh, S. & Selman, M. (2008) EUTROPHICATION AND HYPOXIA IN COASTAL AREAS: A GLOBAL ASSESSMENT OF THE STATE OF KNOWLEDGE. *World Resour. Inst.*, 1. Retrieved from www.wri.org%0Awww.researchgate.net/publication/287774312

Gurlin, D., Gitelson, A.A. & Moses, W.J. (2011) Remote estimation of chl-a concentration in turbid productive waters - Return to a simple two-band NIR-red model? *Remote Sens. Environ.*, 115, 3479–3490, Elsevier Inc. doi:10.1016/j.rse.2011.08.011

Harshada, D., Raman, M. & Jayappa, K.S. (2021) Evaluation of the operational Chlorophyll-a product from global ocean colour sensors in the coastal waters, south-eastern Arabian Sea. *Egypt. J. Remote Sens. Sp. Sci.*, 24, 769–786, National Authority for Remote Sensing and Space Sciences. doi:10.1016/j.ejrs.2021.09.005

Harvey, E.T., Kratzer, S. & Philipson, P. (2015) Satellite-based water quality monitoring for improved spatial and temporal retrieval of chlorophyll-a in coastal waters. *Remote Sens. Environ.*, 158, 417–430, Elsevier Inc. doi:10.1016/j.rse.2014.11.017

Hendry, G.A.F. (1996) Chlorophylls and chlorophyll derivatives. *Nat. Food Color.*, 131–156. doi:10.1007/978-1-4615-2155-6_5

Hu, C., Lee, Z. & Franz, B. (2012) Chlorophyll a algorithms for oligotrophic oceans: A novel approach based on three-band reflectance difference. *J. Geophys. Res. Ocean.*, 117, 1–25. doi:10.1029/2011JC007395

Hyndman, R.J. & Athanasopoulos, G. (2018) *Forecasting: Principles and Practice*. *OTexts*, nd edition., Vol. 19, Melbourne, Australia. doi:10.2307/1054108

IOCCG. (2000) Remote Sensing of Ocean Colour in Coastal, and Other Optically-Complex,Waters. *Reports Int. Ocean. Coord. Gr.*, 59, 144. doi:http://dx.doi.org/10.25607/OBP-95

IOCCG. (2018) *Earth Observations in Support of Global Water Quality Monitoring*. *Reports Monogr. Int. Ocean Colour Coord. Gr.*, Vol. 17.

Kahru, M., Gille, S.T., Murtugudde, R., Strutton, P.G., Manzano-Sarabia, M., Wang, H. & Mitchell, B.G. (2010) Global correlations between winds and ocean chlorophyll. *J. Geophys. Res. Ocean.*, 115, 1–11. doi:10.1029/2010JC006500

Kämpf, J. & Chapman, P. (2016) *Upwelling Systems of the World*. *Upwelling Syst. World*. doi:10.1007/978-3-319-42524-5

Klemas, V. (2011) Remote sensing techniques for studying coastal ecosystems: An overview. *J. Coast. Res.*, 27, 2–17. doi:10.2112/JCOASTRES-D-10-00103.1

Kratzer, S., Therese Harvey, E. & Philipson, P. (2014) The use of ocean color remote sensing in integrated coastal zone management-A case study from Himmerfjärden, Sweden. *Mar. Policy*, 43, 29–39, Elsevier. doi:10.1016/j.marpol.2013.03.023

Krug, L.A., Platt, T., Sathyendranath, S. & Barbosa, A.B. (2017) Unravelling region-specific environmental drivers of phytoplankton across a complex marine domain (off SW Iberia). *Remote Sens. Environ.*, 203, 162–184, Elsevier Inc. doi:10.1016/j.rse.2017.05.029

Krug, L.A., Platt, T., Sathyendranath, S. & Barbosa, A.B. (2017, June 1) Ocean surface partitioning strategies using ocean colour remote Sensing: A review. *Prog. Oceanogr.*, Elsevier Ltd. doi:10.1016/j.pocean.2017.05.013

Leitão, F., Vânia Baptista, Vieira, V., Silva, P.L., Relvas, P. & Teodósio, M.A. (2019) A 60-Year Time Series Analyses of the Upwelling along the Portuguese Coast. *WATER*. doi:10.3390/w11061285

Levier, C.B., Lorente, P., Reffray, G., Sotillo, M., Levier, B., Sotillo, M.G., Sotillo, M.G., *et al.* (2021) Atlantic -Iberian Biscay Irish- IBI Production Centre. *CMEMS*, 1–50.

Loureiro, S., Newton, A. & Icely, J. (2006) Boundary conditions for the European Water Framework Directive in the Ria Formosa lagoon, Portugal (physico-chemical and phytoplankton quality elements). *Estuar. Coast. Shelf Sci.*, 67, 382–398. doi:10.1016/j.ecss.2005.11.029

Loureiro, S., Newton, A. & Icely, J.D. (2005) Microplankton composition , production and upwelling dynamics in Sagres ( SW Portugal ) during the summer of 2001 *, 69, 323–341.

Martinez, E., Antoine, D., D'Ortenzio, F. & Gentili, B. (2009) Climate-driven basin-scale decadal oscillations of oceanic phytoplankton. *Science (80-. ).*, 326, 1253–1256. doi:10.1126/science.1177012

McGillicuddy, D.J., Kosnyrev, V.K., Ryan, J.P. & Yoder, J.A. (2001) Covariation of mesoscale ocean color and sea-surface temperature patterns in the Sargasso Sea. *Deep. Res. Part II Top. Stud. Oceanogr.*, 48, 1823–1836. doi:10.1016/S0967-0645(00)00164-8

McGovern, J.V., Dabrowski, T., Pereiro, D., Gutknecht, E., Lorente, P., Reffray, G. & Sotillo, M.. (2020) Atlantic IBI -Iberian Biscay Irish- Biogeochemical Multi- year Product. in *CMEMS*.

Mélin, F., Vantrepotte, V., Clerici, M., D'Alimonte, D., Zibordi, G., Berthon, J.F. & Canuti, E. (2011) Multi-sensor satellite time series of optical properties and chlorophyll-a concentration in the Adriatic Sea. *Prog. Oceanogr.*, 91, 229–244. doi:10.1016/j.pocean.2010.12.001

Mendes, C.R., Sá, C., Vitorino, J., Borges, C., Tavano Garcia, V.M. & Brotas, V. (2011) Spatial distribution of phytoplankton assemblages in the Nazaré submarine canyon region

(Portugal): HPLC-CHEMTAX approach. *J. Mar. Syst.*, 87, 90–101, Elsevier B.V. doi:10.1016/j.jmarsys.2011.03.005

Moradi, M. (2021) Evaluation of merged multi-sensor ocean-color chlorophyll products in the Northern Persian Gulf. *Cont. Shelf Res.*, 221, Elsevier Ltd. doi:10.1016/j.csr.2021.104415

Moradi, M. (2021) Evaluation of merged multi-sensor ocean-color chlorophyll products in the Northern Persian Gulf. *Cont. Shelf Res.*, 221, 104415, Elsevier Ltd. doi:10.1016/j.csr.2021.104415

Morel, A & Antoine, D. (2007) Pigment Index Retrieval in Case 1 Waters, 26.

Morel, Anclré & Prieur, L. (1977) Analysis of variations in ocean color. *Limnol. Oceanogr.*, 22, 709–722. doi:10.4319/lo.1977.22.4.0709

Moura, D., Aníbal, J., Mendes, I. & Gomes, A. (2019) Introduction. in *Ria Formosa: challenges of a coastal lagoonin a changing environment.* eds. Aníbal, J., Gomes, A., Mendes, I. & Moura, D., pp. 53–60, Faro: University of Algarve. Retrieved from http://hdl.handle.net/10400.1/14018

Nababan, B., Muller-Karger, F.E., Hu, C. & Biggs, D.C. (2011) Chlorophyll variability in the northeastern gulf of Mexico. *Int. J. Remote Sens.*, 32, 8373–8391. doi:10.1080/01431161.2010.542192

Navarro, G. & Ruiz, J. (2006) Spatial and temporal variability of phytoplankton in the Gulf of Cádiz through remote sensing images. *Deep. Res. Part II Top. Stud. Oceanogr.*, 53, 1241–1260. doi:10.1016/j.dsr2.2006.04.014

Novoa, S., Chust, G., Sagarminaga, Y., Revilla, M., Borja, A. & Franco, J. (2012) Water quality assessment using satellite-derived chlorophyll-a within the European directives, in the southeastern Bay of Biscay. *Mar. Pollut. Bull.*, 64, 739–750. doi:10.1016/j.marpolbul.2012.01.020

Racault, M.F., Sathyendranath, S., Brewin, R.J.W., Raitsos, D.E., Jackson, T. & Platt, T. (2017) Impact of El Niño variability on oceanic phytoplankton. *Front. Mar. Sci.*, 4, 133. doi:10.3389/fmars.2017.00133

Ramos, A.M., Cordeiro, A., Sousa, P.M. & Trigo, R.M. (2013) The use of circulation weather types to predict upwelling activity along the western Iberian Peninsula coast. *Cont. Shelf Res.*, 69, 38–51, Elsevier. doi:10.1016/j.csr.2013.08.019

Relvas, P., Luís, J. & Santos, A.M.P. (2009) Importance of the mesoscale in the decadal changes observed in the northern Canary upwelling system. *Geophys. Res. Lett.*, 36, 2–5. doi:10.1029/2009GL040504

Relvas, Paulo & Barton, E.D. (2002) Mesoscale patterns in the Cape São Vicente (Iberian Peninsula) upwelling region. *J. Geophys. Res. Ocean.*, 107, 1–23. doi:10.1029/2000jc000456

Relvas, Paulo & Barton, E.D. (2005) A separated jet and coastal counterflow during upwelling relaxation off Cape Sa ˜ o Vicente ( Iberian Peninsula ), 25, 29–49. doi:10.1016/j.csr.2004.09.006

Rivas, A.L., Dogliotti, A.I. & Gagliardini, D.A. (2006) Seasonal variability in satellite-measured surface chlorophyll in the Patagonian Shelf. *Cont. Shelf Res.*, 26, 703–720. doi:10.1016/j.csr.2006.01.013

Roy, R., Pratihary, A., Mangesh, G. & Naqvi, S.W.A. (2006) Spatial variation of phytoplankton pigments along the southwest coast of India. *Estuar. Coast. Shelf Sci.*, 69, 189–195. doi:10.1016/j.ecss.2006.04.006

Schuckmann, K. Von, Traon, P.Y. Le, Alvarez-Fanjul, E., Axell, L., Balmaseda, M., Breivik, L.A., Brewin, R.J.W., *et al.* (2016) The Copernicus Marine Environment Monitoring Service Ocean State Report. *J. Oper. Oceanogr.*, 9, s235–s320, Taylor & Francis. doi:10.1080/1755876X.2016.1273446

Shahbaba, B. (2009) *Biostatistics with R An Introduction to Statistics Through Biological Data*. *Springer Texts Stat.* doi:10.1007/978-1-4614-1302-8_1

Sheela, A.M., Letha, J., Joseph, S., Ramachandran, K.K. & Sanalkumar, S.P. (2011) Trophic state index of a lake system using IRS (P6-LISS III) satellite imagery. *Environ. Monit. Assess.*, 177, 575–592. doi:10.1007/s10661-010-1658-2

Shen, L., Xu, H. & Guo, X. (2012) Satellite remote sensing of harmful algal blooms (HABs) and a potential synthesized framework. *Sensors (Switzerland)*, 12, 7778–7803. doi:10.3390/s120607778

Shumway, R.H. & Stoffer, D.S. (2011) *Time Series Analysis and Its Applications With R Examples*. *Springer Texts Stat.*

Signorini, S.R., Franz, B.A. & McClain, C.R. (2015) Chlorophyll variability in the oligotrophic

gyres: Mechanisms, seasonality and trends. *Front. Mar. Sci.*, 2, 1–11. doi:10.3389/fmars.2015.00001

Signorini, S.R. & McClain, C.R. (2007) Large-scale forcing impact on biomass variability in the South Atlantic Bight. *Geophys. Res. Lett.*, 34, 1–6. doi:10.1029/2007GL031121

Simon, N., Cras, A., Foulon, E. & Lemée, R. (2009) Diversity and evolution of marine phytoplankton. *C. R. Biol.*, 332, 159–170, Elsevier Masson SAS. doi:10.1016/j.crvi.2008.09.009

Tiffany, A.H.M., Sathyendranath, S. & A., H. (2012) Ocean Color Remote Sensing of Phytoplankton Functional Types. *Remote Sens. Biomass - Princ. Appl.* doi:10.5772/17174

Trees, C.C., Clark, D.K., Bidigare, R.R., Ondrusek, M.E. & Mueller, J.L. (2000) Accessory pigments versus chlorophyll a concentrations within the euphoric zone: A ubiquitous relationship. *Limnol. Oceanogr.*, 45, 1130–1143. doi:10.4319/lo.2000.45.5.1130

Tweddle, J.F., Gubbins, M. & Scott, B.E. (2018) Should phytoplankton be a key consideration for marine management ? *Mar. Policy*, 97, 1–9, Elsevier Ltd. doi:10.1016/j.marpol.2018.08.026

Uitz, J., Claustre, H., Gentili, B. & Stramski, D. (2010) Phytoplankton class-specific primary production in the world's oceans: Seasonal and interannual variability from satellite observations. *Global Biogeochem. Cycles*, 24, 1–19. doi:10.1029/2009GB003680

Volpe, G., Colella, S., Brando, V.E., Forneris, V., Padula, F. La, Cicco, A. Di, Sammartino, M., *et al.* (2019) Mediterranean ocean colour Level 3 operational multi-sensor processing. *Ocean Sci.*, 15, 127–146. doi:10.5194/os-15-127-2019

Waite, J.N. & Mueter, F.J. (2013) Spatial and temporal variability of chlorophyll-a concentrations in the coastal Gulf of Alaska, 1998-2011, using cloud-free reconstructions of SeaWiFS and MODIS-Aqua data. *Prog. Oceanogr.*, 116, 179–192, Elsevier Ltd. doi:10.1016/j.pocean.2013.07.006

Wang, M., Jiang, L., Mikelsons, K. & Liu, X. (2021) Satellite-derived global chlorophyll-a anomaly products. *Int. J. Appl. Earth Obs. Geoinf.*, 97, 102288, Elsevier BV. doi:10.1016/j.jag.2020.102288

Wilson, C. (2011) The rocky road from research to operations for satellite ocean-colour data in fishery management. *ICES J. Mar. Sci.*, 68, 677–686. doi:10.1093/icesjms/fsq168

Wilson, C. & Adamec, D. (2001) Correlations between surface chlorophyll and sea surface height in the tropical Pacific during the 1997-1999 El Niño - Southern Oscillation event. *J. Geophys. Res. Ocean.*, 106, 31175–31188. doi:10.1029/2000jc000724

Wright, S.W. & Jeffrey, S.W. (2006) Pigment markers for phytoplankton production. *Handb. Environ. Chem. Vol. 2 React. Process.*, 2 N, 71–104. doi:10.1007/698_2_003

Wunderlin, D.A., María Del Pilar, D., María Valeria, A., Fabiana, P.S., Cecilia, H.A. & María De Los Ángeles, B. (2001) Pattern recognition techniques for the evaluation of spatial and temporal variations in water quality. A Case Study: Suquía River basin (Córdoba-Argentina). *Water Res.*, 35, 2881–2894. doi:10.1016/S0043-1354(00)00592-3

Xi, H., Losa, S.N., Mangin, A., Soppa, M.A., Garnesson, P., Demaria, J., Liu, Y., *et al.* (2020) Global retrieval of phytoplankton functional types based on empirical orthogonal functions using CMEMS GlobColour merged products and further extension to OLCI data. *Remote Sens. Environ.*, 240, 111704, Elsevier. doi:10.1016/j.rse.2020.111704

Yu, Y., Xing, X., Liu, H., Yuan, Y., Wang, Y. & Chai, F. (2019) The variability of chlorophyll-a and its relationship with dynamic factors in the basin of the South China Sea. *J. Mar. Syst.*, 200, Elsevier B.V. doi:10.1016/j.jmarsys.2019.103230

Zibordi, G., Mélin, F. & Berthon, J.F. (2012) Intra-annual variations of biases in remote sensing primary ocean color products at a coastal site. *Remote Sens. Environ.*, 124, 627–636, Elsevier Inc. doi:10.1016/j.rse.2012.06.016

**R packages Reference**


Alboukadel Kassambara (2020). ggpubr: 'ggplot2' Based Publication Ready Plots. R package version 0.4.0. https://CRAN.R-project.org/package=ggpubr

David Gohel (2020). rvg: R Graphics Devices for Vector Graphics Output. R package version 0.2.5. https://CRAN.R-project.org/package=rvg

David Gohel (2021). officer: Manipulation of Microsoft Word and PowerPoint Documents. R package version 0.4.1. https://CRAN.R-project.org/package=officer

Fox, J., and Bouchet-Valat, M. (2020). Rcmdr: R Commander. R package version 2.7-1.

Hadley Wickham and Jennifer Bryan (2019). readxl: Read Excel Files. R package version 1.3.1. https://CRAN.R-project.org/package=readxl

Hadley Wickham et al., (2019). Welcome to the tidyverse. Journal of Open Source Software, 4(43), 1686, https://doi.org/10.21105/joss.01686

Hadley Wickham H (2016). ggplot2: Elegant Graphics for Data Analysis. Springer-Verlag New York. ISBN 978-3-319-24277-4, https://ggplot2.tidyverse.org.

Hadley Wickham, Romain François, Lionel Henry and Kirill Müller (2021). dplyr: A Grammar of Data Manipulation. R package version 1.0.7. https://CRAN.R-project.org/package=dplyr

Jim Hester and Jennifer Bryan (2021).glue: Interpreted String Literals. R package version 1.5.1. https://CRAN.R-project.org/package=glue

Kirill Müller (2020). here: A Simpler Way to Find Your Files. R package version 1.0.1. https://CRAN.R-project.org/package=here

R Core Team (2021). R: A language and environment for statistical computing. R Foundation for Statistical Computing, Vienna, Austria. URL https://www.R-project.org/.

Simon Garnier, Noam Ross, Robert Rudis, Antônio P. Camargo, Marco Sciaini, and Cédric Scherer (2021). Rvision - Colorblind-Friendly Color Maps for R. R package version 0.6.2.

# APPENDIX-A

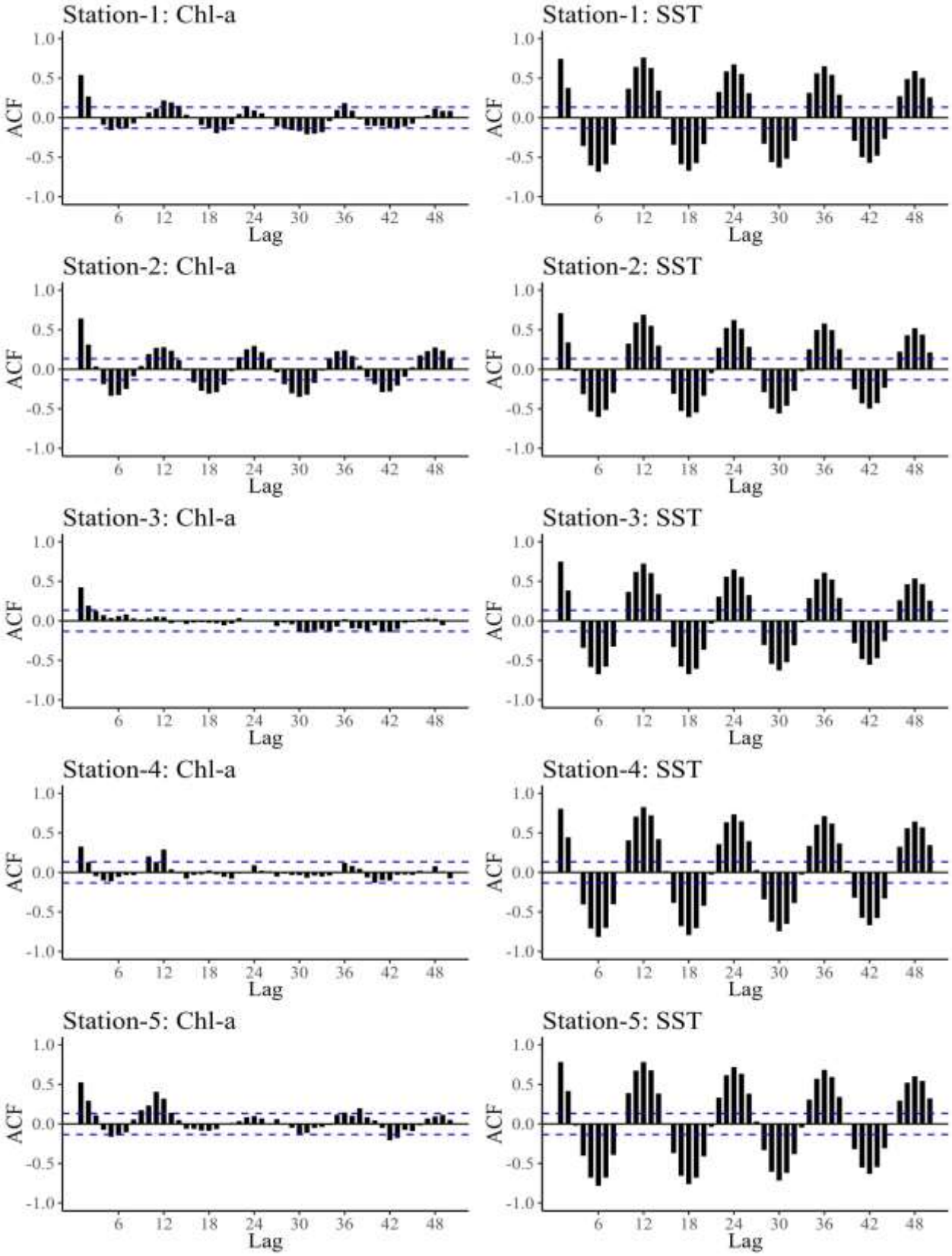


**Fig. A.1.** Autocorrelation function of Chl-*a* and SST time series for all stations.

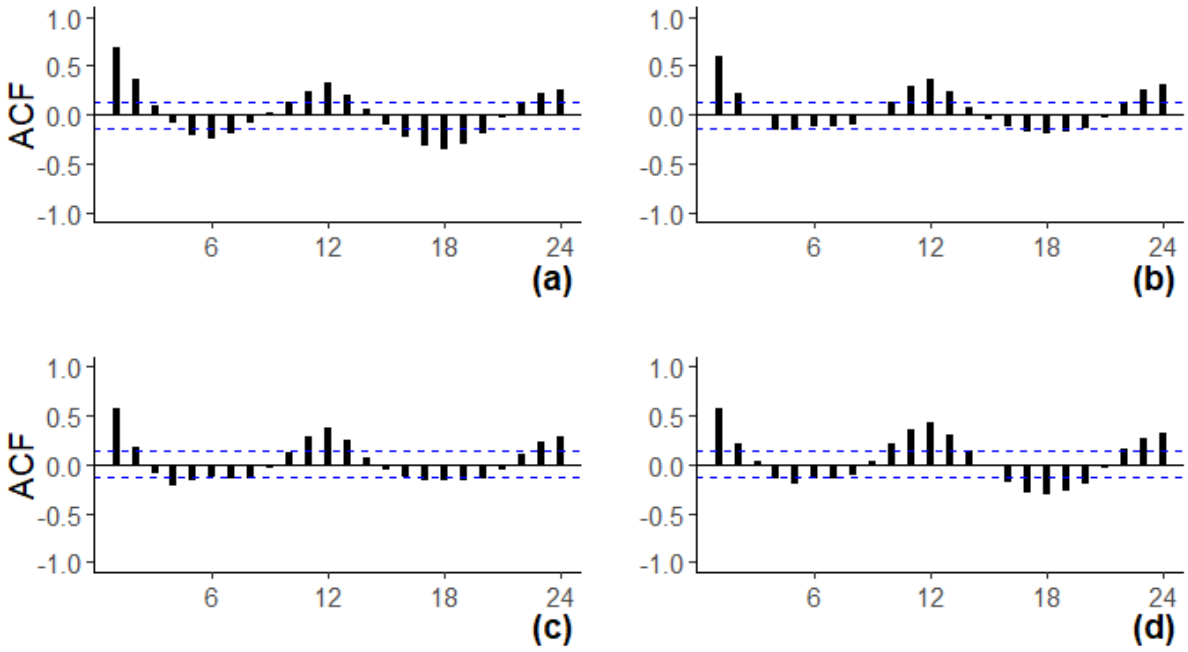


**Fig. A.2.** Autocorrelation function of time series (a) $NH_4^+$, (b) $NO_3^-$ (c) $PO_4^+$ and (d) $SiO_4^{-4}$ for Station 2 (off Sagres).

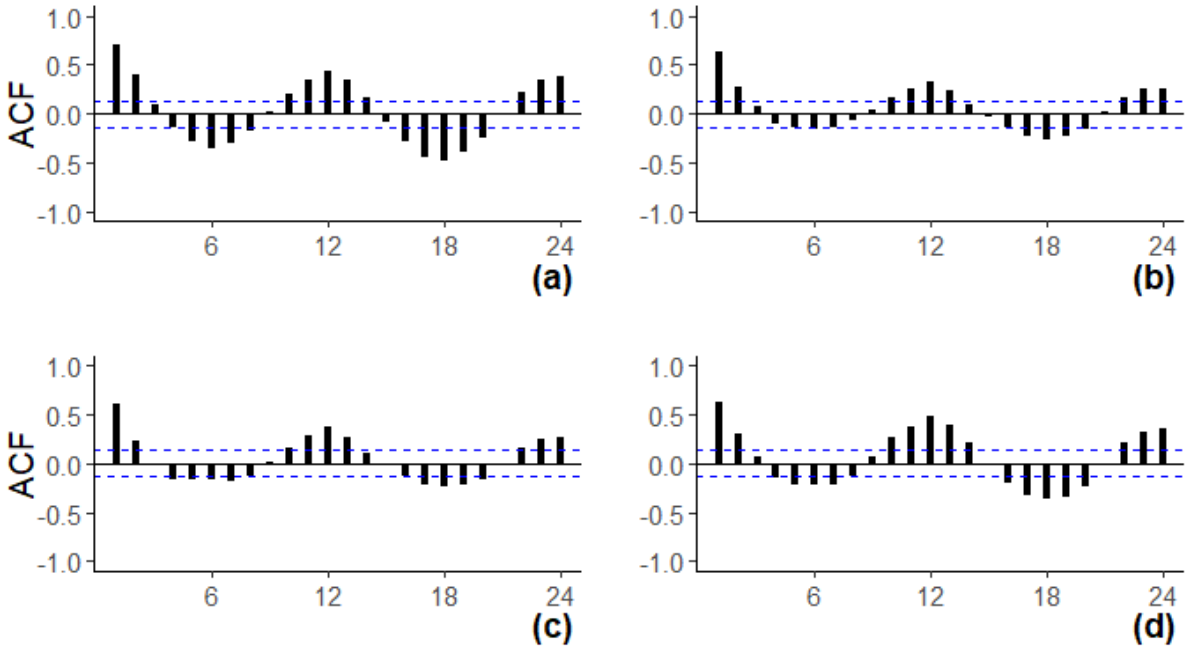


**Fig. A.3.** Autocorrelation function of time series (a) $NH_4^+$, (b) $NO_3^-$ (c) $PO_4^+$ and (d) $SiO_4^{-4}$ for Station 3 (off Portimão).

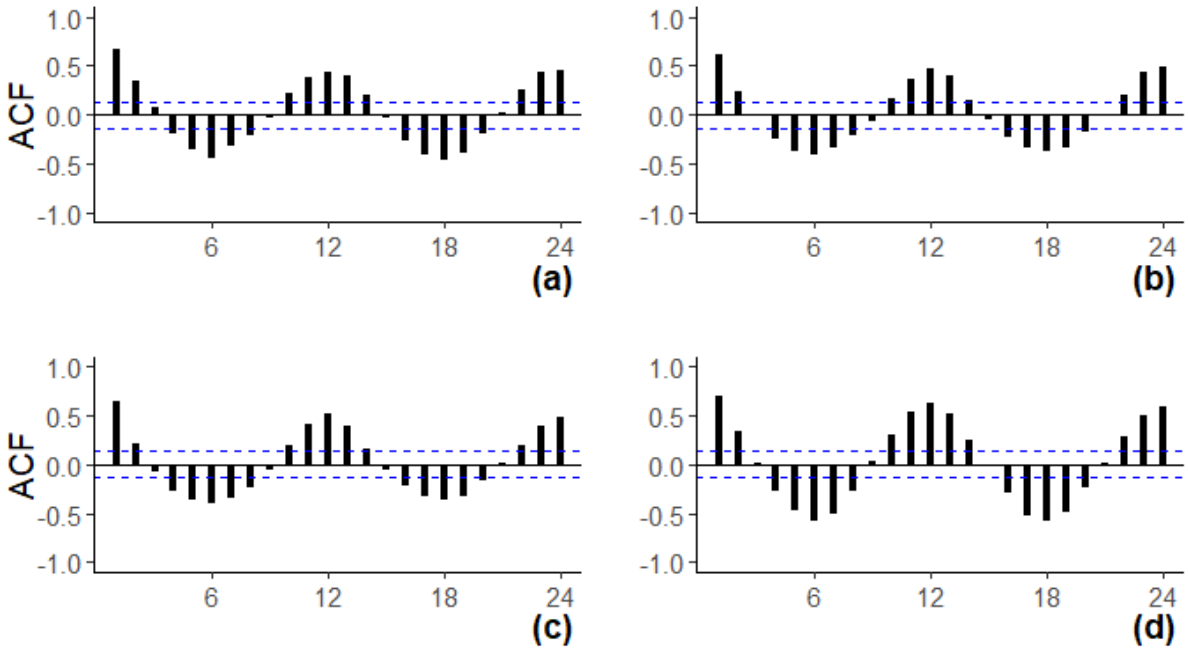


**Fig. A.4.** Autocorrelation function of time series (a) $NH_4^+$, (b) $NO_3^-$ (c) $PO_4^+$ and (d) $SiO_4^{-4}$ for Station 4 (off Ria Formosa).

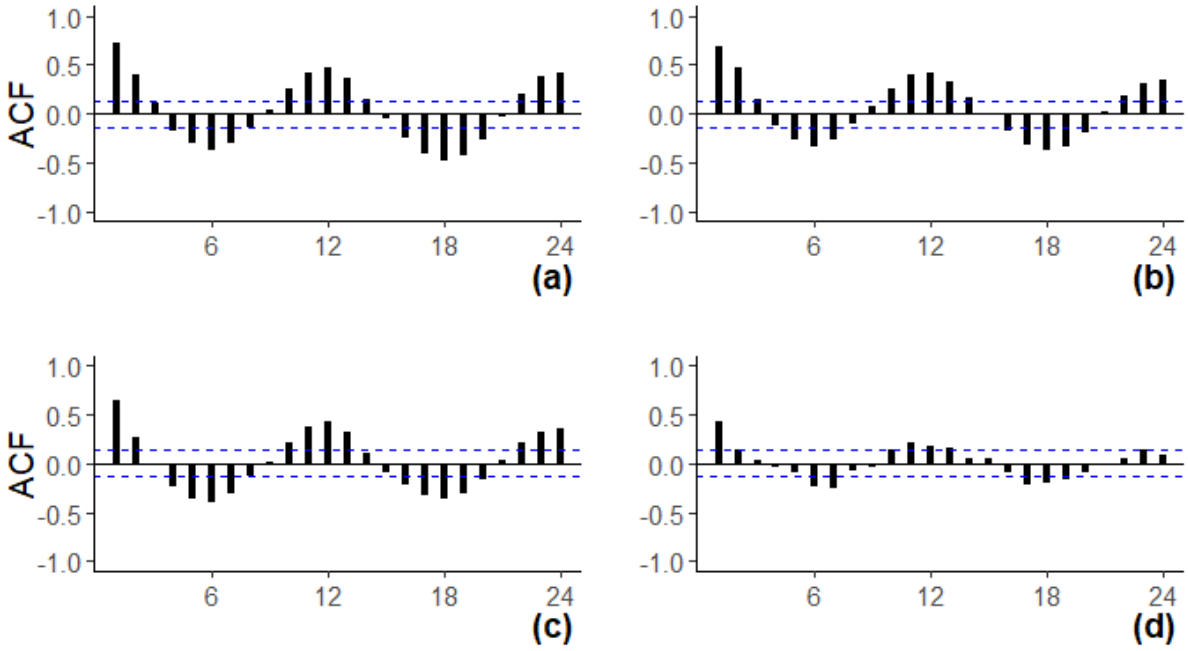


**Fig. A.5.** Autocorrelation function of time series (a) $NH_4^+$, (b) $NO_3^-$ (c) $PO_4^+$ and (d) $SiO_4^{-4}$ for Station 5 (off Guadiana Estuary).

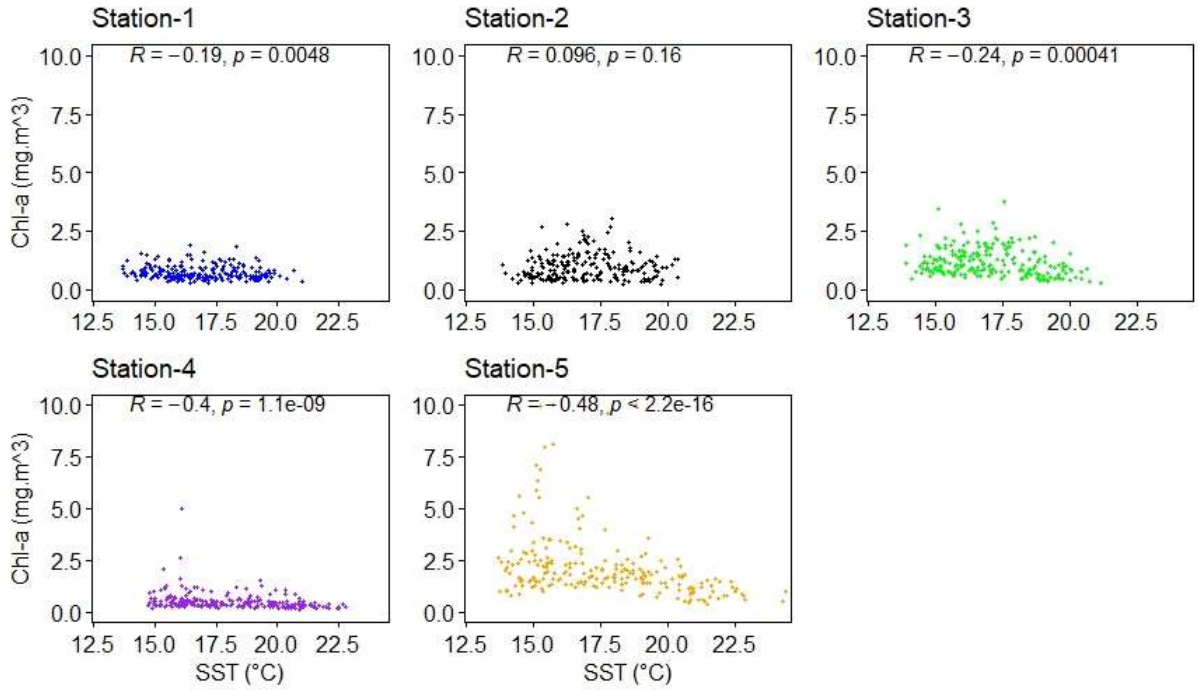


**Fig. A.6.** Scatter plot between Chl-*a* and SST.

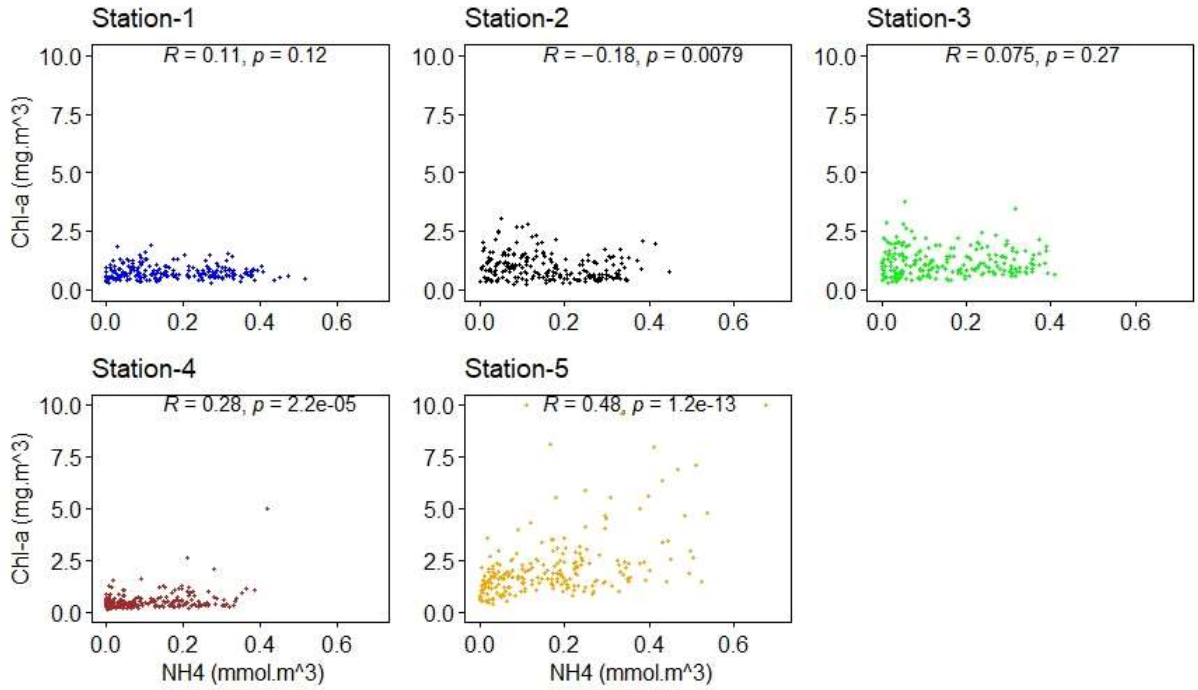


**Fig. A.7.** Scatter plot between Chl-*a* and $NH_4^+$.

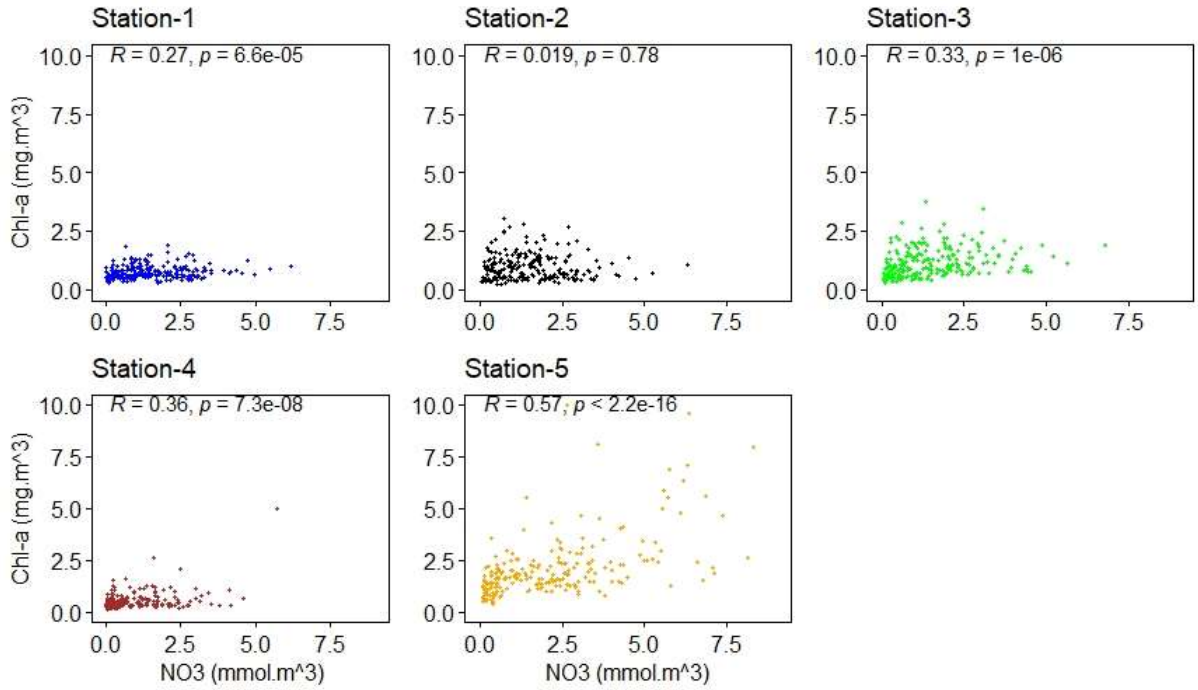


**Fig. A.8**. Scatter plot between Chl-*a* and $NO_3^-$.

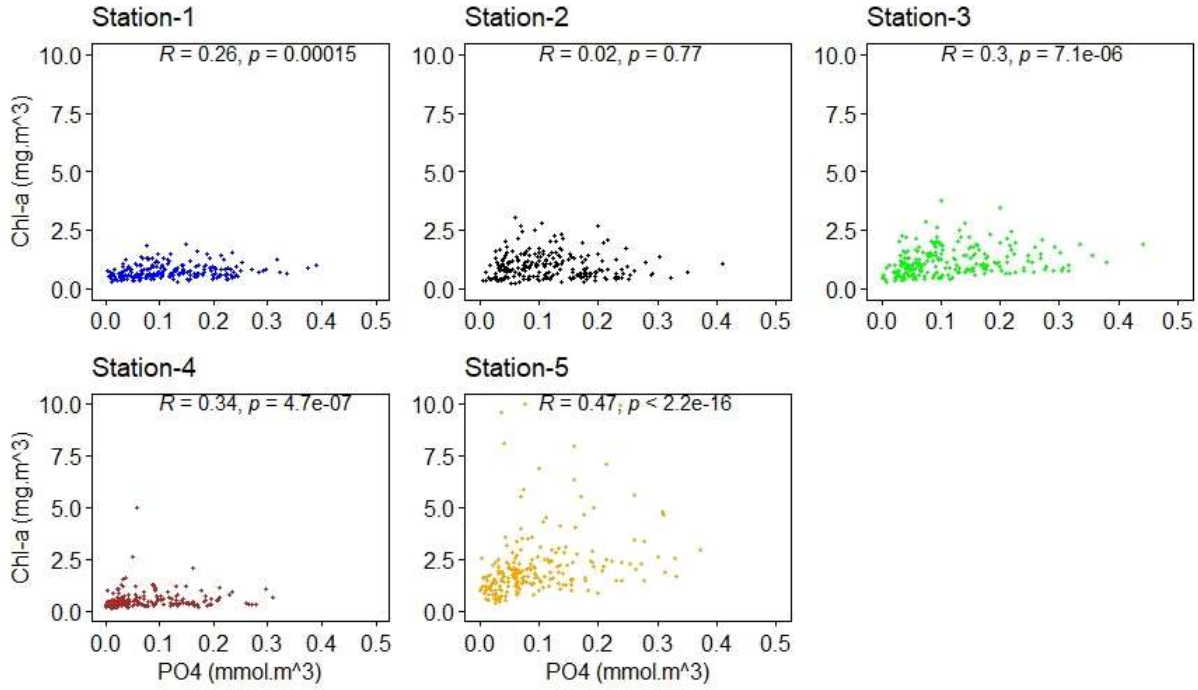


**Fig. A.9.** Scatter plot between Chl-*a* and $PO_4^+$.

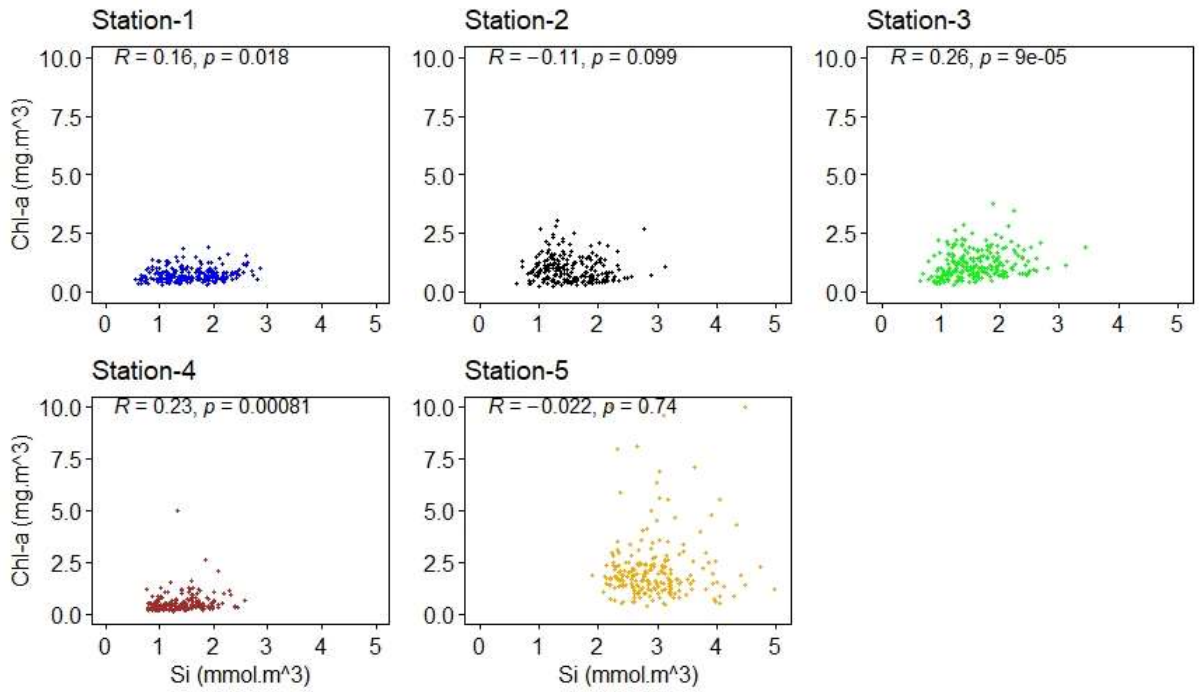


**Fig. A.10.** Scatter plot between Chl-*a* and $SiO_4^{-4}$.